MOMENT METHOD SOLUTION FOR MULTIPLE-STEP DISCONTINUITIES IN WAVEGUIDES

BY

© ABDUL-KADIR M.N. HAMID

A thesis submitted to the faculty of Graduate Studies of the University of Manitoba in partial fulfillment of the requirements of the degree of

MASTER OF SCIENCE

Department of Electrical Engineering

University of Manitoba

July 1988

ISBN 0-315-47893-4

MOMENT METHOD SOLUTION FOR MULTIPLE-STEP DISCONTINUITIES IN WAVEGUIDES

BY

ABDUL-KADIR M.N. HAMID

A thesis submitted to the Faculty of Graduate Studies of the University of Manitoba in partial fulfillment of the requirements of the degree of

MASTER OF SCIENCE

ABSTRACT

The moment method solution is employed in this thesis to analyse the field behaviour and the scattering matrix coefficients describing reflection, transmission, and mode conversions at multiple-step waveguide junctions. The equivalence principle is used to divide the original problem into isolated regions and equivalent magnetic current sheets are used to replace the junctions faces on perfect electric conductors to ensure the continuity of the tangential electric and magnetic field components at each junction. The magnetic current sheets are expressed in terms of infinite series and each term corresponds to a new mode. In the case of double-step two coupled sets of equations in terms of the unknown magnetic current sheets are obtained and solved using the moment method. Some special cases, such as ridged and over-sized double-step discontinuity are considered in detail. The analysis is also extended to include cascaded junctions. The field and scattering matrix coefficients are computed and presented graphically as a function of frequency for various separation between the junctions.

ACKNOWLEDGEMENTS

I wish to express my sincere to Professors I. R. Ciric and M. Hamid for their advise, continuous encouragement and helpful discussion throughout the course of this research.

Thanks to my family and specially my parents for their patience and continuous encouragement.

The auther wishes to acknowledge the financial assistance of the Natural Science and Engineering Research Council of Canada and the Faculty of Graduate studies of the University of Manitoba, which make this research possible.

TABLE OF CONTENTS

LIST OF FIGURES

LIST OF TABLES

LIST OF PRINCIPAL SYMBOLS

A	refers to waveguide A
B	refers to waveguide B
C	refers to waveguide C
j	$\sqrt{-1}$
E	electric field
H	magnetic field
t	refers to the transverse components of the electric and magnetic field
f	frequency
f_c	cutoff frequency
f'_c	cutoff frequency in the connecting waveguide
γ_{ri}	complex attenuation of the i th mode
Y_{ri}	characteristic admittance of the i th mode
λ	wavelength
μ_r	magnetic permeability
r	refers to waveguide A,B, and C, respectively.
u_z	unit vector in z-direction
e_{ri}	modal electric field of i th mode
w_a	width of rectangular waveguide A
w_b	width of rectangular waveguide B
w_c	width of rectangular waveguide C
Γ_o	reflection coefficient of a junction terminated by an electric wall

Γ_e	reflection coefficient of a junction terminated by a magnetic wall
S_1	area of aperture one
S_2	area of aperture two
$M^{(0)}$	magnetic current sheet at S_1
$M^{(L)}$	magnetic current sheet at S_2
$V_p^{(0)}$	coefficient of the p th mode expansion function in aperture S_1
$V_p^{(L)}$	coefficient of the p th mode expansion function in aperture S_2
Q_1	number of unknown coefficients of the transverse electric field in aperture S_1
Q_2	number of unknown coefficients of the transverse electric field in aperture S_2
N_1	number of modes in waveguide A
N_2	number of modes in waveguide B
S	scattering matrix
S_{ip}	element of the scattering matrix S with i, p = a or b : matrix element of the single-junction, with i, p = a or c : matrix element of the double-junction
a_i	coefficient of the i th incident mode in waveguide A
b_i	coefficient of the i th transmitted mode in waveguide B
c_i	coefficient of the i th transmitted mode in waveguide C
d_i	coefficient of the i th reflected mode in waveguide A
f_i	coefficient of the i th reflected mode in waveguide B
L	length of the connecting waveguide

L_t	transformer length
δ_{ip}	kronecker delta (= 0 if i ≠ p; = 1 if i = p)
U	unity matrix
$\vec{I}$	current source
T	transpose matrix
$\vec{O}$	null matrix

CHAPTER 1

INTRODUCTION

The problem of coupling through apertures has many engineering applications, such as waveguide to waveguide coupling, waveguide fed horn coupling, horn to horn coupling, and waveguide fed aperture coupling.

Waveguides with multiple-step discontinuities are encountered in a variety of engineering applications such as transformers to minimize the reflection coefficient [1], band rejection filters [2], and dielectric resonators in waveguides below cutoff [3]. The early work was performed by using the variational method [4,5], Schwarz procedure [6-8], a quasi-optical theory [9], and several numerical methods, some of them based on the moment method solution [10-12]. De Smedt and Denturck [13] used the moment method and point matching solution to obtain the scattering matrix coefficients for a double-step in terms of that for a single step discontinuity, for sufficiently large separation between the junctions. Rozzi and Mecklenbräuker [14,15] proposed a solution based on the variational method and network modeling for interacting inductive irises and steps in rectangular waveguides. The salient feature of their approach is that the solution of the field problem yields a reactance matrix with monotonic convergence properties. Wexler [16] used modal analysis to solve for waveguide discontinuities, the field being expressed in terms of waveguides modes, and obtained a solution for the mode coefficients. Later, a solution for double-plane steps in rectangular waveguides was obtained by Patzelt and Arndt [17] using the method of field expansion into eigenmodes. This method takes into account the influence of the evanescent field modes and power transmitted due the higher order modes. Safavi-Naini and

MacPhie [18,19] used the principle of conservation of complex power to obtain the scattering matrix of two-port network without matrix inversions. The Ray theory method was also applied to study the scattering by a waveguide discontinuity [20-22], where the field at a distant point due to line source excitation is presented as the sum of the fields on the various multiply reflected rays from the source. The ray fields are then converted into a sum of modes, with the amplitude of each mode being determined by the radiation pattern of the source in the two plane wave directions corresponding to the mode. The ray diagram is complicated while the restriction on the dimensions of the scatterer being large relative to the wavelength for a reasonable accuracy makes the method less attractive.

The main objective of this thesis is to present a complete study of the field behavior and the scattering matrix coefficients for single and multi-step waveguide discontinuities for various values of separation length between the junctions.

In chapter 2, we present a moment method procedure for solving the single step discontinuity based on the generalized network representation for aperture problems [23,24]. The method is applied to two infinite rectangular waveguides with a transverse planar junction with an incident field from the smaller waveguide. The field components are expressed in modal form for both the *TE* and *TM* modes. The scattering matrix associated with incident and scattered fields in the smaller waveguide and the transmitted field in the larger waveguide are determined from the analysis. The Reciprocity Theorem permits determination of the scattered and transmitted fields when the incident field is from the larger waveguide. The scattering matrix coefficients are computed and presented graphically as a function of frequency.

In chapter 3, we present the general solution for a double-step waveguide discontinuity. The analysis is extended to a closely separated double-step discontinuity to take into account the near field coupling within the double-step discontinuity and the interaction between the higher order modes. The resulting set of coupled integral equations is solved using the moment method. Quantitative results for the field coefficients are presented for a specific double-step waveguide discontinuity where the separation between the junctions is small compared to the wavelength. Various values of L are considered while the frequency range for computational purposes is from 2.6 to 10 GHz.

Chapter 4 presents an alternative solution to the double-step discontinuity by subjecting the structure to an odd and an even excitation and then superimposing the results to obtain the scattering matrix [13,25]. This is in contrast to classical iterative methods based on the wave matrix approach which employ the scattering matrix for each individual junction and attempt to present the multiple interaction between junctions using the term by term shifting matrix. A series of steps is commonly treated by the transmission matrix parameter[26-28]. In other words, cascaded junctions are always separated by waveguide sections, and those cascaded sections are treated by applying the transmission matrix representation [29], while the cascaded junctions are treated by the scattering matrix scheme for a double-step discontinuity. The only usual restriction is on the connecting waveguide sections which should be sufficiently long relative to the wavelength.

The discussion and conclusions are presented in chapter 5. Appendix A, presents application of the method to a single iris in a rectangular waveguide. The analysis for

these types of discontinuities runs parallel to the foregoing analysis in Chapter 2 with the only difference being in those cases where the waveguide cross-sections are the same.

CHAPTER 2

ANALYSIS OF SINGLE-STEP DISCONTINUITY IN RECTANGULAR WAVEGUIDES

The problem of a single-step waveguide discontinuity is discussed in this chapter. The equivalence principle is used to divide the problem under consideration into two regions [30]. This is can be accomplished by covering the aperture with an electric wall and providing for the unknown tangential electric field in the aperture by attaching magnetic current sheets to both faces of the junction. Continuity of the tangential magnetic field components across the aperture yields an integral equation in terms of the unknown magnetic current sheet. To solve the integral equation, the moment method is used [31]. The unknown magnetic current sheet is expressed as an infinite series with a linear combination of the expansion function. The expansion function is substituted into the integral equation, then a weighting (or testing) function is defined and used to test the integral equation at different points (point matching). Apart from simplicity, the obvious advantage of the moment method is to choose weighting and expansion functions to minimize the computation required for evaluating the inner product [32,33]. A particular choice of expansion functions may be obtained by letting the weighting and basis functions be the same (Galerkin's method) [34,35].

2.1 Formulation

Consider two infinitely long rectangular waveguides having different cross sections as shown in Fig. 2-1. The source is located far enough from the junction in waveguide A where it produces a multimode propagates field. The incident field propagating in the positive z-direction. A part is reflected by the discontinuity and a part is transmitted through the aperture S to waveguide B. The transverse components of the electromagnetic field in modal form are given as follows [31].

$$E_t = \begin{cases} \sum_i a_i e^{-j\gamma_{ai} z} e_{ai} + \sum_i d_i e^{j\gamma_{ai} z} e_{ai} & (z < 0) \\ \sum_i b_i e^{-j\gamma_{bi} z} e_{bi} & (z > 0) \end{cases} \tag{2-1}$$

$$H_t = \begin{cases} \sum_i a_i Y_{ai} e^{-j\gamma_{ai} z} u_z \times e_{ai} - \sum_i d_i Y_{ai} e^{j\gamma_{ai} z} u_z \times e_{ai} & (z < 0) \\ \sum_i b_i Y_{bi} e^{-j\gamma_{bi} z} u_z \times e_{bi} & (z > 0) \end{cases} \tag{2-2}$$

a_i, b_i, and d_i are complex coefficients of the transmitted and reflected mode, γ_{ai} and γ_{bi} are the modal propagation constants, Y_{ai} and Y_{bi} are the modal admittances, e_{ai} and e_{bi} are the modal vectors for the ith mode in waveguides A and B, respectively. The propagation constants are real for propagating modes while in the case of evanescent modes they are imaginary. The normalization of the field is given by [13]

$$\int_S e_{ri} \cdot e_{rp} \, ds = \delta_{ip} \tag{2-3}$$

where r refers to waveguide A or B, respectively.

Using the Equivalence Principle [31,35], the fields in the two regions can be modeled in terms of the equivalent magnetic current sheet M placed over the aperture

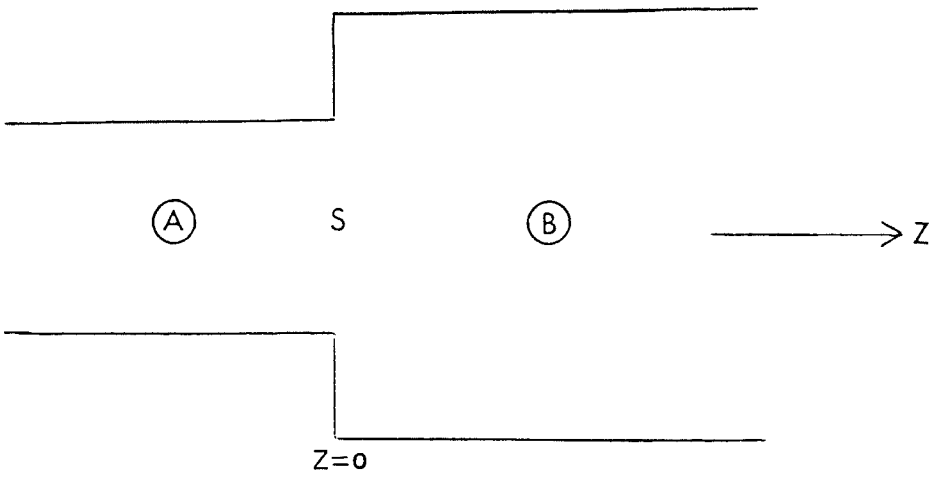

Fig. 2-1: Geometry of single step waveguide discontinuity.

S, as shown in Fig. 2-2, with

$$M = u_z \times E_t \qquad at\ z = 0 \tag{2-4}$$

where u_z is the unit normal and E_t is the unknown electric field in the aperture S which is to be determined. Thus, the field in waveguide A is the incident field plus the field produced by the magnetic sheet M while the field in waveguide B is the field produced by the magnetic current sheet $-M$.

In order to determine the unknown expansion coefficients, we apply the proper boundary conditions. Thus the continuity of the tangential electric field components across the aperture S at z = 0, requires that

$$\sum_i a_i\ u_z \times e_{ai} + \sum_i d_i\ u_z \times e_{ai} = M = \sum_i b_i\ u_z \times e_{bi} \tag{2-5}$$

Also the continuity of the tangential magnetic field components across the aperture S at z = 0, requires that

$$\sum_i a_i\ Y_{ai}\ u_z \times e_{ai} - \sum_i d_i\ Y_{ai}\ u_z \times e_{ai} = \sum_i b_i\ Y_{bi}\ u_z \times e_{bi} \tag{2-6}$$

If equations (2-5) and (2-6) could be satisfied exactly, we would obtain the true solution. To obtain an approximate solution, we apply the moment method.

2.2 Moment method solution

To apply the moment method, we expand the magnetic current sheet M as

$$M = \sum_{p=1}^{Q} V_p\ M_p \qquad at\ z=0 \tag{2-7}$$

where V_p are unknown complex coefficients to be evaluated, and M_p are known vector basis functions. The above summation is limited to a finite number of terms Q. By substituting (2-7) into (2-5), we obtain

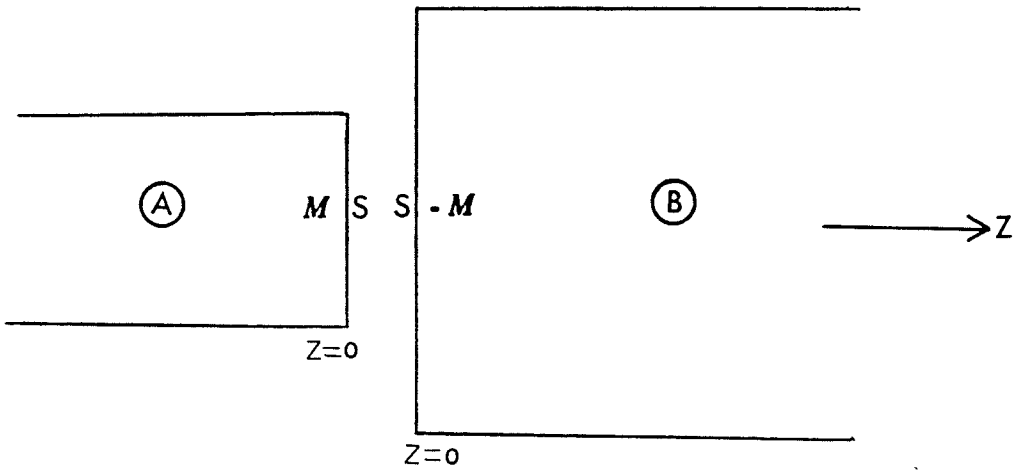

Fig. 2-2: Equivalence for waveguides A and B.

$$\sum_{i=1}^{N} a_i \; u_z \times e_{ai} + \sum_{i=1}^{N} d_i \; u_z \times e_{ai} = \sum_{p=1}^{Q} V_p \; M_p \tag{2-8}$$

and

$$\sum_{i=1}^{N} b_i u_z \times e_{bi} = \sum_{p=1}^{Q} V_p \; M_p \tag{2-9}$$

Next, multiplying equation (2-8) by $u_z \times e_{ak}$ and equation (2-9) by $u_z \times e_{bk}$ (k = 1,2,..., N), and integrating over the corresponding aperture S, we obtain

$$\sum_{i=1}^{N} a_i \int_S u_z \times e_{ai} \cdot u_z \times e_{ak} \; ds + \sum_{i=1}^{N} d_i \int_S u_z \times e_{ai} \cdot u_z \times e_{ak} \; ds =$$

$$\sum_{p=1}^{Q} V_p \int_S M_p \cdot u_z \times e_{ak} \; ds \tag{2-10}$$

and

$$\sum_{i=1}^{N} b_i \int_S u_z \times e_{bi} \cdot u_z \times e_{bk} \; ds = \sum_{p=1}^{Q} V_p \int_S M_p \cdot u_z \times e_{bk} \; ds \tag{2-11}$$

Because of the orthogonality condition (2-3), all the terms in the summations on the left hand side are equal to zero except the i = k term. This leads to

$$a_i + d_i = \sum_{p=1}^{Q} V_p \; h_{aip} \qquad (i = 1,2,..., N) \tag{2-12}$$

$$b_i = \sum_{p=1}^{Q} V_p \; h_{bip} \qquad (i = 1,2,..., N) \tag{2-13}$$

where

$$h_{rip} = \int_S M_p \cdot u_z \times e_{ri} \; ds \qquad (r = a,b) \tag{2-14}$$

Equation (2-14) can be written in matrix form as

$$H_r = [h_{rip}]_{N \times Q} \tag{2-15}$$

Next, define an inner product as in [31],

$$<W\ ,\ G> = \int_S W \cdot G\ ds \tag{2-16}$$

and a set of testing functions $\{W_p,\ p = 1,2,...,Q\}$, which may or may not be equal to the expansion functions. We take the inner product of (2-6) with the testing function W_k, and obtain

$$\sum_{i=1}^{N} a_i Y_{ai} \int_S W_k \cdot u_z \times e_{ai}\ ds = \sum_{i=1}^{N} \left[\sum_{p=1}^{Q} V_p h_{aip} - a_i \right] Y_{ai} \int_S W_k \cdot u_z \times e_{ai}\ ds +$$

$$\sum_{i=1}^{N} \left[\sum_{p=1}^{Q} V_p h_{bip} \right] Y_{bi} \int_S W_k \cdot u_z \times e_{bi}\ ds \tag{2-17}$$

Equation (2-17) can be simplified as

$$2\sum_{i=1}^{N} a_i Y_{ai} W_{aik} = \sum_{i=1}^{N} \left[\sum_{p=1}^{Q} V_p h_{aip} \right] Y_{ai} W_{aik} +$$

$$\sum_{i=1}^{N} \left[\sum_{p=1}^{Q} V_p h_{bip} \right] Y_{bi} W_{bik} \qquad (k = 1,2,...,Q) \tag{2-18}$$

where

$$W_{rik} = \int_S W_k \cdot u_z \times e_{ri}\ ds \qquad (r = a,b) \tag{2-19}$$

The above equation can be written as in (2-15), *i.e.*

$$W_r = [W_{rik}]_{N \times Q} \tag{2-20}$$

Following Mautz *et al* [24,36-38] equation (2-18) may be re-written in the generalized admittance form as

$$\vec{I} = [\bar{Y}_a + \bar{Y}_b]\ \vec{V} \tag{2-21}$$

where

$$\vec{I} = 2W_a^T Y_a \vec{\alpha} \tag{2-22}$$

$$\bar{Y}_r = W_r^T Y_r H_r \qquad (r = a,b) \tag{2-23}$$

$$\vec{a} = [a_i]_{N\times 1} \tag{2-24}$$

$$\vec{V} = [V_p]_{Q\times 1} \tag{2-25}$$

With Y_r being the diagonal matrix of the modal admittances in the corresponding waveguide A or B, $\vec{a}$ and $\vec{V}$ are the column matrices of the quantities a_i and V_p, and T is the matrix transpose. Equation (2-21) can be interpreted as two networks $[\overline{Y}_a]$ and $[\overline{Y}_b]$ in parallel with the current source $\vec{I}$ as shown in Fig. 2-3. It is important to know that $[\overline{Y}_a]$ represents waveguide A and $[\overline{Y}_b]$ represents waveguide B, which may be computed separately, then the results are combined to yield the solution of the problem.

2.3 Galerkin's method solution

Since the aperture S has the same cross-section as waveguide A, we may let the weighting and basis functions be the same and equal to [23]

$$M_p = W_p = u_z \times e_{ap} \qquad (p=1,2,\ldots, Q) \tag{2-26}$$

Also, we let $N = Q$ and $e_{ap} = e_{bp}$. This leads to

$$H_r = W_r = U \qquad (r = a, b) \tag{2-27}$$

where U is the identity matrix. Equations (2-22) and (2-23) reduce to

$$\vec{I} = 2Y_a \vec{a} \tag{2-28}$$

$$\overline{Y}_r = Y_r \tag{2-29}$$

Substituting (2-28) and (2-29) into (2-21), we obtain

$$\vec{I} = [Y_a + Y_b]\,\vec{V} \tag{2-30}$$

Equation (2-30) represents a $(N\times N)$ system of linear equations. Its solution through equations (2-12)-(2-13) yields the electric and magnetic fields in equations (2-1) and (2-2). The final stage in this chapter is to obtain the scattering matrix coefficients for

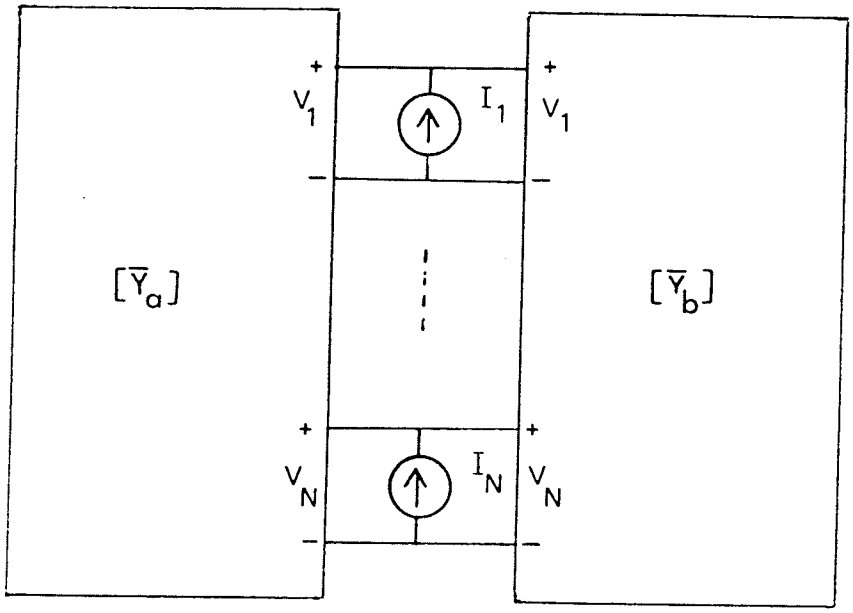

Fig. 2-3: The generalized network presentation of equation (2-21).

the single-step discontinuity.

2.4 Scattering matrix formulation

The scattering matrix for the single step discontinuity is given by [39]

$$S = \begin{bmatrix} S_{aa} & S_{ab} \\ S_{ba} & S_{bb} \end{bmatrix} \tag{2-31}$$

Let the subscripts a and b denote the left and right side regions of the junctions, respectively. The complex reflection coefficients S_{aa} can be obtained from (2-12) as

$$\vec{d} = \vec{V} - \vec{a} \tag{2-32}$$

where $\vec{V}$ is obtained from (2-30) as

$$\vec{V} = 2\,(Y_a + Y_b)^{-1}\, Y_a \vec{a} \tag{2-33}$$

Substituting (2-33) into (2-32) leads to

$$\vec{d} = 2\,(Y_a + Y_b)^{-1}\, Y_a \vec{a} - \vec{a} \tag{2-34}$$

Therefore, the submatrix S_{aa} can be written as

$$S_{aa} = \frac{\vec{d}}{\vec{a}} = (Y_a + Y_b)^{-1}\,(Y_a - Y_b) \tag{2-35}$$

Similarly, the complex transmission coefficients can be obtained from (2-13) as

$$\vec{b} = 2\,(Y_a + Y_b)^{-1}\, Y_a \vec{a} \tag{2-36}$$

Therefore, the submatrix S_{ba} may be written as

$$S_{ba} = \frac{\vec{b}}{\vec{a}} = 2\,(Y_a + Y_b)^{-1}\, Y_a \tag{2-37}$$

The submatrices S_{ab} and S_{bb} due to the excitation in waveguide B may be obtained in a similar manner since the situation is reciprocal to the above submatrices S_{aa} and S_{ba} due to the excitation in waveguide A. Therefore, the source vector $\vec{I}$ can be written in this case as

$$\vec{I} = 2Y_b \vec{a} \tag{2-38}$$

Now, it can be shown that the submatrices S_{ab} and S_{bb} are given by

$$S_{ab} = 2\,(Y_a + Y_b)^{-1} Y_b \tag{2-39}$$

and

$$S_{bb} = -S_{aa} = (Y_a + Y_b)^{-1}(Y_b - Y_a) \tag{2-40}$$

2.5 Numerical results

We consider the structure shown in Fig. 2-2 where waveguide A has a width w_a = 7.214 cm, with height d = 3.404 cm and cutoff frequency f_c = 2.08 GHz, while waveguide B has a width w_b = 4.50 cm, with the same height as waveguide A and cutoff frequency f'_c = 3.33 GHz = 1.603 f_c. These dimensions and frequencies were selected to permit numerical comparison with published data by others using different methods of solution. The magnitude and phase of S_{aa}, S_{ab}, and S_{ba} are plotted as a function of frequency. Different values of N are considered *e.g.* N = 1,3,5, with N=5 yielding to a satisfactory accuracy. The results are compared with the values calculated by De Smedt *et al* [13] and the range of frequency is extended to 5 GHz. It is seen from Fig. 2-4 that the magnitude of reflection coefficient is unity between 2.6 GHz and 3.33 GHz and the agreement between the two curves is excellent below 3.6 GHz. Fig. 2-5 shows the magnitude of S_{ab} as zero at 3.33 GHz, the cutoff frequency of waveguide B, while the magnitude of S_{ab} and S_{ba} can exceed unity because of the normalization in equation (2-3) [13]. In Fig. 2-7 we present the phase of S_{aa}, S_{ab}, and S_{ba} in degrees, where the phase of S_{aa} and S_{ba} are above zero degrees while the phase of S_{ab} is below zero degrees between 2.6 GHz and 3.4 GHz. The phase of S_{aa}, S_{ab}, and S_{ba} is zero degrees above 3.4 GHz. The impedance mismatch that occurs when

two waveguides are connected together may be represented by the voltage standing wave ratio (VSWR) in the waveguide containing the incident wave [29,40-42], *i.e.*

$$VSWR = \frac{1 + |S_{aa}|}{1 - |S_{aa}|} \tag{2-41}$$

The results are presented at various frequencies in Fig. 2-8.

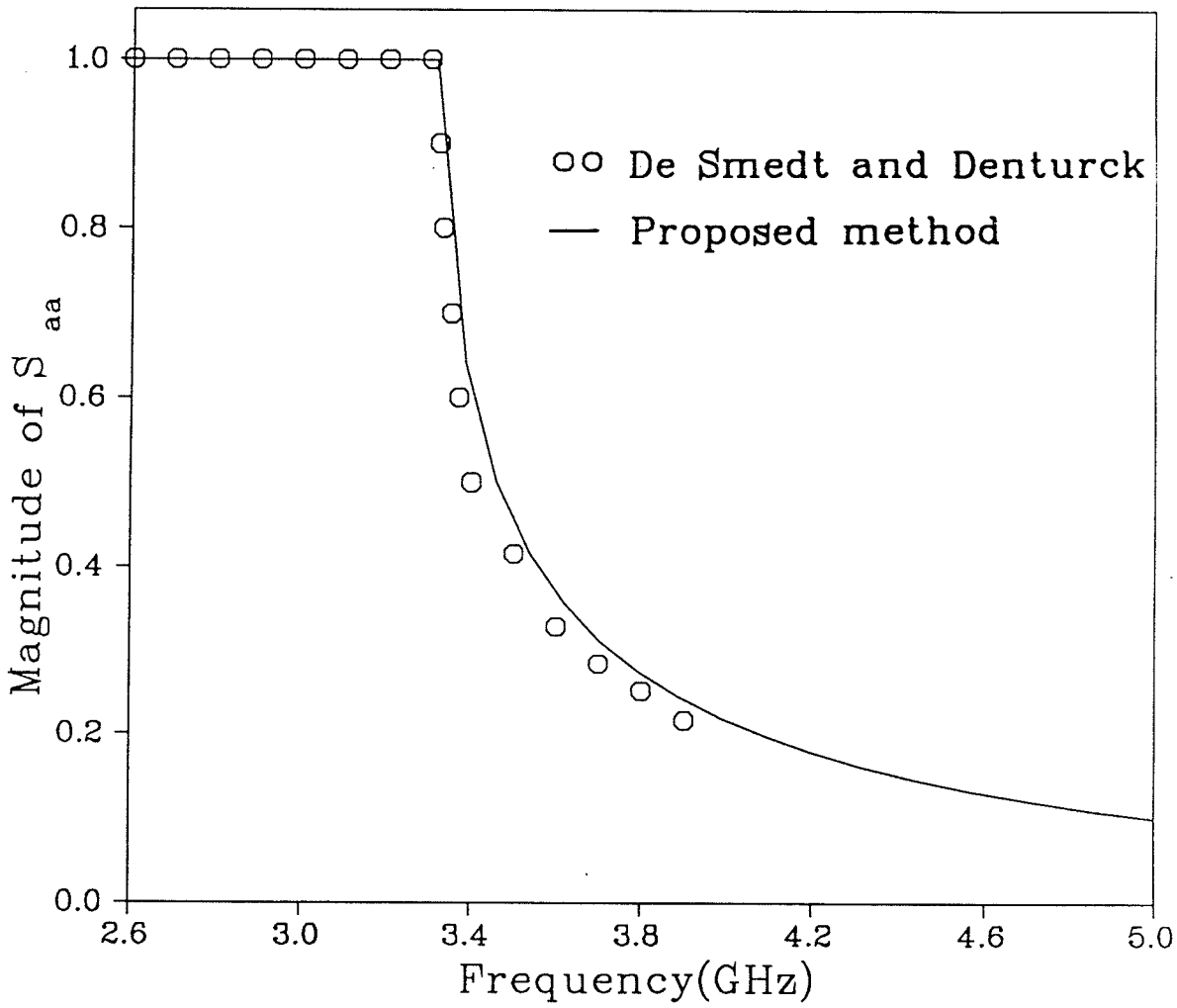

Fig. 2-4: Magnitude of S_{aa} for single step discontinuity.

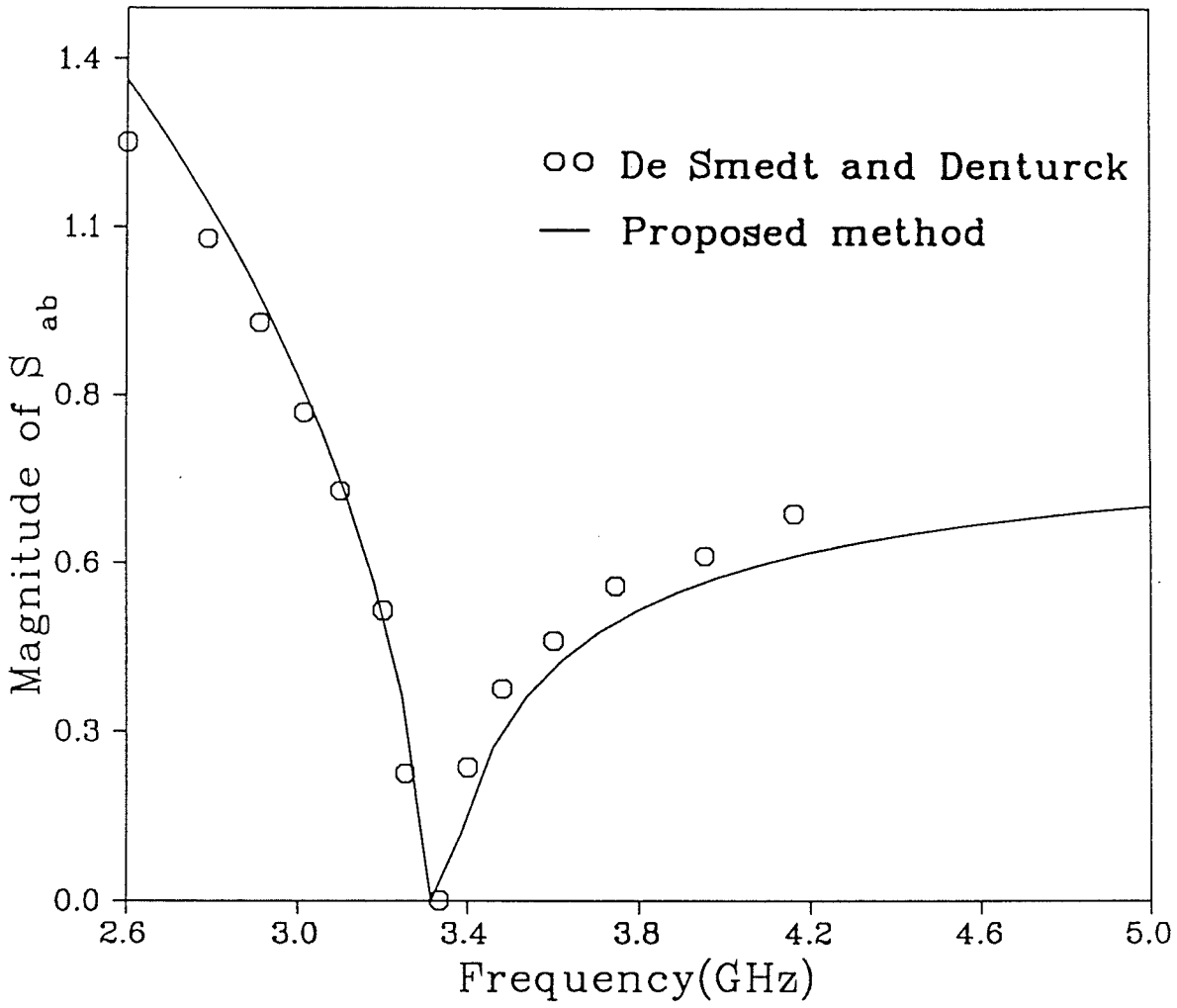

Fig. 2-5: Magnitude of S_{ab} for single step discontinuity.

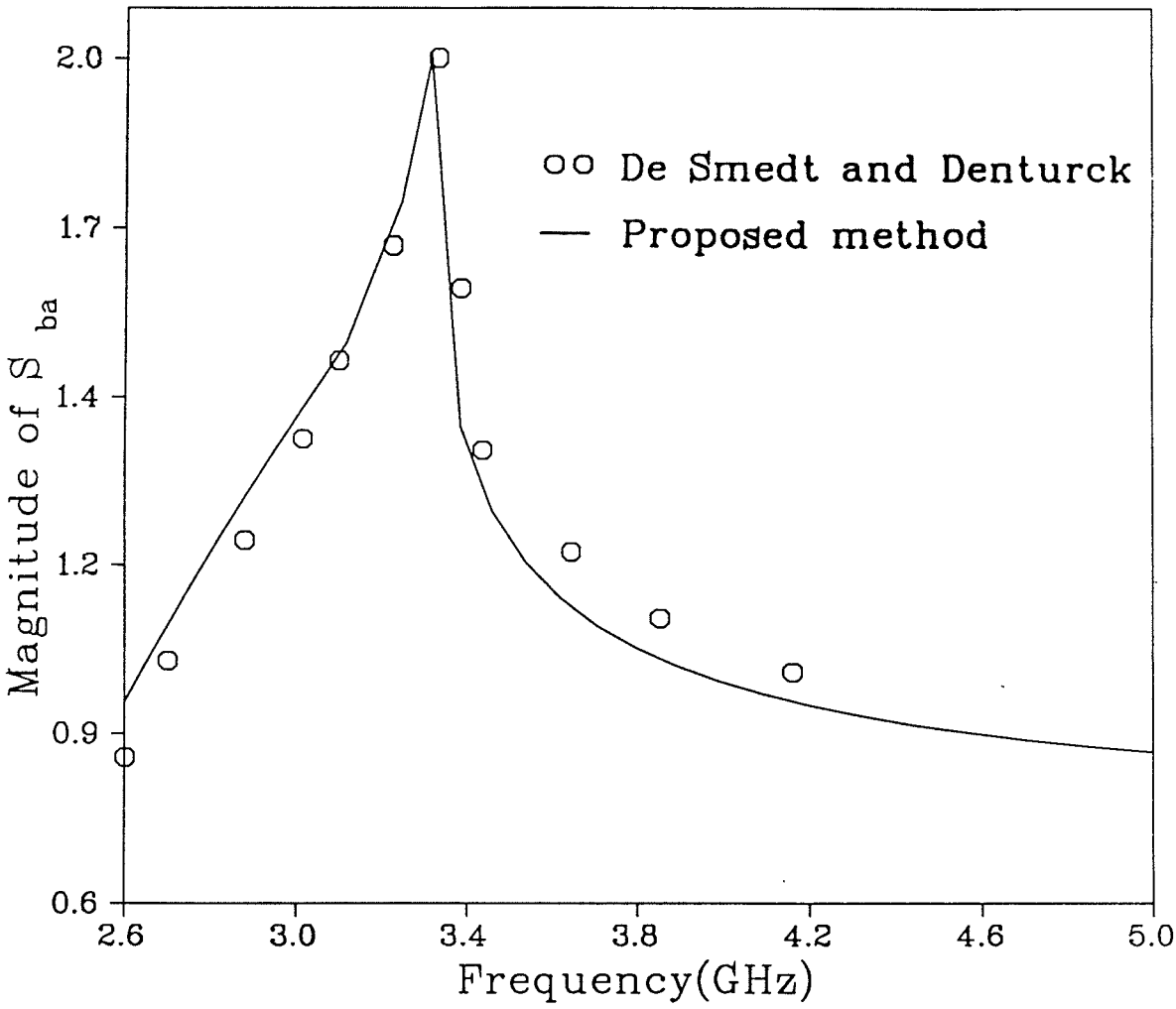

Fig. 2-6: Magnitude of S_{ba} for single step discontinuity.

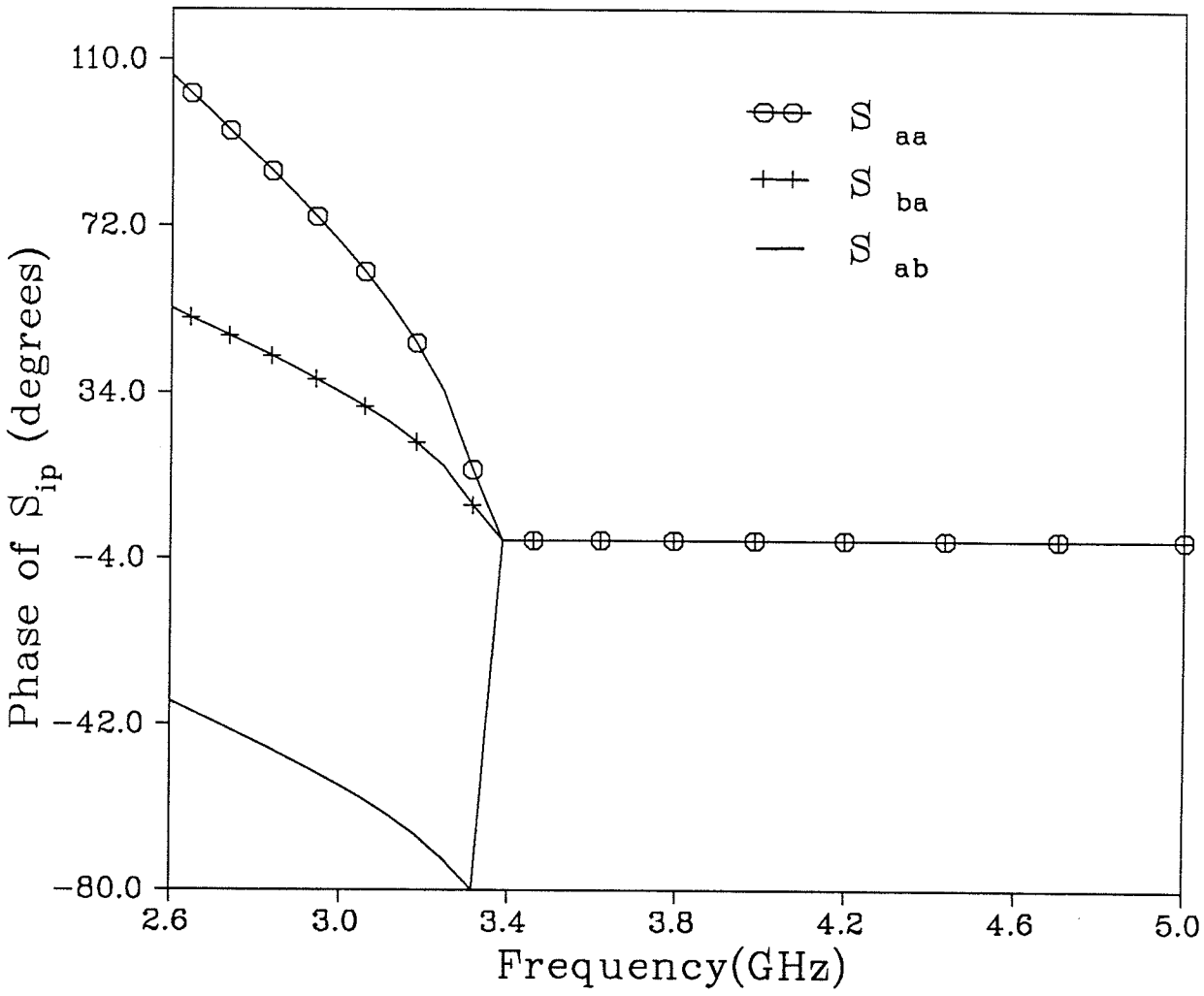

Fig. 2-7: Phases of the scattering matrix elements.

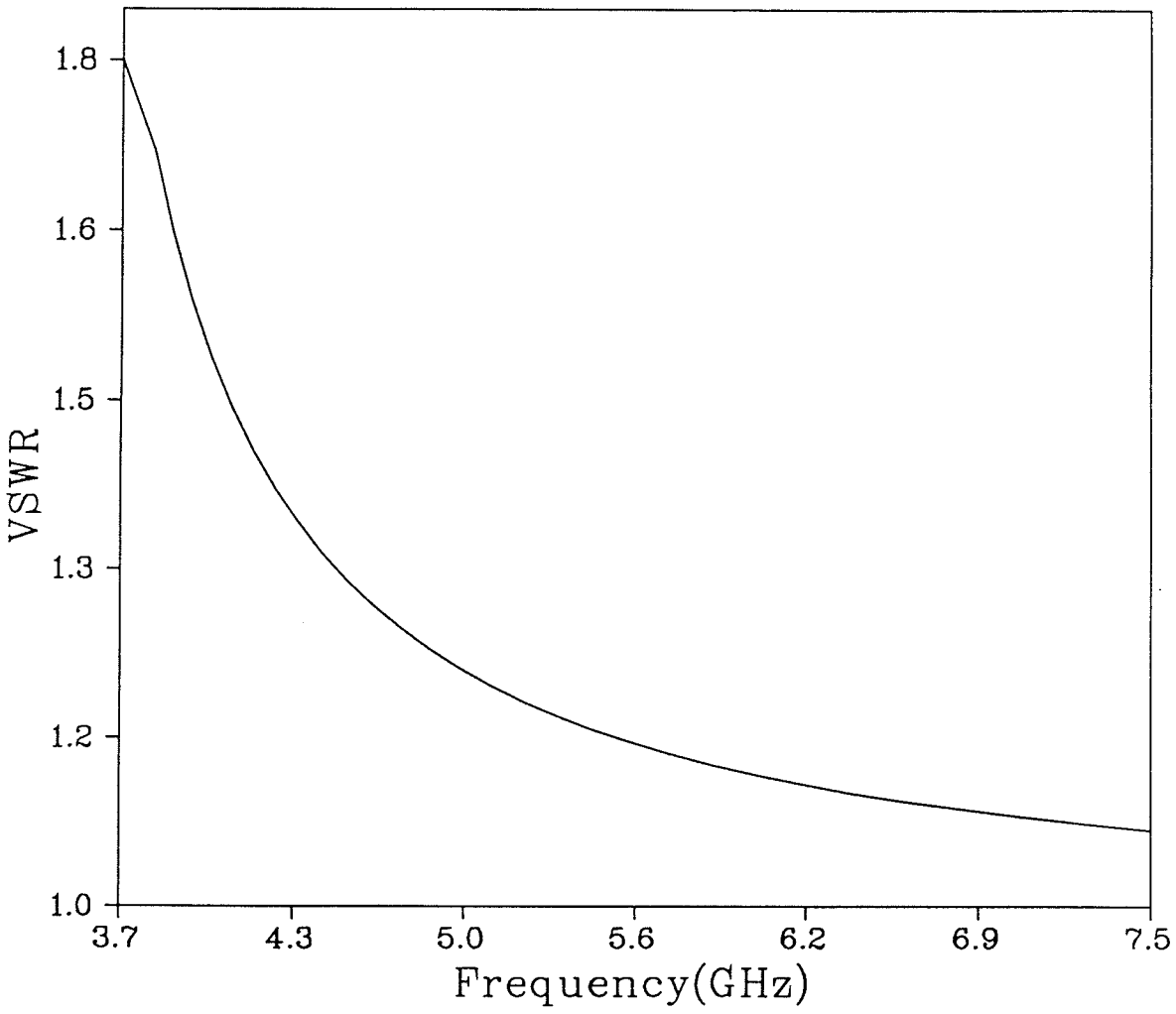

Fig. 2-8: Magnitude of *VSWR* for single step discontinuity.

CHAPTER 3

ANALYSIS OF DOUBLE-STEP DISCONTINUITIES IN RECTANGULAR WAVEGUIDES

In this chapter the problem of double-step discontinuities in rectangular waveguides is discussed. The analysis developed in chapter 2 for the single-step discontinuity (two regions problem) is extended to double-step discontinuities (three regions problem). To accomplish this, the Equivalence Principle is used to replace both faces of each junction by electric walls, each of which carries magnetic current sheets on both sides. The problem is divided into three separate regions which are coupled by the magnetic current sheets. Continuity of the tangential magnetic field components across the two apertures results into two coupled equations involving the unknown magnetic current sheets. These equations are expressed in matrix form using the moment method. The results can be interpreted in terms of the admittance matrices computed separately for each region.

3.1 Formulation

Consider the double-step discontinuities in rectangular waveguides as shown in Fig. 3-1. The problem consists of three regions A, B, and C, respectively, which are separated by two boundaries (junctions faces). The fields transverse to the positive z-direction may be written in modal form as follows [25,31].

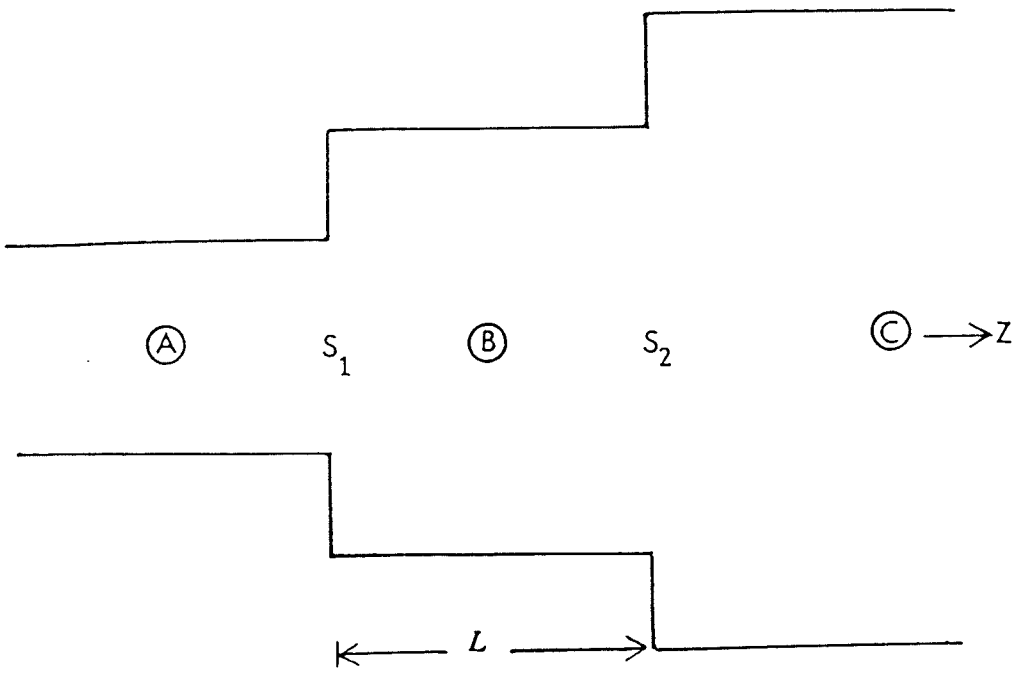

Fig. 3-1: Geometry of general double-step waveguide discontinuities.

In region A

$$E_t = \sum_i (a_i e^{-j\gamma_{ai} z} + d_i e^{j\gamma_{ai} z})\, e_{ai}$$

$$H_t = \sum_i Y_{ai} (a_i e^{-j\gamma_{ai} z} - d_i e^{j\gamma_{ai} z})\, u_z \times e_{ai} \ ; \tag{3-1a}$$

in region B

$$E_t = \sum_i (b_i e^{-j\gamma_{bi} z} + f_i e^{j\gamma_{bi} z})\, e_{bi}$$

$$H_t = \sum_i Y_{bi} (b_i e^{-j\gamma_{bi} z} - f_i e^{j\gamma_{bi} z})\, u_z \times e_{bi} \ , \tag{3-1b}$$

and in region C

$$E_t = \sum_i c_i e^{-j\gamma_{ci} (z-L)} e_{ci}$$

$$H_t = \sum_i c_i Y_{ci} e^{-j\gamma_{ci} (z-L)}\, u_z \times e_{ci} \ . \tag{3-1c}$$

a_i, b_i, and c_i are complex coefficients of the transmitted modes, d_i and f_i are complex coefficients of the reflected modes, γ_{ai}, γ_{bi}, and γ_{ci} are the modal propagation constants, Y_{ai}, Y_{bi}, and Y_{ci} are the modal admittances, and e_{ai}, e_{bi}, and e_{ci} are the modal vectors for the ith mode in regions A,B , and C, respectively.

Using the Equivalence Principle, the fields in the three regions can be modeled in terms of the equivalent magnetic current sheets $M^{(0)}$ and $M^{(L)}$ placed over the apertures S_1 and S_2, respectively, as shown in Fig. 3-2, with

$$M^{(0)} = u_z \times E_t^{(0)} \qquad at\ z = 0 \tag{3-2}$$

$$M^{(L)} = u_z \times E_t^{(L)} \qquad at\ z = L \tag{3-3}$$

where $E_t^{(0)}$ and $E_t^{(L)}$ are the total electric fields in the apertures S_1 and S_2, respectively, which are to be determined later. The field in region A is the incident field plus the field produced by the magnetic sheet $M^{(0)}$, which is identical to (3-1a). The

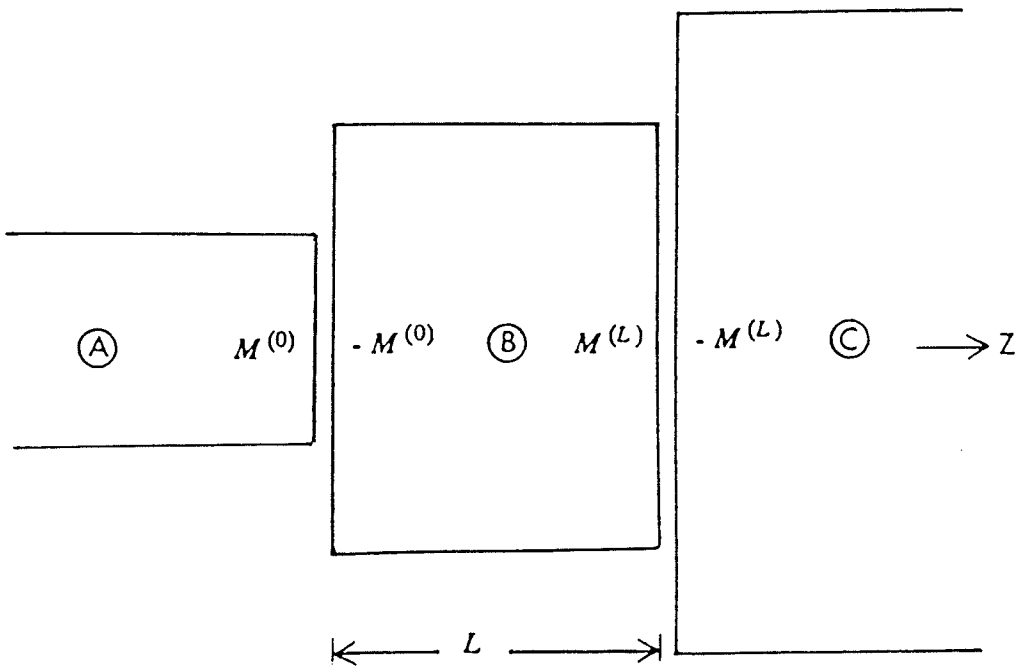

Fig. 3-2: Equivalance for waveguides A,B, and C.

field in region B (resonator box) is the total field produced by the two magnetic current sheets $-M^{(0)}$ and $M^{(L)}$, which is identical to (3-1b). The field in region C is the field produced by the magnetic current sheet $-M^{(L)}$, which is identical to (3-1c).

In order to determine the unknown expansion coefficients, we apply the proper boundary conditions at the various junctions. Thus the continuity of the tangential electric field components across the apertures S_1 and S_2 requires that

$$\sum_i a_i \; u_z \times e_{ai} + \sum_i d_i \; u_z \times e_{ai} = M^{(0)}$$

$$= \sum_i b_i \; u_z \times e_{bi} + \sum_i f_i \; u_z \times e_{bi} \qquad at \; z = 0 \qquad (3\text{-}4)$$

and

$$\sum_i b_i e^{-j\gamma_{bi} L} \; u_z \times e_{bi} + \sum_i f_i e^{j\gamma_{bi} L} \; u_z \times e_{bi} = M^{(L)}$$

$$= \sum_i c_i \; u_z \times e_{ci} \qquad at \; z = L \qquad (3\text{-}5)$$

Also the continuity of the tangential magnetic field components across the apertures S_1 and S_2 requires that

$$\sum_i a_i Y_{ai} u_z \times e_{ai} - \sum_i d_i Y_{ai} u_z \times e_{ai} =$$

$$\sum_i b_i Y_{bi} u_z \times e_{bi} - \sum_i f_i Y_{bi} u_z \times e_{bi} \qquad at \; z = 0 \qquad (3\text{-}6)$$

and

$$\sum_i b_i Y_{bi} e^{-j\gamma_{bi} L} u_z \times e_{bi} - \sum_i f_i Y_{bi} e^{j\gamma_{bi} L} u_z \times e_{bi} =$$

$$\sum_i c_i Y_{ci} u_z \times e_{ci} \qquad at \; z = L \qquad (3\text{-}7)$$

Since in general it is not possible to obtain closed form solutions for the unknowns in equations (3–4) through (3–7), we apply the moment method.

3.2 Moment method solution

To apply the moment method, we expand the magnetic current sheets $M^{(0)}$ and $M^{(L)}$ as

$$M^{(0)} = \sum_{p=1}^{Q_1} V_p^{(0)} M_p^{(0)} \qquad at\ S_1 \tag{3-8}$$

and

$$M^{(L)} = \sum_{p=1}^{Q_2} V_p^{(L)} M_p^{(L)} \qquad at\ S_2 \tag{3-9}$$

where $V_p^{(0)}$ and $V_p^{(L)}$ are unknown complex coefficients to be evaluated, $M_p^{(0)}$ and $M_p^{(L)}$ are known vector basis functions. The above summations are limited to a finite number of terms Q_1 and Q_2. By substituting (3-8) and (3-9) into (3-4) and (3-5), we obtain

$$\sum_{i=1}^{N_1} a_i\ u_z \times e_{ai} + \sum_{i=1}^{N_1} d_i\ u_z \times e_{ai} = \sum_{p=1}^{Q_1} V_p^{(0)} M_p^{(0)} \tag{3-10}$$

$$\sum_{i=1}^{N_1} b_i\ u_z \times e_{bi} + \sum_{i=1}^{N_1} f_i\ u_z \times e_{bi} = \sum_{p=1}^{Q_1} V_p^{(0)} M_p^{(0)} \tag{3-11}$$

$$\sum_{i=1}^{N_2} b_i e^{-j\gamma_{bi} L}\ u_z \times e_{bi} + \sum_{i=1}^{N_2} f_i e^{j\gamma_{bi} L}\ u_z \times e_{bi} = \sum_{p=1}^{Q_2} V_p^{(L)} M_p^{(L)} \tag{3-12}$$

$$\sum_{i=1}^{N_2} c_i\ u_z \times e_{ci} = \sum_{p=1}^{Q_2} V_p^{(L)} M_p^{(L)} \tag{3-13}$$

The summations on the left hand sides of the above equations may be truncated to a finite numbers of modes N_1 and N_2. Next, multiplying equations (3-10) by $u_z \times e_{ak}$, (3-11) and (3-12) by $u_z \times e_{bk}$, and (3-13) by $u_z \times e_{ck}$, and integrating over the corresponding apertures S_1 and S_2, respectively, we obtain

$$\sum_{i=1}^{N_1} a_i \int_{S_1} u_z \times e_{ai} \cdot u_z \times e_{ak}\, ds_1 + \sum_{i=1}^{N_1} d_i \int_{S_1} u_z \times e_{ai} \cdot u_z \times e_{ak}\, ds_1 =$$

$$\sum_{p=1}^{Q_1} V_p^{(0)} \int_{S_1} M_p^{(0)} \cdot u_z \times e_{ak}\, ds_1 \tag{3-14}$$

$$\sum_{i=1}^{N_1} b_i \int_{S_1} u_z \times e_{bi} \cdot u_z \times e_{bk}\, ds_1 + \sum_{i=1}^{N_1} f_i \int_{S_1} u_z \times e_{bi} \cdot u_z \times e_{bk}\, ds_1 =$$

$$\sum_{p=1}^{Q_1} V_p^{(0)} \int_{S_1} M_p^{(0)} \cdot u_z \times e_{bk}\, ds_1 \tag{3-15}$$

$$\sum_{i=1}^{N_2} b_i e^{-j\gamma_{bi} L} \int_{S_2} u_z \times e_{bi} \cdot u_z \times e_{bk}\, ds_2 + \sum_{i=1}^{N_2} f_i e^{j\gamma_{bi} L} \int_{S_2} u_z \times e_{bi} \cdot u_z \times e_{bk}\, ds_2 =$$

$$\sum_{p=1}^{Q_2} V_p^{(L)} \int_{S_2} M_p^{(L)} \cdot u_z \times e_{bk}\, ds_2 \tag{3-16}$$

and

$$\sum_{i=1}^{N_2} c_i \int_{S_2} u_z \times e_{ci} \cdot u_z \times e_{ck}\, ds_2 = \sum_{p=1}^{Q_2} V_p^{(L)} \int_{S_2} M_p^{(L)} \cdot u_z \times e_{ck}\, ds_2 \tag{3-17}$$

Because of the orthogonality condition for the mode functions in each region (2-3), all the terms in the summations on the left hand side are equal to zero except for the i = k term. This leads to

$$a_i + d_i = \sum_{p=1}^{Q_1} V_p^{(0)}\, h_{aip}^{(0)} \tag{3-18}$$

$$b_i + f_i = \sum_{p=1}^{Q_1} V_p^{(0)}\, h_{bip}^{(0)} \tag{3-19}$$

$$b_i e^{-j\gamma_{bi} L} + f_i e^{j\gamma_{bi} L} = \sum_{p=1}^{Q_2} V_p^{(L)}\, h_{bip}^{(L)} \tag{3-20}$$

$$c_i = \sum_{p=1}^{Q_2} V_p^{(L)}\, h_{cip}^{(L)} \tag{3-21}$$

where

$$h_{aip}^{(0)} = \int_{S_1} M_p^{(0)} \cdot u_z \times e_{ai}\, ds_1 \tag{3-22}$$

$$h_{bip}^{(0)} = \int_{S_1} M_p^{(0)} \cdot u_z \times e_{bi}\, ds_1 \tag{3-23}$$

$$h_{bip}^{(L)} = \int_{S_2} M_p^{(L)} \cdot u_z \times e_{bi}\, ds_2 \tag{3-24}$$

$$h_{cip}^{(L)} = \int_{S_2} M_p^{(L)} \cdot u_z \times e_{ci}\, ds_2 \tag{3-25}$$

Solving for b_i and f_i from (3–19) and (3–20), and applying a simple elimination procedure yields

$$b_i = \frac{-j}{2 \sin(\gamma_{bi} L)} \left[e^{j\gamma_{bi} L} \sum_{p=1}^{Q_1} V_p^{(0)} h_{bip}^{(0)} - \sum_{p=1}^{Q_2} V_p^{(L)} h_{bip}^{(L)} \right] \tag{3-26}$$

$$f_i = \frac{-j}{2 \sin(\gamma_{bi} L)} \left[\sum_{p=1}^{Q_2} V_p^{(L)} h_{bip}^{(L)} - e^{-j\gamma_{bi} L} \sum_{p=1}^{Q_1} V_p^{(0)} h_{bip}^{(0)} \right] \tag{3-27}$$

Next, taking the inner product (as defined in (2-16)) of (3-6) and (3-7) with the testing functions $W_k^{(0)}$ and $W_k^{(L)}$, respectively, we obtain

$$\sum_{i=1}^{N_1} a_i Y_{ai} \int_{S_1} W_k^{(0)} \cdot u_z \times e_{ai}\, ds_1 = \sum_{i=1}^{N_1} \left[\sum_{p=1}^{Q_1} V_p^{(0)} h_{aip}^{(0)} - a_i \right] Y_{ai} \int_{S_1} W_k^{(0)} \cdot u_z \times e_{ai}\, ds_1 +$$

$$\sum_{i=1}^{N_1} \frac{-jY_{bi}}{2\sin(\gamma_{bi} L)} \left[e^{j\gamma_{bi} L} \sum_{p=1}^{Q_1} V_p^{(0)} h_{bip}^{(0)} - \sum_{p=1}^{Q_2} V_p^{(L)} h_{bip}^{(L)} \right] \int_{S_1} W_k^{(0)} \cdot u_z \times e_{bi}\, ds_1 +$$

$$\sum_{i=1}^{N_1} \frac{jY_{bi}}{2\sin(\gamma_{bi} L)} \left[\sum_{p=1}^{Q_2} V_p^{(L)} h_{bip}^{(L)} - e^{-j\gamma_{bi} L} \sum_{p=1}^{Q_1} V_p^{(0)} h_{bip}^{(0)} \right] \int_{S_1} W_k^{(0)} \cdot u_z \times e_{bi}\, ds_1 \tag{3-28}$$

and

$$\sum_{i=1}^{N_2} \frac{-jY_{bi} e^{-j\gamma_{bi} L}}{2\sin(\gamma_{bi} L)} \left[e^{\gamma_{bi} L} \sum_{p=1}^{Q_1} V_p^{(0)} h_{bip}^{(0)} - \sum_{p=1}^{Q_2} V_p^{(L)} h_{bip}^{(L)} \right] \int_{S_2} W_k^{(L)} \cdot u_z \times e_{bi}\, ds_2 +$$

$$\sum_{i=1}^{N_2} \frac{jY_{bi}\, e^{j\gamma_{bi} L}}{2\sin(\gamma_{bi} L)} \left[\sum_{p=1}^{Q_2} V_p^{(L)} h_{bip}^{(L)} - e^{-j\gamma_{bi} L} \sum_{p=1}^{Q_1} V_p^{(0)} h_{bip}^{(0)} \right] \int_{S_2} W_k^{(L)} \cdot u_z \times e_{bi}\, ds_2 =$$

$$\sum_{i=1}^{N_2} \left[\sum_{p=1}^{Q_2} V_p^{(L)} h_{cip} \right] Y_{ci} \int_{S_2} W_k^{(L)} \cdot u_z \times e_{ci}\, ds_2 \qquad (3\text{-}29)$$

The above set of coupled integral equations can be expressed in the simplified forms

$$2\sum_{i=1}^{N_1} a_i Y_{ai} W_{aik}^{(0)} = \sum_{i=1}^{N_1} \left[\sum_{p=1}^{Q_1} V_p^{(0)} h_{aip}^{(0)} \right] Y_{ai} W_{aik}^{(0)} + \sum_{i=1}^{N_1} \frac{-jY_{bi}}{\sin(\gamma_{bi} L)}$$

$$\left[\cos(\gamma_{bi} L) \sum_{p=1}^{Q_1} V_p^{(0)} h_{bip}^{(0)} - \sum_{p=1}^{Q_2} V_p^{(L)} h_{bip}^{(L)} \right] W_{bik}^{(0)} \qquad (k = 1,2,\ldots,Q_1) \qquad (3\text{-}30)$$

and

$$\sum_{i=1}^{N_2} \frac{-jY_{bi}}{\sin(\gamma_{bi} L)} \left[\sum_{p=1}^{Q_1} V_p^{(0)} h_{bip}^{(0)} - \cos(\gamma_{bi} L) \sum_{p=1}^{Q_2} V_p^{(L)} h_{bip}^{(L)} \right] W_{bik}^{(L)} =$$

$$\sum_{i=1}^{N_2} \left[\sum_{p=1}^{Q_2} V_p^{(L)} h_{cip}^{(L)} \right] Y_{ci} W_{cik}^{(L)} \qquad (k = 1,2,\ldots,Q_2) \qquad (3\text{-}31)$$

where

$$W_{aik}^{(0)} = \int_{S_1} W_k^{(0)} \cdot u_z \times e_{ai}\, ds_1 \qquad (3\text{-}32)$$

$$W_{bik}^{(0)} = \int_{S_1} W_k^{(0)} \cdot u_z \times e_{bi}\, ds_1 \qquad (3\text{-}33)$$

$$W_{bik}^{(L)} = \int_{S_2} W_k^{(L)} \cdot u_z \times e_{bi}\, ds_2 \qquad (3\text{-}34)$$

$$W_{cik}^{(L)} = \int_{S_2} W_k^{(L)} \cdot u_z \times e_{ci}\, ds_2 \qquad (3\text{-}35)$$

The above equations can be written in matrix form [43,44] as

$$\vec{I} = \left[\overline{Y}_a - j\cot(\gamma_{bi} L)\, \overline{Y}_b^{11} \right] \vec{V}^{(0)} + \left[\frac{j}{\sin(\gamma_{bi} L)} \overline{Y}_b^{12} \right] \vec{V}^{(L)} \qquad (3\text{-}36)$$

$$\vec{O} = \left[\frac{j}{\sin(\gamma_{bi} L)} \bar{Y}_b^{21} \right] \vec{V}^{(0)} + \left[-jcot(\gamma_{bi} L) \bar{Y}_b^{22} + \bar{Y}_c \right] \vec{V}^{(L)} \tag{3-37}$$

where $\vec{O}$ is the null matrix and

$$\vec{I} = 2W_a^{(0)T} Y_a \vec{a} \tag{3-38}$$

$$\bar{Y}_a = W_a^{(0)T} Y_a H_a^{(0)} \tag{3-39}$$

$$\bar{Y}_b^{11} = W_b^{(0)T} Y_b H_b^{(0)} \tag{3-40}$$

$$\bar{Y}_b^{12} = W_b^{(0)T} Y_b H_b^{(L)} \tag{3-41}$$

$$\bar{Y}_b^{21} = W_b^{(L)T} Y_b H_b^{(0)} \tag{3-42}$$

$$\bar{Y}_b^{22} = W_b^{(L)T} Y_b H_b^{(L)} \tag{3-43}$$

$$\bar{Y}_c = W_c^{(L)T} Y_c H_c^{(L)} \tag{3-44}$$

$$H_r^{(0)} = [h_{rip}^{(0)}]_{N_1 \times Q_1} \qquad (r = a, b) \tag{3-45}$$

$$H_r^{(L)} = [h_{rip}^{(L)}]_{N_2 \times Q_2} \qquad (r = b, c) \tag{3-46}$$

with Y_a, Y_b, and Y_c being the diagonal matrices of the modal admittances in the corresponding regions A, B, and C, respectively. Equations (3-36) and (3-37) are $(Q_1 + Q_2) \times (Q_1 + Q_2)$ coupled sets of complex equations which suggest the generalized network representation as shown in Fig. 3-3, and should be solved simultaneously in order to yield the unknown coefficient matrices $\vec{V}^{(0)}$ and $\vec{V}^{(L)}$, respectively. The system of matrices in equations (3-36) and (3-37) are composed of an admittance matrix $\bar{Y}_a$ of region A and an admittance matrix $\bar{Y}_c$ of region C which are coupled by the coupling matrix $\bar{Y}_b$, where

$$\bar{Y}_b = \begin{bmatrix} \bar{Y}_b^{11} & \bar{Y}_b^{12} \\ \bar{Y}_b^{21} & \bar{Y}_b^{22} \end{bmatrix} \tag{3-47}$$

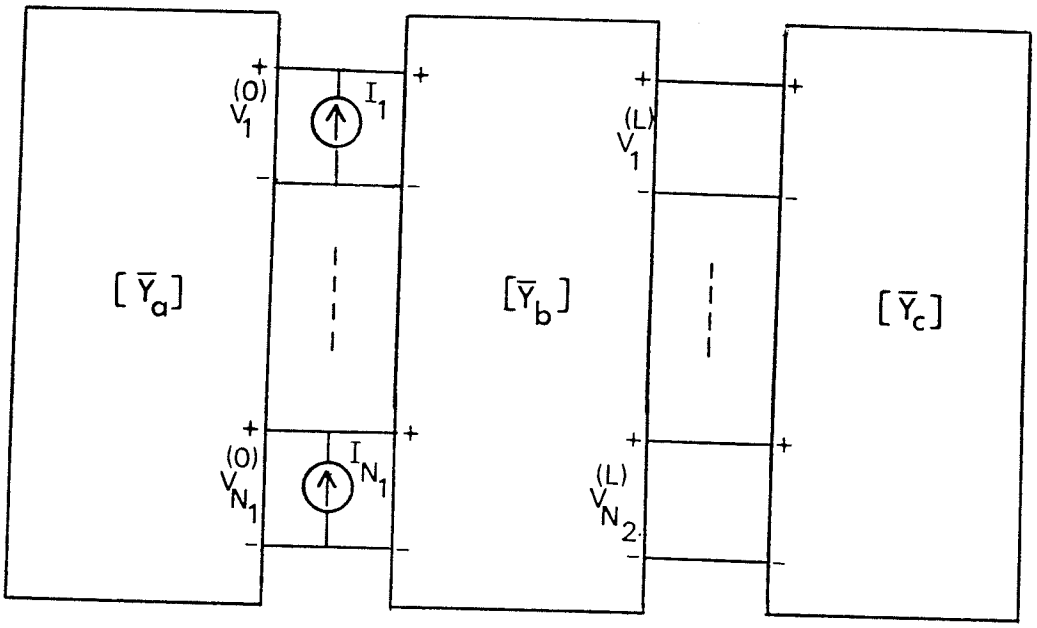

Fig. 3-3: The generalized network presentation of equations (3-36) and (3-37).

3.3 Galerkin's method solution

For the special case of a symmetric double step discontinuity (waveguides A and C have the same cross section), we let

$$M_p^{(0)} = M_p^{(L)} = W_p^{(0)} = W_p^{(L)} = u_z \times e_{ap} \qquad (p = 1,2,...,Q) \tag{3-48}$$

Also, we set $Q_1 = Q_2 = N_1 = N_2 = N$ and $e_{ap} = e_{bp}$. This leads to

$$H_a^{(0)} = H_b^{(0)} = H_b^{(L)} = H_c^{(L)} = U \tag{3-49}$$

$$W_a^{(0)} = W_b^{(0)} = W_b^{(L)} = W_c^{(L)} = U \tag{3-50}$$

where U is the identity matrix. Therefore, equations (3-38) through (3-44) reduce to

$$\vec{I} = 2Y_a \vec{a} \tag{3-51}$$

$$\overline{Y}_a = Y_a \tag{3-52}$$

$$\overline{Y}_b^{11} = \overline{Y}_b^{12} = \overline{Y}_b^{21} = \overline{Y}_b^{22} = Y_b \tag{3-53}$$

$$\overline{Y}_c = Y_c \tag{3-54}$$

By substituting (3-51) through (3-54) into (3-36) and (3-37), we obtain

$$\vec{I} = \left[Y_a - jcot\ (\gamma_{bi}\ L)\ Y_b \right] \vec{V}^{(0)} + \left[\frac{j}{\sin\ (\gamma_{bi}\ L)} Y_b \right] \vec{V}^{(L)} \tag{3-55}$$

$$\vec{O} = \left[\frac{j}{\sin\ (\gamma_{bi}\ L)}\ Y_b \right] \vec{V}^{(0)} + \left[-jcot\ (\gamma_{bi}\ L) Y_b + Y_c \right] \vec{V}^{(L)} \tag{3-56}$$

Adding (3-55) to (3-56), we obtain

$$\vec{I} = \left[Y_a + j \tan\ (\frac{\gamma_{bi}\ L}{2}) Y_b \right] \left[\vec{V}^{(0)} + \vec{V}^{(L)} \right] \tag{3-57}$$

Similarly, subtracting (3-56) from (3-55), we obtain

$$\vec{I} = \left[Y_a - jcot\ (\frac{\gamma_{bi}\ L}{2}) Y_b \right] \left[\vec{V}^{(0)} - \vec{V}^{(L)} \right] \tag{3-58}$$

Equations (3-57) and (3-58) represent in matrix form a decoupled system of $(2N \times 2N)$

linear equations. Its solution provides through equations (3-18)-(3-21) the solution for the fields in equations (3-1).

3.4 Numerical results

We consider the structure shown in Fig. 3-4 where waveguides A and C have width w_a = 7.214 cm, and height d = 3.40 cm, while waveguide B has width w_b = 4.50 cm and the same height as waveguide A. The separation between the junctions for the first case is taken to be L = 7.98 cm. To obtain the electric field distribution at the junctions, the sum of the solutions of equations (3-56) and (3-57) yields twice the electric field distribution at z = 0, while their difference yields the electric field distribution at $z = L$. For computation of the field coefficients, different values of N are considered *e.g.* N = 5,7,9,11,13, with N = 15, the field coefficient has a magnitude less than 0.5 percent of that of the first coefficient with N = 1.

In Fig. 3-5 we have plotted the magnitude of the field coefficients $V_1^{(0)}$ and $V_1^{(L)}$ as a function of frequency. The value of $V_1^{(0)}$ varies between 1.8 at f = 3.35 GHz and 1.0 at f = 3.75 and 5.0 GHz, respectively, while the value of $V_1^{(L)}$ is unity between f = 3.75 and 5.0 GHz. Fig. 3-6 shows the phase of $V_1^{(0)}$ and $V_1^{(L)}$; they differ by 32 degrees at f = 2.6 GHz, but they are almost equal at 3.8 GHz. On the other hand, there is a sudden change in phase for both coefficients at 3.8 GHz. In Fig. 3-7 we have plotted the magnitude of the field coefficient $V_1^{(0)}$ versus frequency with L (length of the smaller waveguide) as a parameter. It can be seen that by decreasing the value of L the magnitude of $V_1^{(0)}$ decreases as well. For example, the value of $V_1^{(0)}$ drops from 1.65 to 1.06 as the length decreases from 4 cm to 1 cm at f = 3.4 GHz, while Fig. 3-8 shows that the magnitude of $V_1^{(L)}$ increases from 0.38 to 0.88 at f = 2.8 GHz. In Figs.

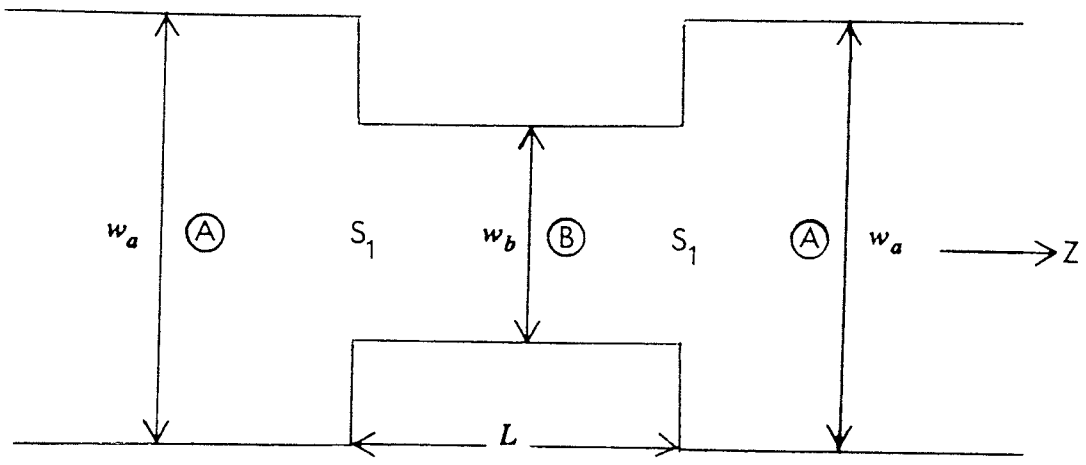

Fig. 3-4: **Geometry of symmetric double-step waveguide discontinuities.**

3-9 and 3-10 we plot the phases of the field coefficients, where the phase of $V_1^{(0)}$ varies between -50 and 50 degrees while the phase of $V_1^{(L)}$ remains negative. Again this is obtained by decreasing the value of L from 4 cm to 1 cm. Tables 3-1 and 3-2 present the field coefficients of a symmetric double-step discontinuity computed as a function of the separation length L, the value of the field coefficient $V_1^{(0)}$ varies between 1.0 and 1.96 while the value of $V_1^{(L)}$ slightly change by increasing the length L at 5 GHz. At higher frequencies, namely f = 10 GHz, the field coefficients remain approximately constant for the same variation of L.

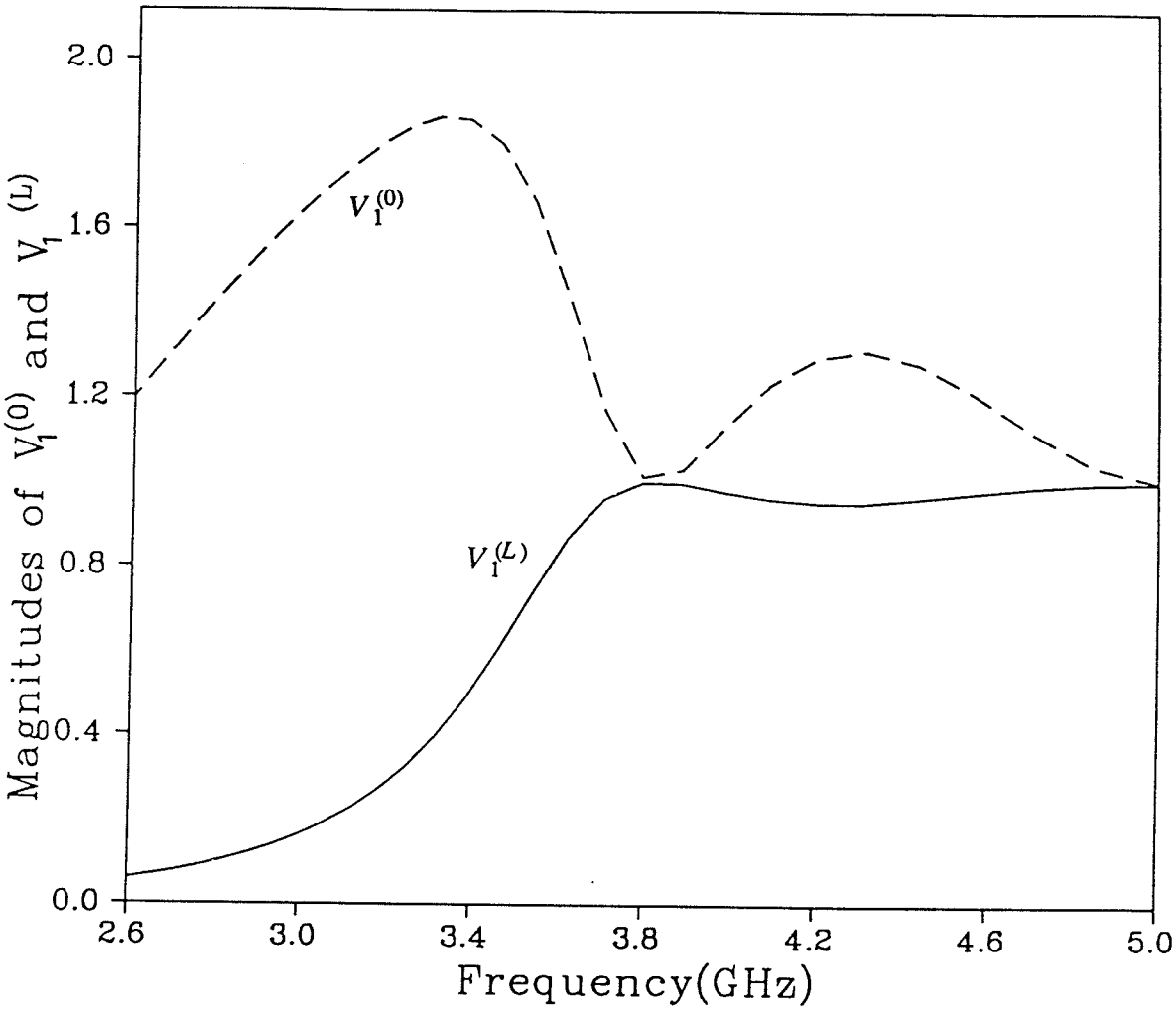

Fig. 3-5: Magnitude of field coefficients for double-step with L = 7.98 cm.

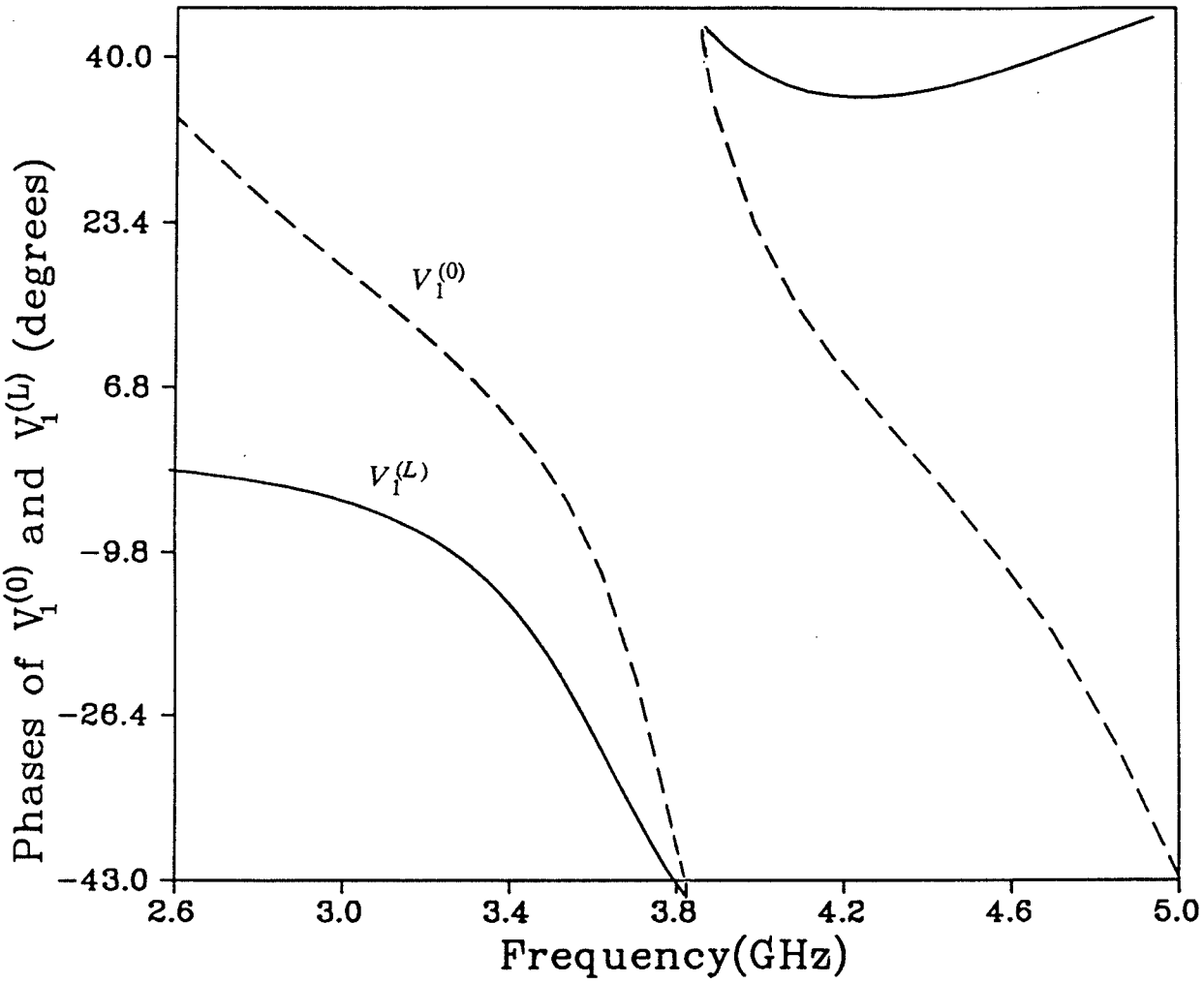

Fig. 3-6: Phase of field coefficients for double-step with L = 7.98 cm.

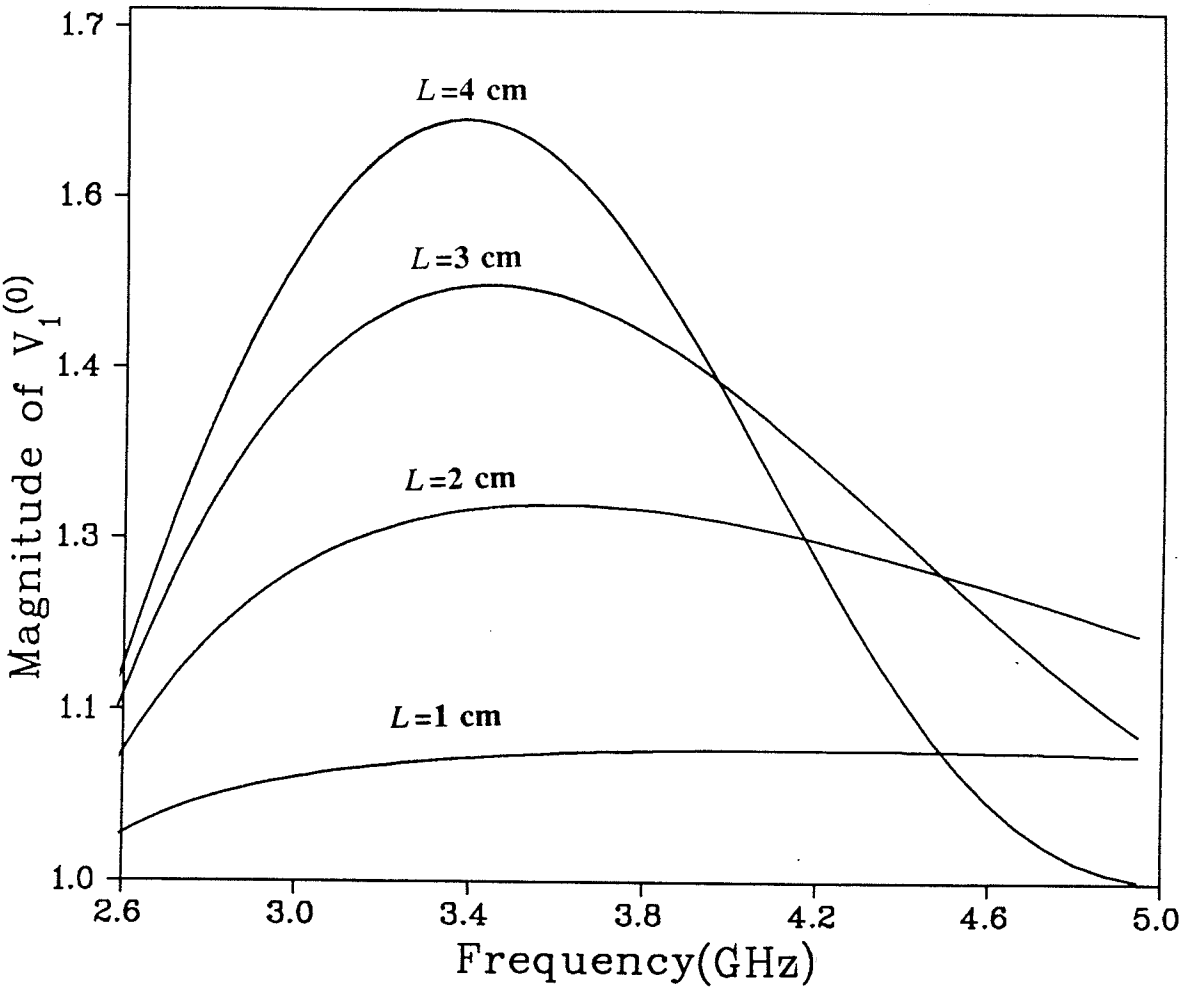

Fig. 3-7: Magnitude of $V_1^{(0)}$ with L as a parameter.

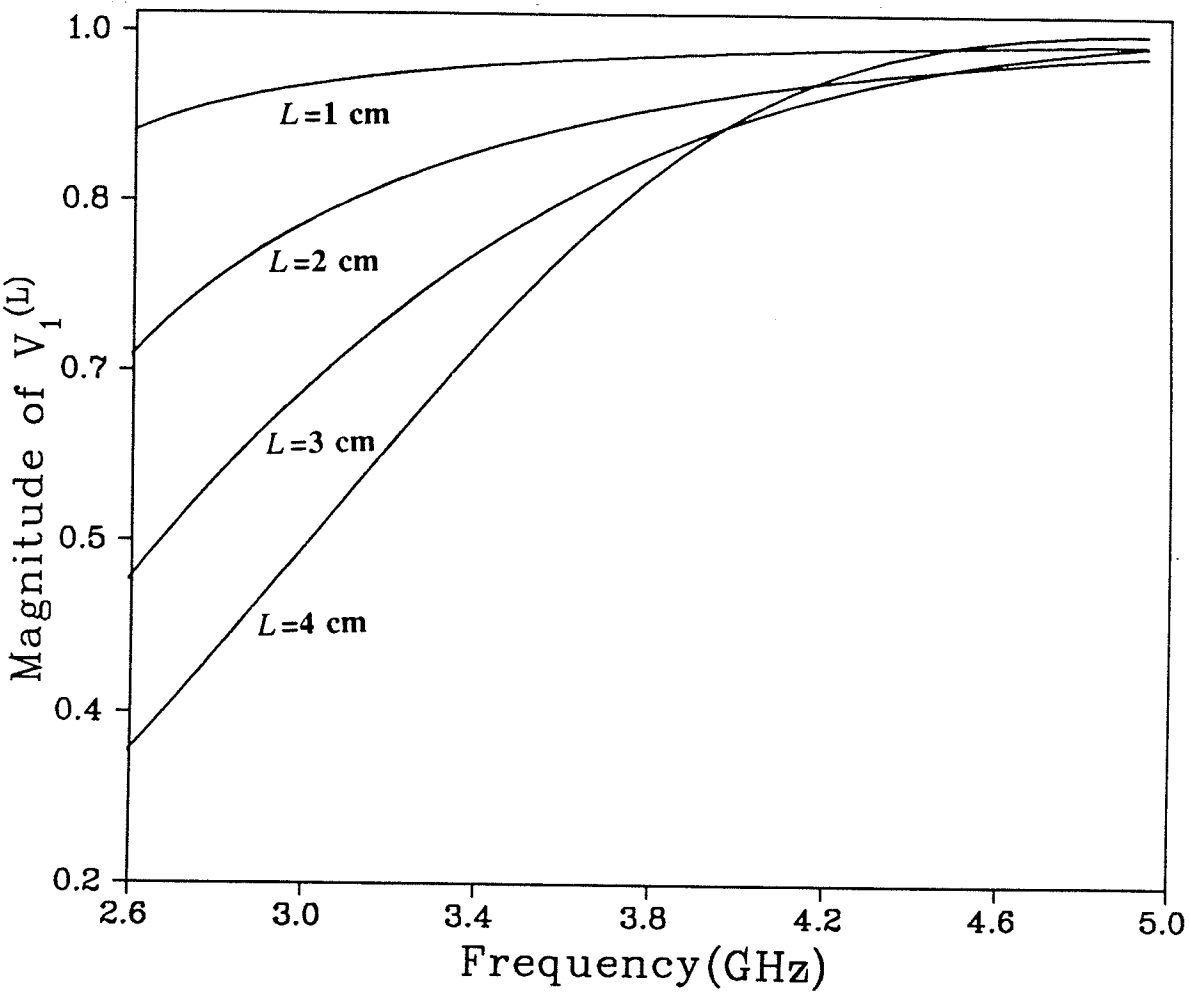

Fig. 3-8: Magnitude of $V_1^{(L)}$ with L as a parameter.

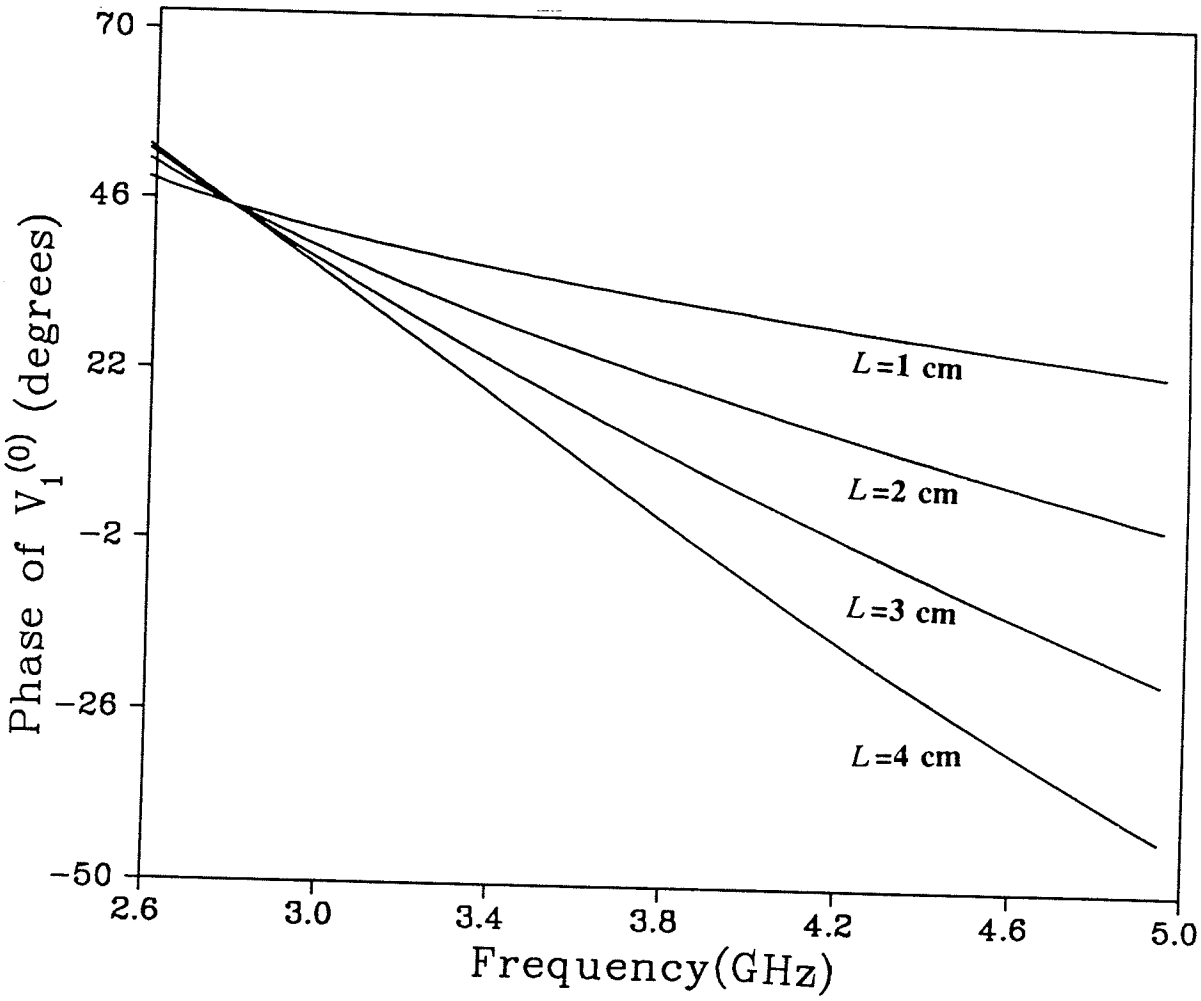

Fig. 3-9: Phase of $V_1^{(0)}$ with L as a parameter.

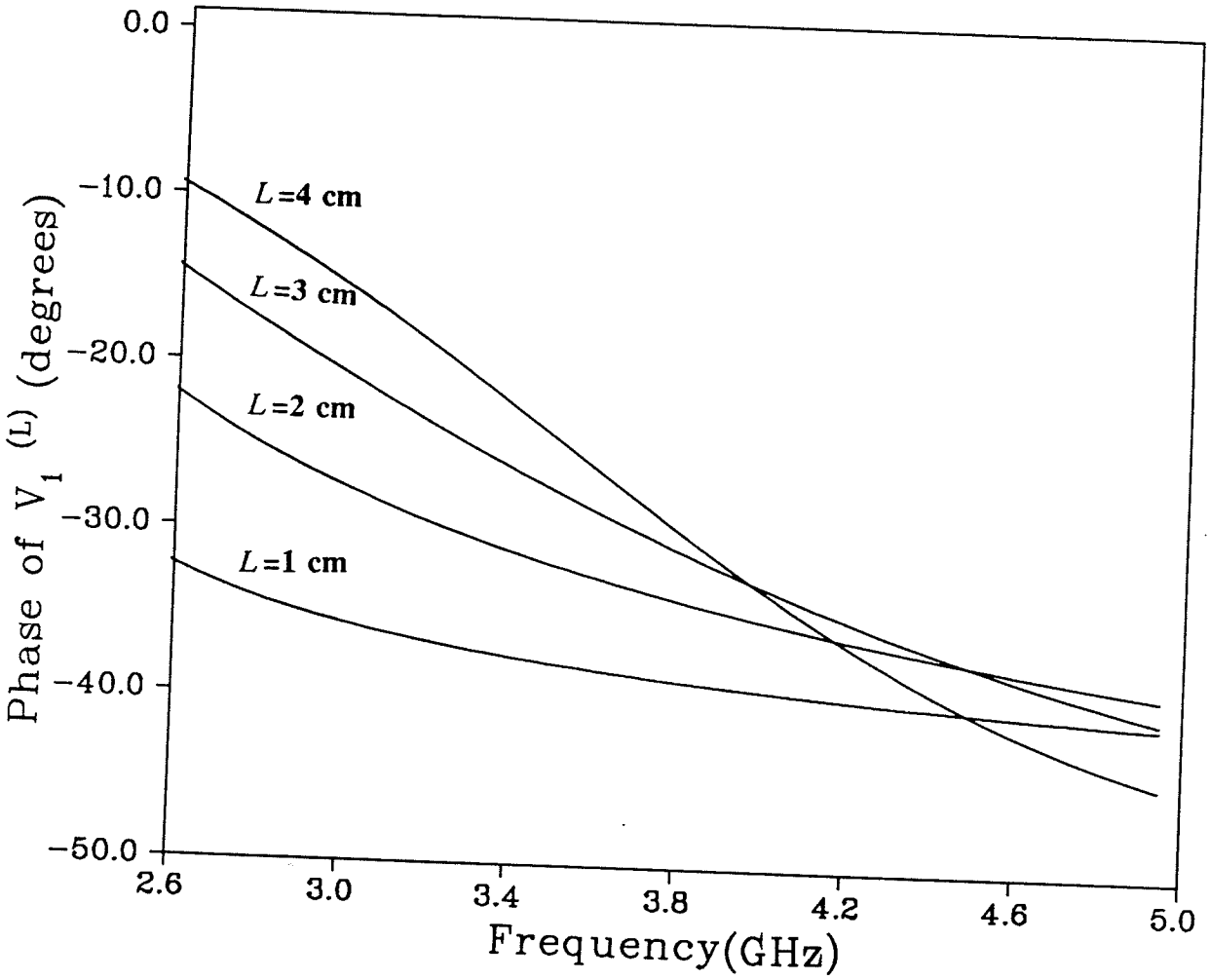

Fig. 3-10: Phase of $V_1^{(L)}$ with L as a parameter.

Table 3-1. Field coefficients as a function of separation length for w_b/w_a = 0.624, f = 5 GHz.

	Magnitude		Phase (degrees)	
Separation, L (cm)	$V_1^{(0)}$	$V_1^{(L)}$	$V_1^{(0)}$	$V_1^{(L)}$
1	1.103	0.990	17.660	27.229
2	1.196	0.980	0.196	22.284
3	1.107	0.989	-17.138	26.968
4	1.000	0.999	-44.206	44.434
5	1.099	0.991	18.190	-27.500
6	1.195	0.980	0.586	-22.289
7	1.111	0.989	-16.622	-26.714
8	1.000	0.999	-43.412	-43.869
9	1.095	0.990	18.726	27.779
10	1.195	0.980	0.978	22.300
11	1.115	0.989	-16.114	26.469
12	1.000	0.999	-42.620	43.305
13	1.092	0.991	19.270	-28.068
14	1.960	0.981	1.370	-26.232
15	1.119	0.988	-15.611	-26.232

Table 3-2. Field coefficients as a function of separation length for w_b/w_a = 0.624, f = 10 GHz.

	Magnitude		Phase (degrees)	
Separation, L (cm)	$V_1^{(0)}$	$V_1^{(L)}$	$V_1^{(0)}$	$V_1^{(L)}$
1	1.031	0.999	-9.240	26.889
2	1.019	0.999	18.401	-30.038
3	1.000	0.999	-32.173	-37.176
4	1.038	0.999	-0.997	25.746
5	1.010	0.999	29.207	-35.477
6	1.016	0.999	-20.901	-31.163
7	1.033	0.999	7.146	26.431
8	1.000	0.999	41.747	-42.976
9	1.028	0.999	-11.391	-27.470
10	1.022	0.999	16.000	29.054
11	1.003	0.999	-35.243	38.994
12	1.036	0.999	-2.996	-25.855
13	1.009	0.999	26.355	33.912
14	1.013	0.999	-23.513	32.434
15	1.035	0.999	5.096	-26.089

CHAPTER 4

ALTERNATIVE SOLUTION FOR SYMMETRIC DOUBLE-STEP DISCONTINUITIES IN RECTANGULAR WAVEGUIDES

In this chapter the problem of symmetric double-step discontinuities is discussed. The problem can be simplified by considering the two special cases of even and odd excitation modes and then superimposing the results. In the case of even excitation modes, waves of equal amplitude but opposite in phase are assumed propagating in regions A and C simultaneously [11,25]. Since the field distribution is symmetrical about $z=0$ as shown in Fig. 4-1, a magnetic wall (open circuit) may be placed at the symmetry plane $z=0$. In the case of odd excitation, waves with opposite in amplitude and phase are propagating in regions A and C simultaneously. Since the field in this case is anti-symmetric, this allows an electric wall to be placed at the symmetry plane $z=0$. Addition of the two excitations results in twice the amplitude of the excitations in region A and zero excitation in region C. Therefore, the problem is reduced to a single step discontinuity and terminated alternately by a magnetic or electric wall as shown in Fig. 4-2. The analysis for this type of structure runs parallel to the analysis in chapter 2, the only difference being that waveguide B is not infinitely long in this case, being bounded by an alternate magnetic or electric wall at z=0 which requires one more boundary condition to be considered in the analysis.

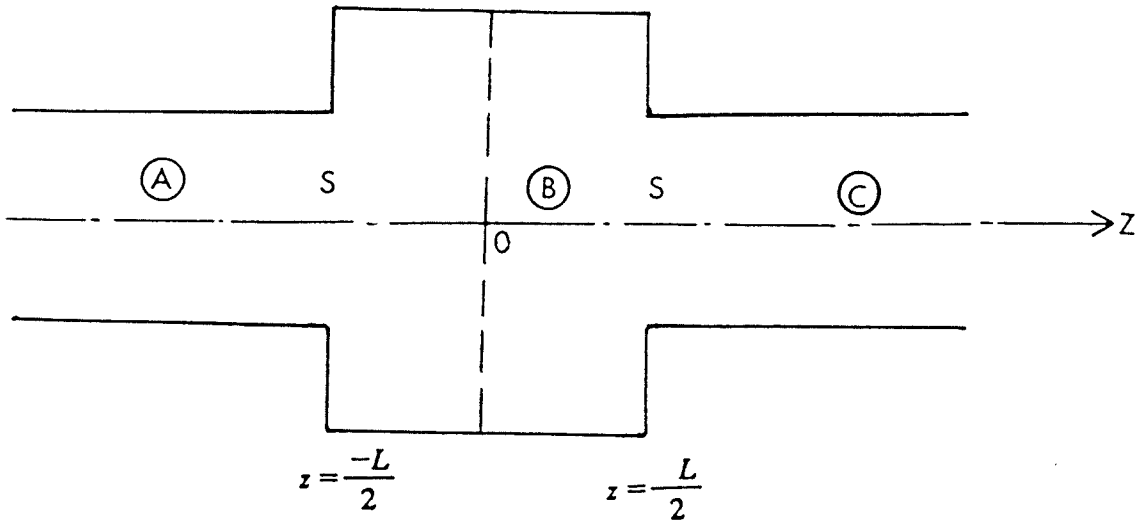

Fig. 4-1: Geometry of symmetric double-step waveguide discontinuities.

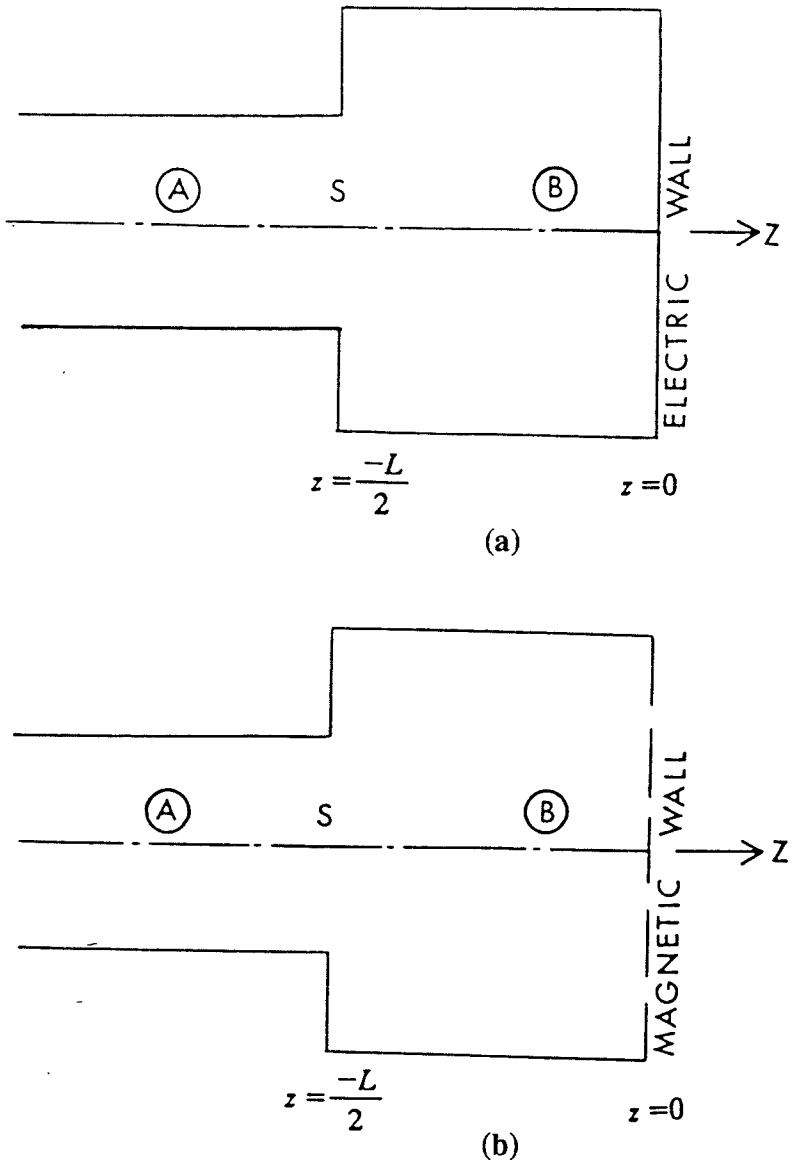

Fig. 4-2: (a) Short-circuit bisection. (b) Open-circuit bisection.

4.1 Formulation

Consider the structure shown in Fig. 4-2, with an incident field propagating in the positive z-direction. A part of it is scattered by the discontinuity and a part is transmitted to waveguide B. The transmitted waves are totally reflected at z=0 plane. Thus, the transverse components of fields are given in modal form as follows.

$$E_t = \begin{cases} \sum_i a_i e^{-j\gamma_{ai}\,(z+\frac{L}{2})} e_{ai} + \sum_i d_i e^{j\gamma_{ai}\,(z+\frac{L}{2})} e_{ai} & z < -L/2 \\ \sum_i b_i e^{-j\gamma_{bi}\,z} e_{bi} + \sum_i \varepsilon\, b_i e^{j\gamma_{bi}\,z} e_{bi} & -L/2 < z < 0 \end{cases} \tag{4-1}$$

$$H_t = \begin{cases} \sum_i a_i Y_{ai} e^{-j\gamma_{ai}\,(z+\frac{L}{2})} u_z \times e_{ai} - \sum_i d_i Y_{ai} e^{j\gamma_{ai}\,(z+\frac{L}{2})} u_z \times e_{ai} & z < -L/2 \\ \sum_i b_i Y_{bi} e^{-j\gamma_{bi}\,z} u_z \times e_{bi} - \sum_i \varepsilon\, b_i Y_{bi} e^{j\gamma_{bi}\,z} u_z \times e_{bi} & -L/2 < z < 0 \end{cases} \tag{4-2}$$

a_i, b_i, and d_i are complex coefficients of the transmitted and reflected modes, γ_{ai} and γ_{bi} are the modal propagation constants, Y_{ai} and Y_{bi} are the modal admittances, and e_{ai} and e_{bi} are the modal vectors for the ith mode in the corresponding waveguides A and B, respectively. For the case of an electric wall ε = -1 while in the case of a magnetic wall ε = 1.

Using the Equivalence Principle, the fields in the two regions can be modeled in terms of the equivalent magnetic current sheet M placed over the aperture S, as shown in Fig. 4-3, with

$$M = u_z \times E_t \qquad at\ z = -\frac{L}{2} \tag{4-3}$$

where E_t is the unknown electric field in the aperture to be determined. The field in waveguide A is the incident field plus the field produced by the magnetic sheet M.

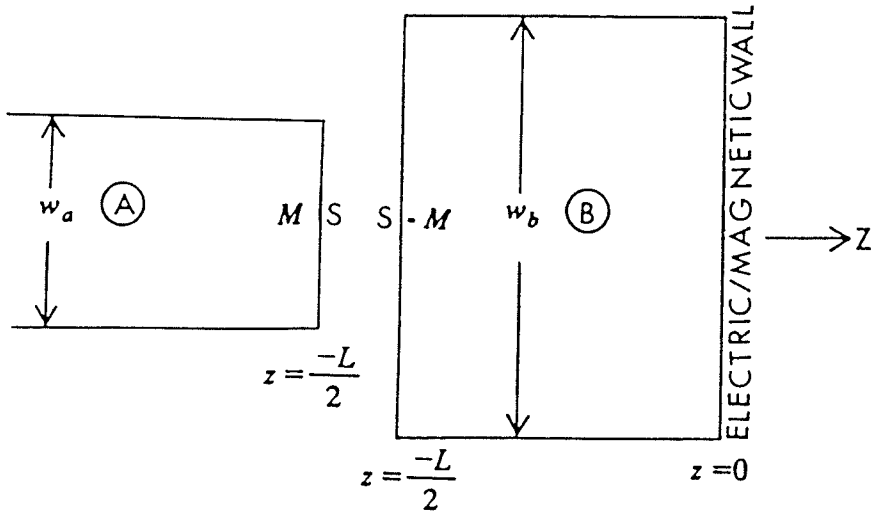

Fig. 4-3: Equivalence for waveguides A and B.

The field in waveguide B (resonator box) is the total field produced by the magnetic current sheet $-M$ plus the field totally reflected by the magnetic or electric wall at the boundary z = 0.

In order to determine the unknown expansion coefficients, we apply the proper boundary conditions. Thus the continuity of the tangential electric field components across the aperture S at $z = -\frac{L}{2}$, requires that

$$\sum_i a_i \; u_z \times e_{ai} + \sum_i d_i \; u_z \times e_{ai} = M$$

$$\sum_i b_i e^{j\gamma_{bi}\frac{L}{2}} u_z \times e_{bi} + \sum_i \varepsilon \; b_i e^{-j\gamma_{bi}\frac{L}{2}} u_z \times e_{bi} \qquad (4\text{-}4)$$

Also the continuity of the tangential magnetic field components across the aperture S at $z = -\frac{L}{2}$, requires that

$$\sum_i a_i Y_{ai} u_z \times e_{ai} - \sum_i d_i Y_{ai} u_z \times e_{ai} =$$

$$\sum_i b_i Y_{bi} e^{j\gamma_{bi}\frac{L}{2}} u_z \times e_{bi} - \sum_i \varepsilon b_i Y_{bi} e^{-j\gamma_{bi}\frac{L}{2}} u_z \times e_{bi} \qquad (4\text{-}5)$$

To obtain an approximate solution for equations (4-4) and (4-5), we apply the moment method.

4.3 Moment-method solution

To apply the moment method, we expand the magnetic current sheet M as

$$M = \sum_{p=1}^{Q} V_p \; M_p \qquad at \; z = -\frac{L}{2} \qquad (4\text{-}6)$$

where V_p are unknown complex coefficients to be evaluated, and M_p are known vector basis functions. The above summation is limited to a finite number of terms Q. By substituting (4–6) into (4–4) and applying the orthogonality condition (2-3) for the

mode functions in each region and simplifying, we obtain

$$a_i + d_i = \sum_{p=1}^{Q} V_p \; h_{aip} \qquad (i = 1,2,..., N) \tag{4-7}$$

$$b_i = \frac{1}{e^{j\gamma_{bi}\frac{L}{2}} + \varepsilon\, e^{-j\gamma_{bi}\frac{L}{2}}} \sum_{p=1}^{Q} V_p \; h_{bip} \qquad (i = 1,2,..., N) \tag{4-8}$$

where

$$h_{rip} = \int_S M_p \cdot u_z \times e_{ri} \; ds \qquad (r = a,b) \tag{4-9}$$

Equation (4-9) can be written in matrix form as

$$H_r = [h_{rip}]_{N \times Q} \tag{4-11}$$

Taking the inner product of (4–5) (as defined in (2-16)) with the testing function W_k on the aperture S, we obtain [46],

$$2\sum_{i=1}^{N} a_i Y_{ai} W_{aik} = \sum_{i=1}^{N} \left[\sum_{p=1}^{Q} V_p h_{aip} \right] Y_{ai} W_{aik} +$$

$$\sum_{i=1}^{N} \frac{e^{j\gamma_{bi}\frac{L}{2}} - \varepsilon\, e^{-j\gamma_{bi}\frac{L}{2}}}{e^{j\gamma_{bi}\frac{L}{2}} + \varepsilon\, e^{-j\gamma_{bi}\frac{L}{2}}} \left[\sum_{p=1}^{Q} V_p h_{bip} \right] Y_{bi} W_{bik} \qquad (k = 1,2,...,Q) \tag{4-12}$$

where

$$W_{rik} = \int_S W_k \cdot u_z \times e_{ri} \; ds \qquad (r = a,b) \tag{4-13}$$

The above equations can be written in matrix form

$$W_r = [W_{rik}]_{N \times Q} \tag{4-14}$$

Following Mautz *et al* [24] equation (4-12) may be written in the generalized admittance form

$$\vec{I} = \left[\overline{Y}_a + \frac{e^{j\gamma_{bi}\frac{L}{2}} - \varepsilon\, e^{-j\gamma_{bi}\frac{L}{2}}}{e^{j\gamma_{bi}\frac{L}{2}} + \varepsilon\, e^{-j\gamma_{bi}\frac{L}{2}}} \overline{Y}_b \right] \vec{V} \tag{4-15}$$

where

$$\vec{I} = 2W_a^T \overline{Y}_a \vec{a} \tag{4-16}$$

$$\overline{Y}_r = W_r^T Y_r H_r \qquad (r = a, b) \tag{4-17}$$

$$\vec{a} = [a_i]_{N\times 1} \tag{4-18}$$

$$\vec{V} = [V_p]_{Q\times 1} \tag{4-19}$$

With Y_r being the diagonal matrix of the modal admittances in the corresponding waveguide A or B while $\vec{a}$ and $\vec{V}$ are the column matrices of the quantities a_i and V_p, respectively.

4.3 Galerkin's method solution

As the aperture S occupies the cross-section of the smaller waveguide A, we may let

$$M_p = W_p = u_z \times e_{ap} \qquad (p = 1,2,\ldots, Q) \tag{4-20}$$

Also, we let $Q = N$ and $e_{ap} = e_{bp}$. This leads to

$$H_r = W_r = U \qquad (r = a, b) \tag{4-21}$$

where U is the identity matrix. Equations (4-16) and (4-17) reduce to

$$\vec{I} = 2Y_a \vec{a} \tag{4-22}$$

$$\overline{Y}_r = Y_r \tag{4-23}$$

Substituting (4-22) and (4-23) into (4-15), we obtain

$$\vec{I} = \left[Y_a + \frac{e^{j\gamma_{bi}\frac{L}{2}} - \varepsilon\, e^{-j\gamma_{bi}\frac{L}{2}}}{e^{j\gamma_{bi}\frac{L}{2}} + \varepsilon\, e^{-j\gamma_{bi}\frac{L}{2}}} Y_b \right] \vec{V} \tag{4-24}$$

In the case of even excitation ($\varepsilon = 1$), equation (4-24) reduces to

$$\vec{I} = \left[Y_a + j\tan\left(\frac{\gamma_{bi}L}{2}\right) Y_b \right] \vec{V} \tag{4-25}$$

while in the case of odd excitation ($\varepsilon = -1$),

$$\vec{I} = \left[Y_a - j\cot\left(\frac{\gamma_{bi}L}{2}\right) Y_b \right] \vec{V} \tag{4-26}$$

Equations (4-25) and (4-26) represent ($N \times N$) systems of linear equations. Its solution through equations (4-7)-(4-8) yields the field distributions in equations (4-1) and (4-2). The final step of the presented analysis is to formulate the scattering matrix for the double-step discontinuity.

4.4 Scattering matrix formulation

The ($2N \times 2N$) scattering matrix for the double-step waveguide discontinuity may be written as [13]

$$S = \begin{bmatrix} S_{aa} & S_{ac} \\ S_{ca} & S_{cc} \end{bmatrix} = \frac{1}{2} \begin{bmatrix} \Gamma_e + \Gamma_o & \Gamma_e - \Gamma_o \\ \Gamma_e - \Gamma_o & \Gamma_e + \Gamma_o \end{bmatrix} \tag{4-27}$$

where Γ_e is the reflection coefficient matrix due to even excitation while Γ_o is the reflection coefficient matrix due to odd excitation. For the even excitation, the complex reflection coefficients can be obtained from (4-7) as

$$\vec{d} = \vec{V} - \vec{a} \tag{4-28}$$

where $\vec{V}$ may be obtained from (4-25) as

$$\vec{V} = 2\left[Y_a + j\tan\left(\frac{\gamma_{bi}L}{2}\right) Y_b\right]^{-1} Y_a\vec{a} \tag{4-29}$$

Substituting (4-29) into (4-28), we get

$$\vec{d} = 2\left[Y_a + j\tan\left(\frac{\gamma_{bi}L}{2}\right) Y_b\right]^{-1} Y_a\vec{a} - \vec{a} \tag{4-30}$$

Therefore, the $(N\times N)$ submatrix Γ_e is obtained in the form

$$\Gamma_e = \frac{\vec{d}}{\vec{a}} = \left[Y_a + j\tan\left(\frac{\gamma_{bi}L}{2}\right) Y_b\right]^{-1}\left[Y_a - j\tan\left(\frac{\gamma_{bi}L}{2}\right) Y_b\right] \tag{4-31}$$

The submatrix Γ_o due to the odd excitation may be obtained in a similar manner, as

$$\Gamma_o = \left[Y_a - jcot\left(\frac{\gamma_{bi}L}{2}\right) Y_b\right]^{-1}\left[Y_a + jcot\left(\frac{\gamma_{bi}L}{2}\right) Y_b\right] \tag{4-32}$$

Comparing the above scattering matrix with the one obtained by De Smedt *et al* [13] in terms of that for a single-step is

$$S_{aa} = S_{cc} = S_{aa}^{(s)} + S_{bb}^{(s)}\, S_{ac}^{(s)}\, e^{-\gamma_1 L} \tag{3-33}$$

and

$$S_{ac} = S_{ca} = \frac{S_{ab}^{(s)}\, S_{ba}^{(s)}\, e^{-\gamma_1 L}}{1 - S_{bb}^{(s)2}\, e^{-2\gamma_1 L}} \tag{3-34}$$

The above scattering matrix needs more computation than the one obtained in equation (4-27) because in using the above equations we have to combine the scattering matrix at each junction to obtain the overall scattering matrix. In addition the length L has to be sufficiently large compared to the wavelength. This is in contrast with the obtained scattering matrix which handles two consecutive junctions at a time, in other words, the amount of computation is reduced to one half by using equation (4-27).

4.5 Cascaded junctions

In this section we present a solution for the scattering matrix when a number of junctions (more than two) are considered together in a cascade as shown in Fig. 4-4. It is convenient to present each two consecutive junctions by their scattering matrix (equation (4-27)). The scattering matrix of a cascade of waveguide junctions may be obtained by multiplication of the scattering matrices of each two consecutive junctions. The only restriction is that the length L_t has to be sufficiently large compared to the wavelengh.

4.6 Scattering matrix for cascaded junctions

To obtain the scattering matrix for the structure comprised of waveguides A and E as shown in Fig. 4-4, it is first necessary to express the scattering matrix of the double-step between waveguides A and C as shown in Fig. 4-5 (a) as

$$b_1^{(A)} = S_{aa}^{(d)}\, a_1^{(A)} + S_{ac}^{(d)}\, b_1^{(C)} \tag{4-35}$$

$$a_1^{(C)} = S_{ca}^{(d)}\, a_1^{(A)} + S_{cc}^{(d)}\, b_1^{(C)} \tag{4-36}$$

This is to be combined with the scattering matrix of the double-step between waveguides C and E and with the help of the transmission matrix, *i.e.*

$$b_1^{(C)}\, e^{\gamma_1 L_t} = S_{cc}^{(d)}\, e^{-\gamma_1 L_t}\, a_1^{(C)} + S_{ce}^{(d)}\, a_1^{(E)} \tag{4-37}$$

$$b_1^{(E)} = S_{ec}^{(d)}\, e^{-\gamma_1 L_t}\, a_1^{(C)} + S_{ee}^{(d)} a_1^{(E)} \tag{4-38}$$

With the elimination of the internal variables (see Appendix B), the overall combined scattering matrix shown in Fig. 4-5 (b) reduces to

$$S_{aa} = S_{aa}^{(d)} + \frac{S_{ac}^{(d)}\, S_{cc}^{(d)}\, S_{ca}^{(d)}\, e^{-2\gamma_1 L_t}}{1 - S_{cc}^{(d)2}\, e^{-2\gamma_1 L_t}} \tag{4-38}$$

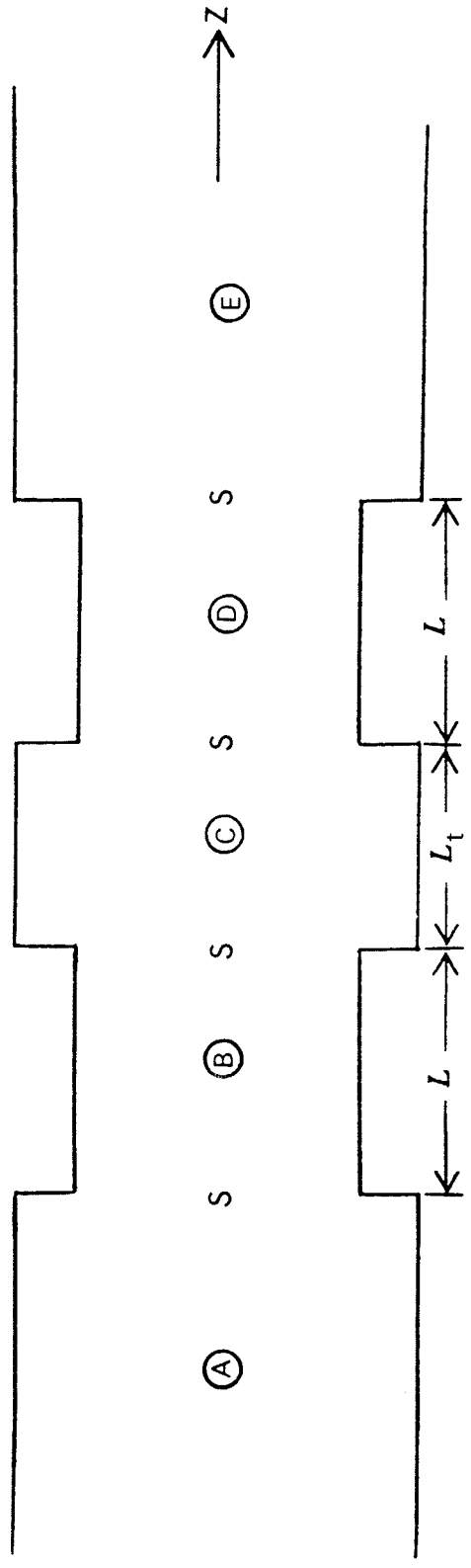

Fig. 4-4: Geometry of multiple-step dicontinuities in waveguides.

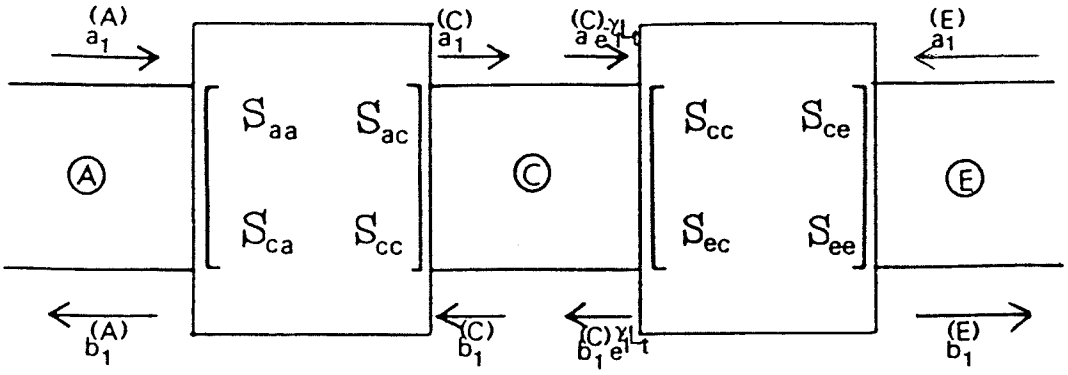

(a)

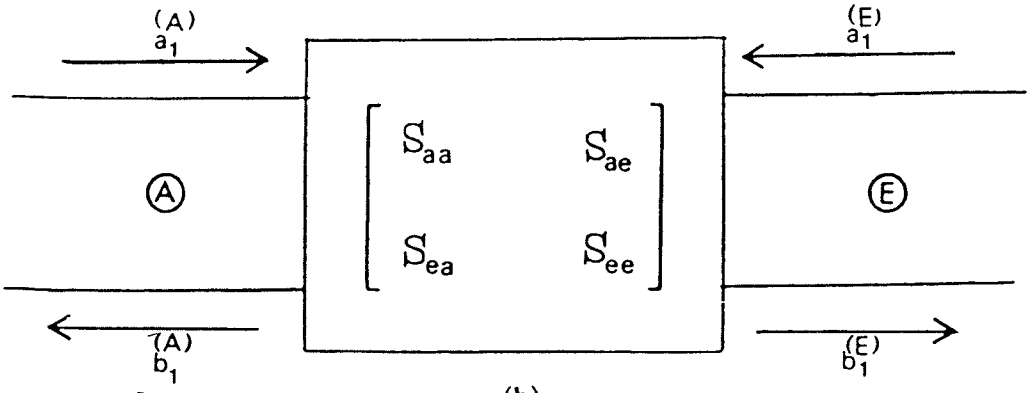

(b)

Fig. 4-5: Scattering matrix representation of cacaded discontinuities.

$$S_{ae} = \frac{S_{ac}^{(d)} S_{ce}^{(d)} e^{-\gamma_1 L_t}}{1 - S_{cc}^{(d)2}\, e^{-2\gamma_1 L_t}} \tag{4-39}$$

$$S_{ea} = \frac{S_{ec}^{(d)} S_{ca}^{(d)} e^{-\gamma_1 L_t}}{1 - S_{cc}^{(d)2}\, e^{-2\gamma_1 L_t}} \tag{4-40}$$

$$S_{ee} = S_{ee}^{(d)} + \frac{S_{ec}^{(d)}\, S_{cc}^{(d)}\, S_{ce}^{(d)}\, e^{-2\gamma_1 L_t}}{1 - S_{cc}^{(d)2}\, e^{-2\gamma_1 L_t}} \tag{4-41}$$

Since the input waveguides are identical, we may obtain the following simplifications

$$S_{aa}^{(d)} = S_{cc}^{(d)} = S_{ee}^{(d)} \tag{4-42}$$

$$S_{ca}^{(d)} = S_{ec}^{(d)} \tag{4-43}$$

$$S_{ac}^{(d)} = S_{ce}^{(d)} \tag{4-44}$$

4.6 Numerical results

We consider three numerical examples, namely, ridged, over-sized and a cascaded double-step waveguide discontinuity. The purpose of doing this is to make sure that the analysis presented is valid for these structures and also for various values of L by comparing with available data for these examples.

4.6.1 Ridged double-step waveguide discontinuity

Consider the structure shown in Fig. 3-4 where the dimensions are stated in section 3.3. The magnitude and phase of S_{aa} and S_{ac} are plotted as a function of frequency. Different values of N were considered *i.e.* N = 3,5,...,9, with N = 9 yielding a satisfactory accuracy. The results are compared with the experimental values obtained by De Smedt and Denturck while the frequency range is extended to 5 GHz in order to show the interference of higher order modes. It is seen from Fig. 4-6 that

the two curves for the reflection coefficient are virtually identical below 3.3 GHz. Even at higher frequencies, the agreement is close. Resonance occurred at 3.75 GHz in the smaller waveguide (between the junctions) which is slightly towards higher frequencies. Fig. 4-7 shows the magnitude of the transmission coefficient, the difference between the two curves being about -4 dB at 2.6 GHz. The agreement is also good at higher frequencies, while the magnitude of S_{ac} for frequencies above 3.8 GHz is 0 dB (unity). Fig. 4-8 shows the phase of the reflection coefficient, and the difference between the curves is about 8 degrees in the range 2.6 GHz to 3.6 GHz. The agreement is also good at higher frequencies than 3.6 GHz. On the other hand, Fig. 4-9 shows the phase of S_{ac}, the agreement between the two curves is good at frequencies higher than 3.1 GHz. We have plotted in Fig. 4-10 the variation of S_{aa} and S_{ac} in dB versus frequency with L as a parameter. Here the magnitude of the reflection coefficient dropped to - 50 dB and the resonance occurred at 4.1 GHz for L = 6.0 cm and at 4.75 GHz for L = 4.50 cm, the latter separation length being the same as the width of the smaller waveguide. Figs. 4-10 and 4-11 show that the magnitude of the reflection and transmission coefficient improve by varying L. For example, the magnitude of the transmission coefficient increases from -9.8 dB to -1 dB as the length L decreases from 4 cm to 1 cm. We have plotted the *VSWR* versus frequency for different lengths in Fig. 4-12, where the results show that decreasing the value of L results in increasing the magnitude of *VSWR* at the normalized frequency 1.8. The computations were again extended up to 5 GHz.

4.6.2 Over-sized double-step waveguide discontinuity

We consider the structure shown in Fig. 4-3 where waveguide A has a width w_a 2.286 cm and a cutoff frequency f_c = 13.12 GHz, while waveguide B has a width w_b = 4.572 cm and a cutoff frequency f'_c = 6.56 GHz = 0.5 f_c. The separation between the junctions is assumed to be L = 2.743 cm.

Fig. 4-13 shows the computed magnitude of the reflection coefficient of an oversized double step waveguide discontinuity, while the frequency range is taken between 7 and 19 GHz. Different values of N were considered, with N = 11 yielding to a satisfactory accuracy. The results are checked against the values calculated by Rozzi *et al* [14]. It is seen that the two curves are very close between f = 7 and 10.4 GHz. The results obtained by the presented method lead to values of S_{aa} which vanish at different frequencies, namely f = 11.2,14.1,17.2 GHz.

Tables 4.1 through 4.4 for the scattering matrix coefficients and the voltage standing wave ratio *VSWR* are computed using equations (4-27) and (2-41), respectively. The results presented in tables 4.1 and 4.2 are obtained for w_b/w_a =1.2, and propagating frequencies f = 8 GHz and f = 15 GHz. The magnitude of *VSWR* is higher at f = 8 GHz, while it stays approximately constant at higher frequencies.

Tables 4.3 and 4.4 present results are obtained for w_b/w_a = 2.0 and the same propagating freqencies stated before in the previous cases. It is interesting to note that increasing the width of waveguide B to twice the width of waveguide A results in increasing the magnitude of the *VSWR*, this is due to the interaction of TE_{30} mode.

4.6.3 Cascaded double-step junctions

Consider the structure shown in Fig. 4-4 where the dimensions are the same as

stated in section 3.3. The magnitude and the phase of S_{aa} and S_{ae} are plotted versus frequency. Fig. 4-14 shows the magnitude of S_{aa} is 0 dB between 2.6 and 3.55 GHz, where the separation between the junctions is taken to be L = 7.98 cm and the transformer section L_t = 10 cm. In the case of the double-step, the resonance occured at 3.75 GHz in the frequency range 2.6 to 5 GHz, while in this case three resonances occured, namely at 3.55, 3.95, and 4.4 GHz, respectively. Also it can be seen that the magnitude of S_{ae} is 0 dB in the range 3.55-5.0 GHz and varies between -47 and -4.0 dB in the range 2.6-3.55 GHz. Fig. 4-15 shows the phase of the scattering matrix while Figs. 4-16 and 4-17 are another examples where the separation L and the transformer section L_t are the same and equal to 7.98 cm. We have plotted the magnitude of *VSWR* versus frequency with L as aparameter and L_t = 7.98 cm in Fig. 4-18, where the results show that decreasing the value of L from 6 to 4 cm results in increasing the value of *VSWR* from 3.1 to 9.3 at the normalized frequency 1.8.

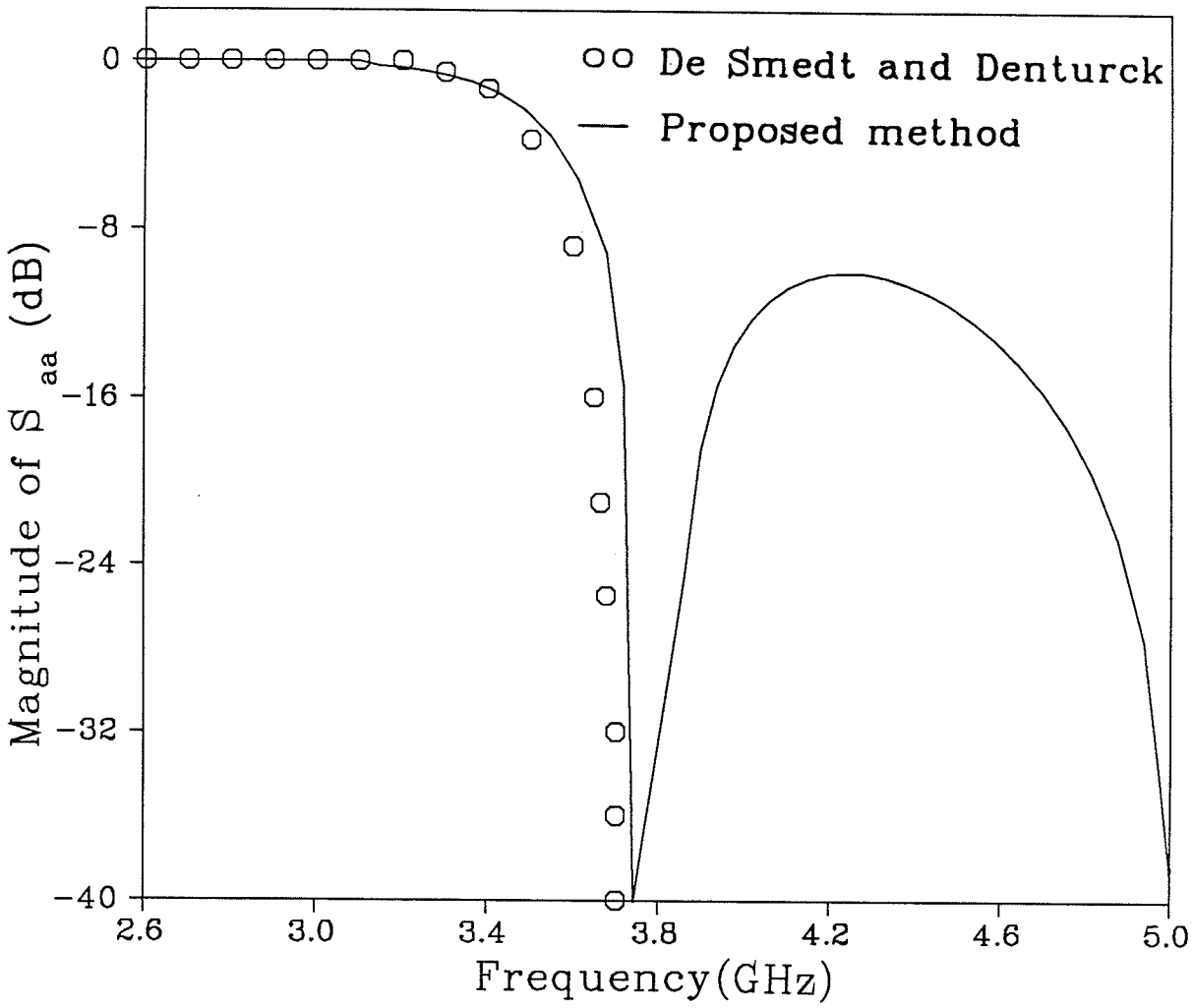

Fig. 4-6: Magnitude of S_{aa} for double-step with L = 7.98 cm.

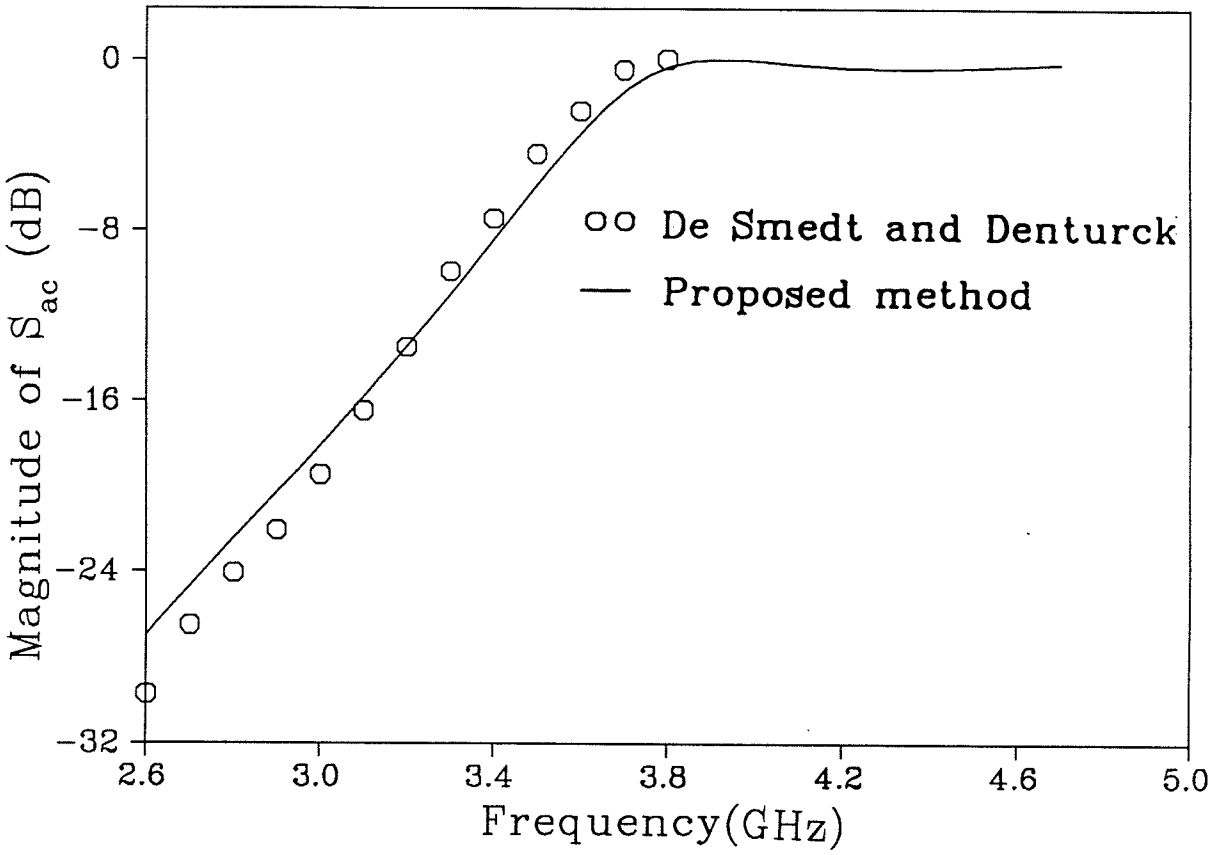

Fig. 4-7: Magnitude of S_{ac} for double-step with L = 7.98 cm.

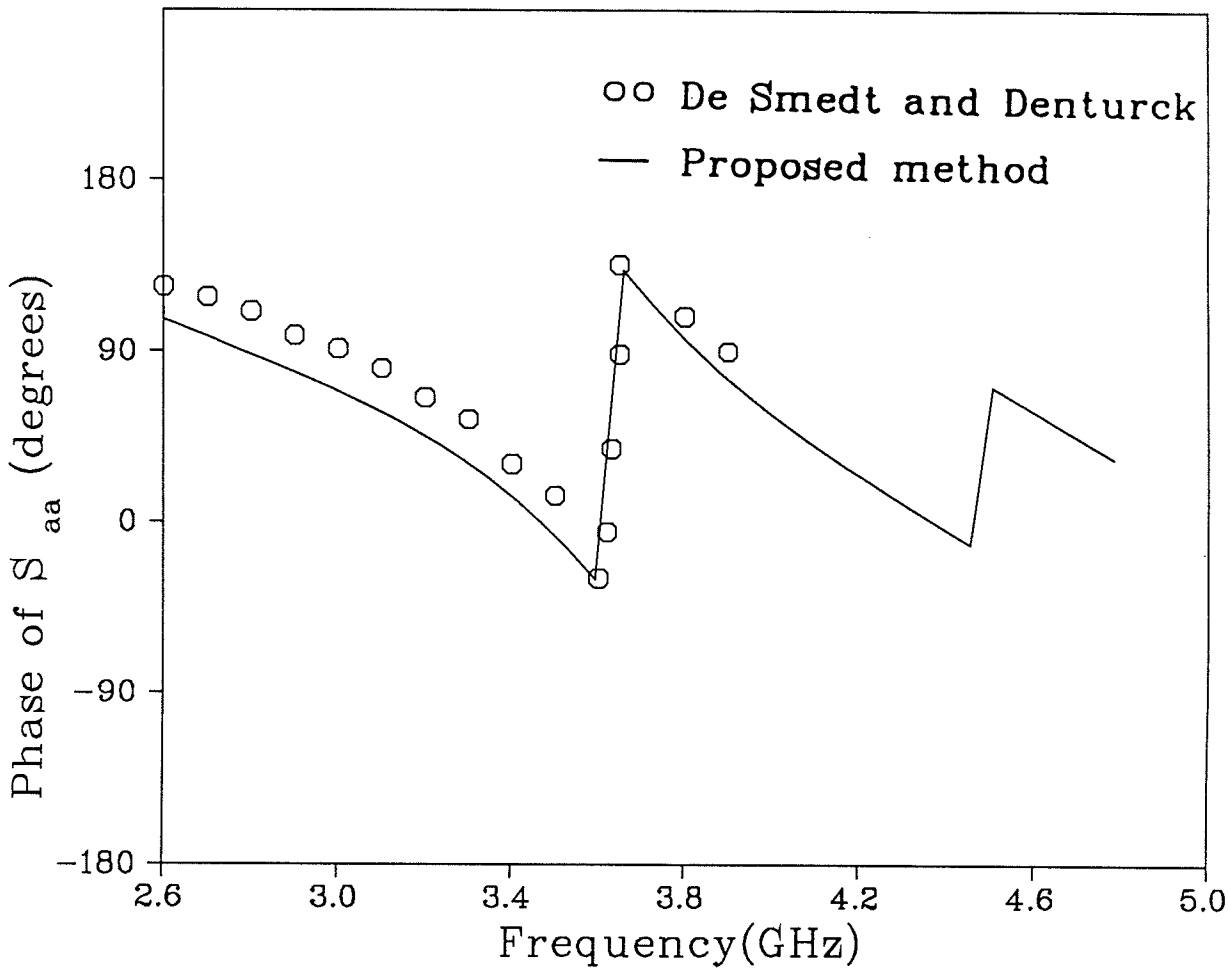

Fig. 4-8: Phase of S_{aa} for double-step with L = 7.98 cm

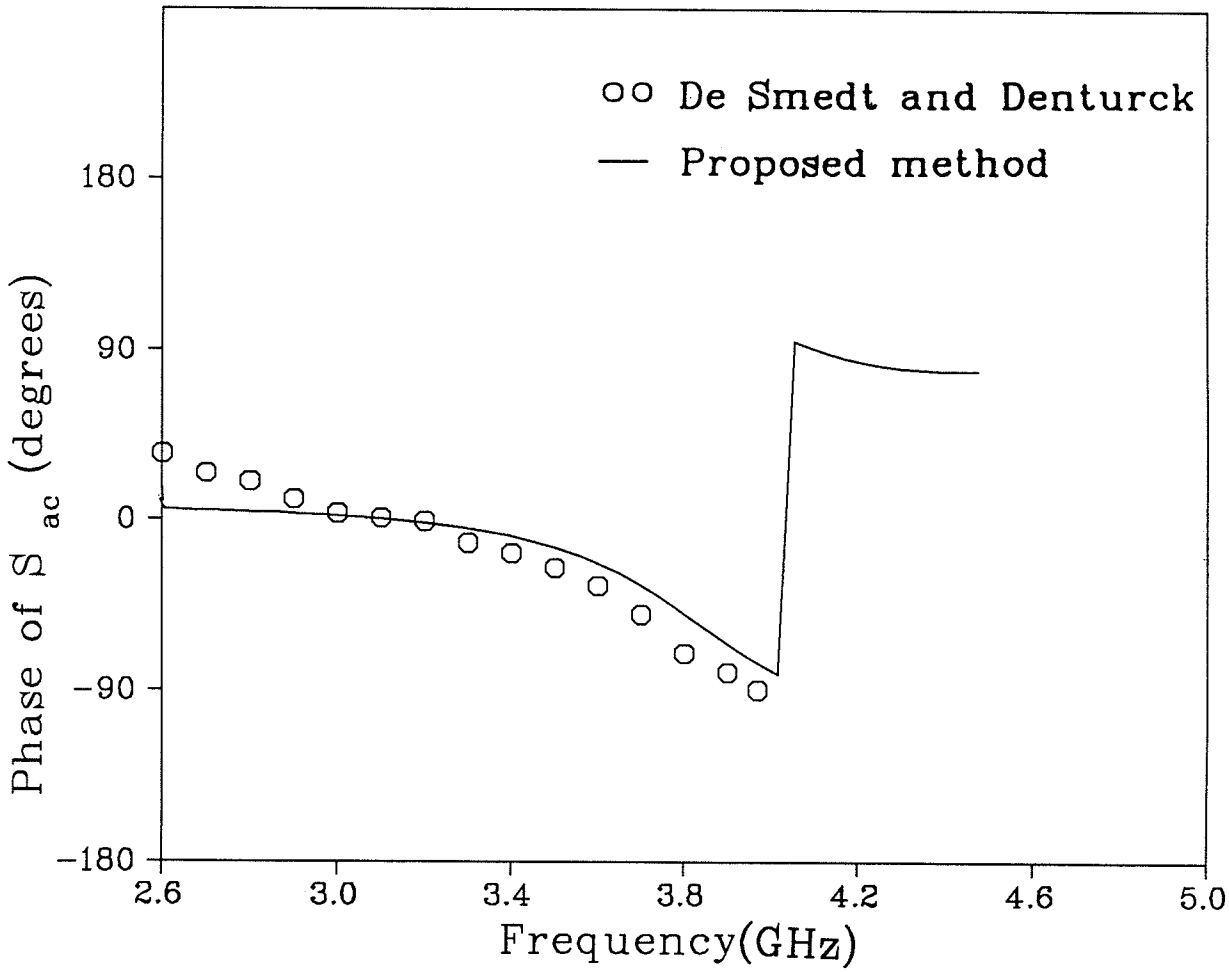

Fig. 4-9: Phase of S_{ac} for double-step with L = 7.98 cm

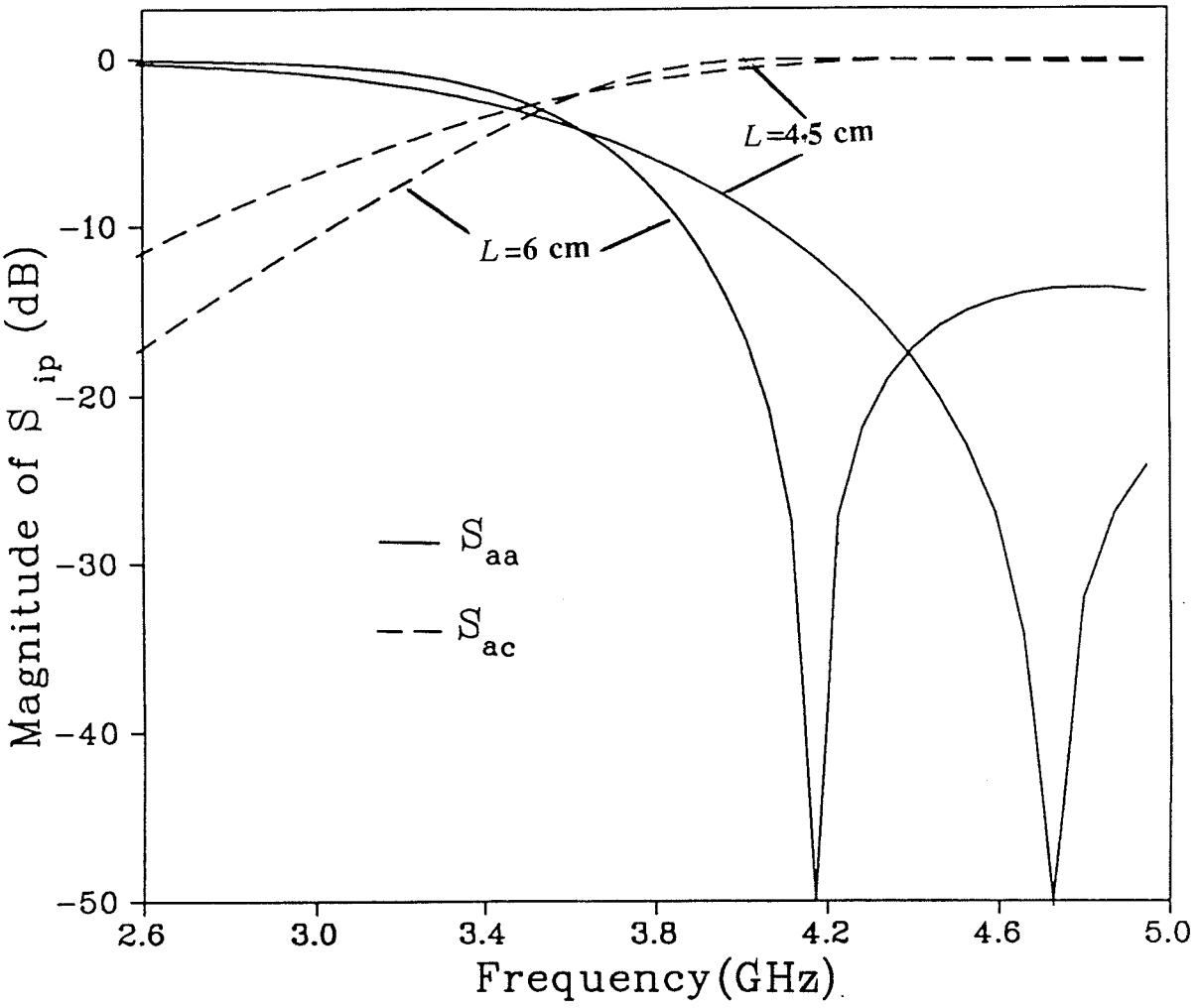

Fig. 4-10: Magnitude of S_{ip} with L as a parameter.

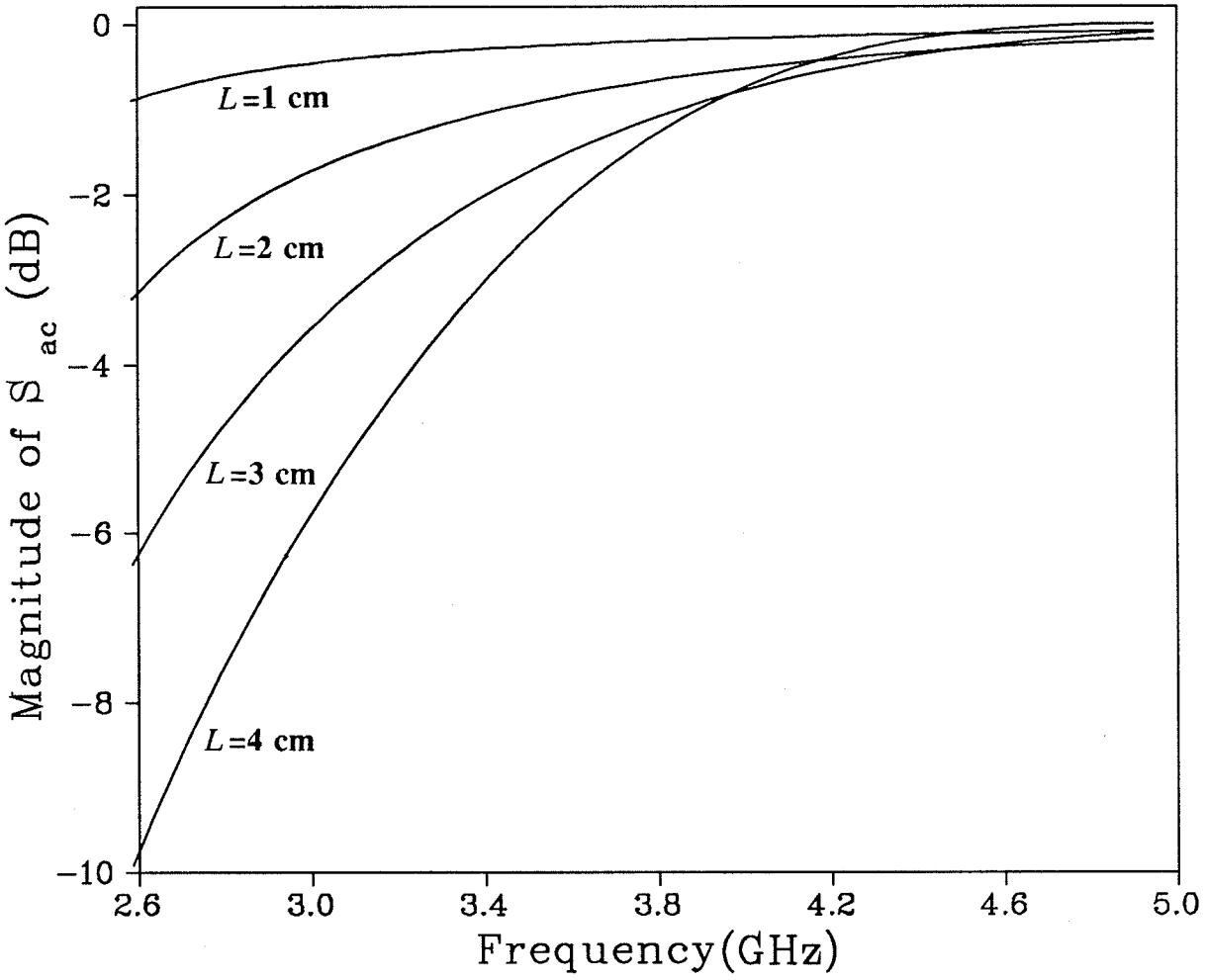

Fig. 4-11: Magnitude of S_{ac} with L as a parameter.

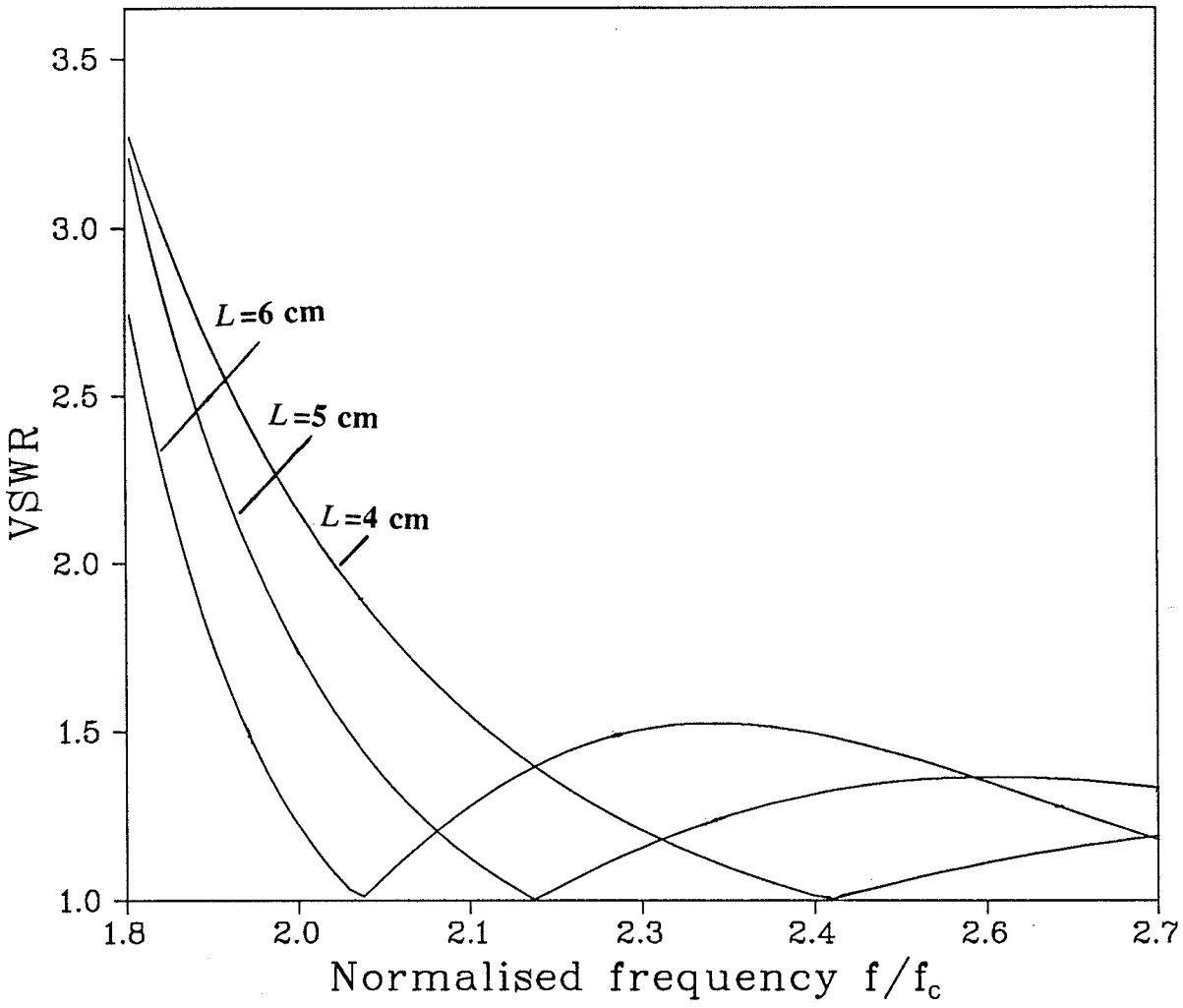

Fig. 4-12: Magnitude of *VSWR* with L as a parameter.

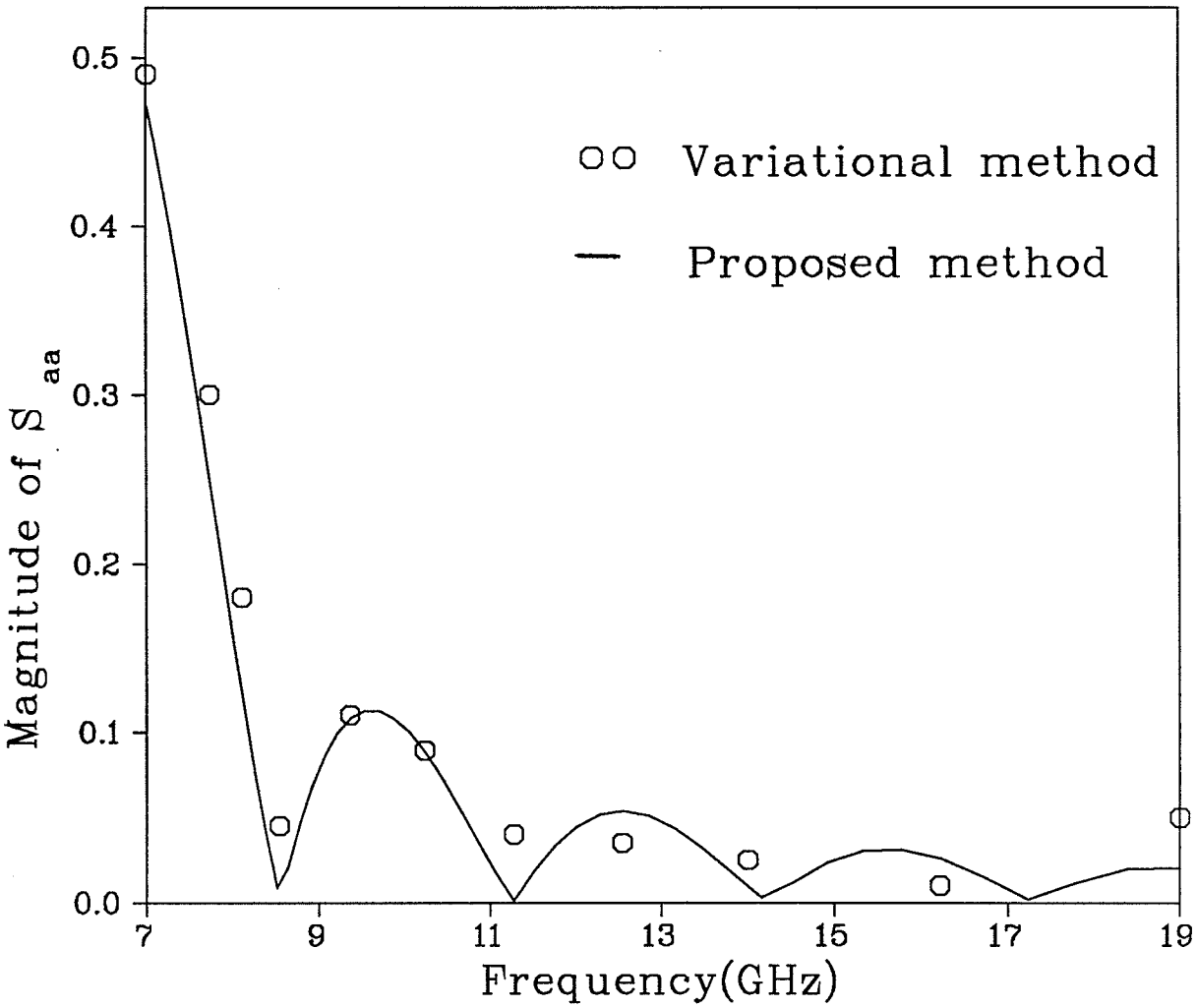

Fig. 4-13: Magnitude of S_{aa} for double-step with L = 2.743 cm.

Table 4-1. Scattering cofficients as a function of separation length for w_b/w_a = 1.2, f = 8 GHz.

Separation, L (cm)	S_{aa}	S_{ac}	$VSWR$
1	-0.2127-j0.7485	0.3235-j0.9189	1.582
2	-0.1016+j0.1182	-0.7491-j0.6439	1.369
3	-0.0633-j0.1054	-0.8510+j0.5106	1.280
4	-0.2318+j0.4089	0.1687+j0.9571	1.616
5	-0.0071 +j0.0452	0.9843+j0.1720	1.086
6	-0.1834-j0.1009	0.4716-j0.8566	1.530
7	-0.1415+j0.1174	-0.6277-j0.7564	1.451
8	-0.0311-j0.0804	-0.9291+j0.3596	1.888
9	-0.2389+j0.0027	0.0111+j0.9709	1.628
10	-0.0274+j0.0761	0.9379+j0.3374	1.176
11	-0.1469-j0.1163	0.6096-j0.7702	1.461
12	-0.1787+j0.1038	-0.4915-j0.8460	1.530
13	-0.0092-j0.0459	-0.9796+j0.1955	1.098
14	-0.2335-j0.0357	-0.1470+j0.9605	1.618
15	-0.0584+j0.1023	0.8634+j0.4905	1.268

Table 4-2. Scattering cofficients as a function of separation length for w_b/w_a = 1.2, f = 15 GHz.

Separation, L (cm)	S_{aa}	S_{ac}	*VSWR*
1	-0.0016+j0.0073	-0.9766-j0.2146	1.015
2	-0.0061+j0.0133	0.9078+j0.4198	1.029
3	-0.0127+j0.0168	-0.7966-j0.6041	1.043
4	-0.0202+j0.0172	0.6484+j0.7608	1.054
5	-0.0272+j0.0145	-0.4700-j0.8820	1.064
6	-0.0323+j0.0090	0.2700+j0.9622	1.069
7	-0.0347+j0.0020	-0.5743-j0.9977	1.072
8	-0.0340-j0.0054	-0.1578+j0.9868	1.071
9	-0.0302-j0.0118	0.3657-j0.9301	1.067
10	-0.0240-j0.0161	-0.5567+j0.8301	1.059
11	-0.0166-j0.0174	0.7219-j0.6915	1.050
12	-0.0094-j0.0155	-0.8536+j0.5206	1.037
13	-0.0037-j0.0107	0.9455-j0.3253	1.023
14	-0.0005-j0.0039	-0.9933+j0.1148	1.008
15	-0.0004+j0.0035	0.9949+j0.1011	1.007

Table 4-3: Scattering coefficients as a function of separation length for w_b/w_a = 2.0, f = 8 GHz.

Separation, L (cm)	S_{aa}	S_{ac}	*VSWR*
1	-0.4347-j0.0167	0.0350-j0.8998	2.395
2	-0.0039+j0.0409	-0.9947-j0.0945	1.086
3	-0.4295-j0.0498	-0.1038+j0.8957	2.524
4	-0.0154+j0.0804	0.9789+j0.1874	1.178
5	-0.4194-j0.0817	0.1731-j0.8874	2.492
6	-0.0339+j0.1167	-0.9531-j0.2770	1.277
7	-0.4043-j0.1120	-0.2424+j0.8749	2.445
8	-0.0586+j0.1486	0.9183+j0.3623	1.380
9	-0.3844-j0.1398	0.3119-j0.8572	2.385
10	-0.08843+j0.1751	-0.8753-j0.4419	1.488
11	-0.1100-j0.1644	-0.3813+j0.8353	2.311
12	-0.1220+j0.1955	0.8255+j0.5152	1.699
13	-0.3320-j0.1852	0.4505-j0.8078	2.226
14	-0.1582+j0.2094	-0.7699-j0.5817	1.712
15	-0.300-j0.2013	-0.5190+j0.7745	2.133

Table 4-4. Scattering cofficients as a function of separation length for w_b/w_a = 2.0, f = 15 GHz.

Separation, L (cm)	S_{aa}	S_{ac}	*VSWR*
1	-0.0005+j0.0062	-0.9971-j0.0763	1.012
2	-0.0018+j0.0122	0.9883+j0.1520	1.025
3	-0.0042+j0.0180	-0.9737-j0.2269	1.037
4	-0.0074+j0.0233	0.9535+j0.3004	1.050
5	-0.0112+j0.0282	-0.9277-j0.3721	1.063
6	-0.0159+j0.0323	0.8964+j0.4416	1.075
7	-0.0211+j0.0357	-0.8600-j0.5085	1.087
8	-0.0268+j0.0383	0.8186+j0.5724	1.098
9	-0.0327+j0.0399	-0.7725-j0.6328	1.109
10	-0.0389+j0.0407	0.7220+j0.6895	1.119
11	-0.0451+j0.0405	-0.6674-j0.7423	1.129
12	-0.0512+j0.0394	0.6090+j0.7906	1.138
13	-0.0570+j0.03737	-0.5470-j0.8343	1.146
14	-0.0625+j0.0344	0.4820+j0.8732	1.154
15	-0.0674+j0.0308	-0.4143-j0.9071	1.160

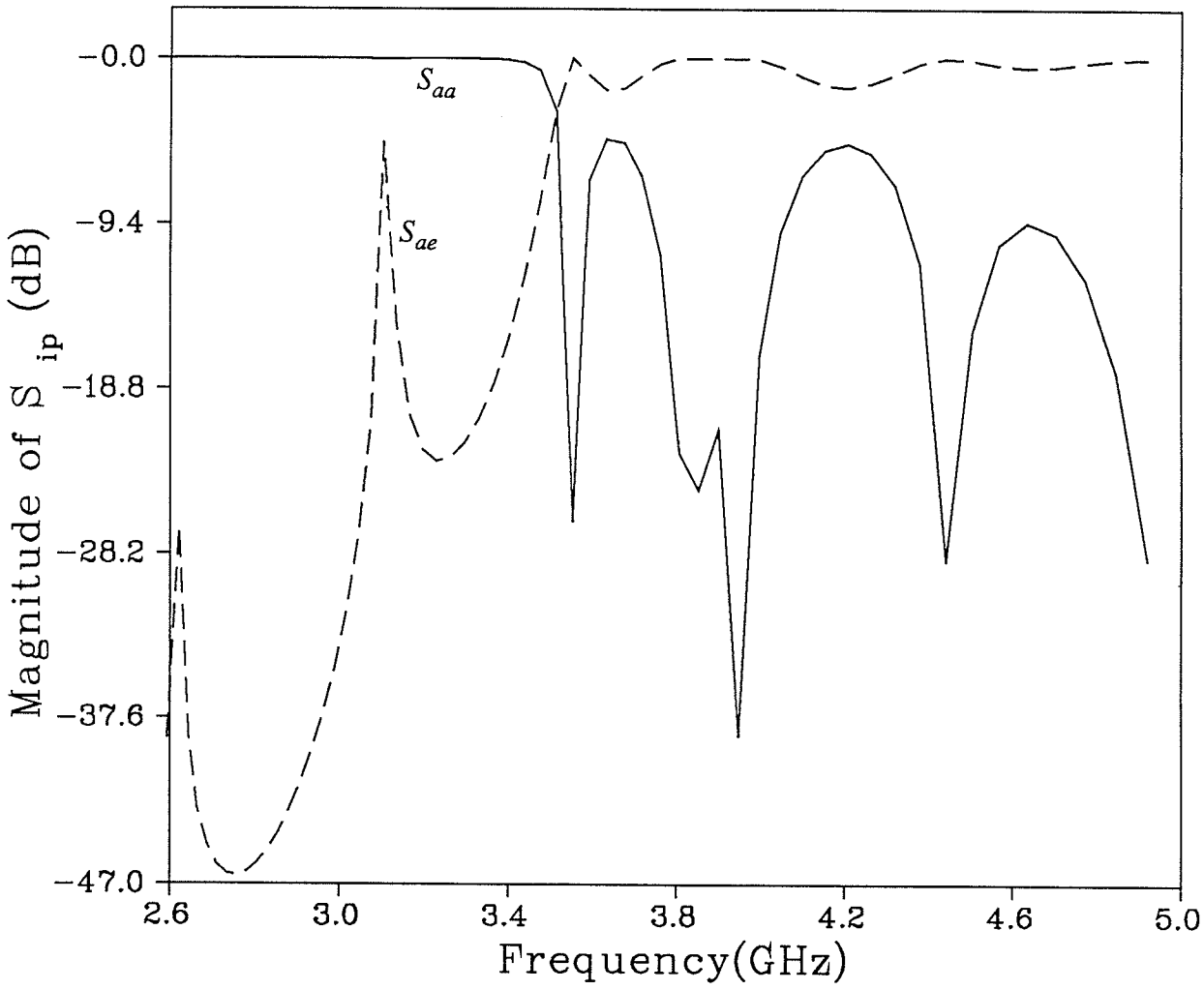

Fig. 4-14: Magnitude of S_{ip} for multiple-step with L = 7.98 cm and L_t = 10 cm.

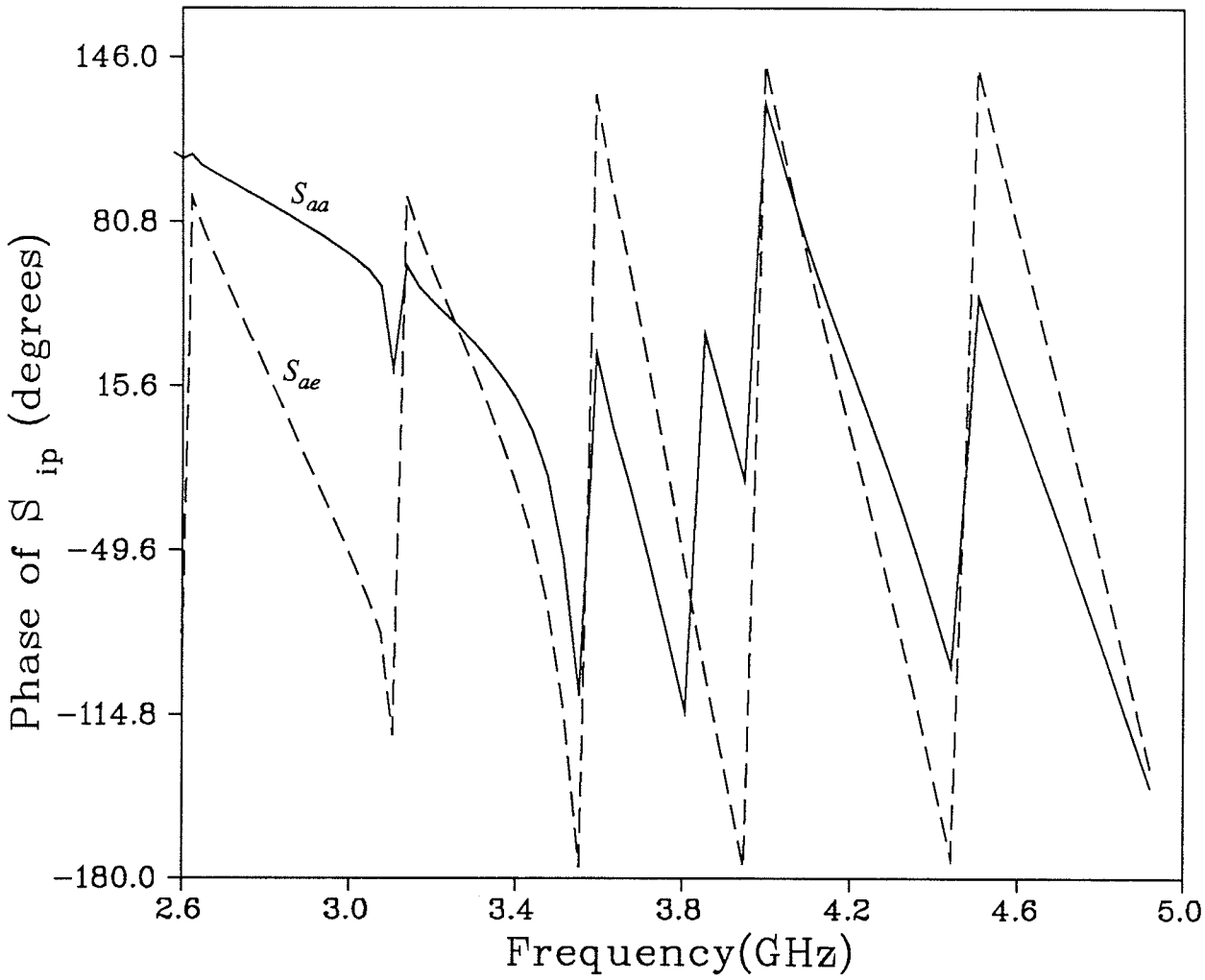

Fig. 4-15: Phase of S_{ip} for multiple-step with L = 7.98 cm and L_t = 10 cm.

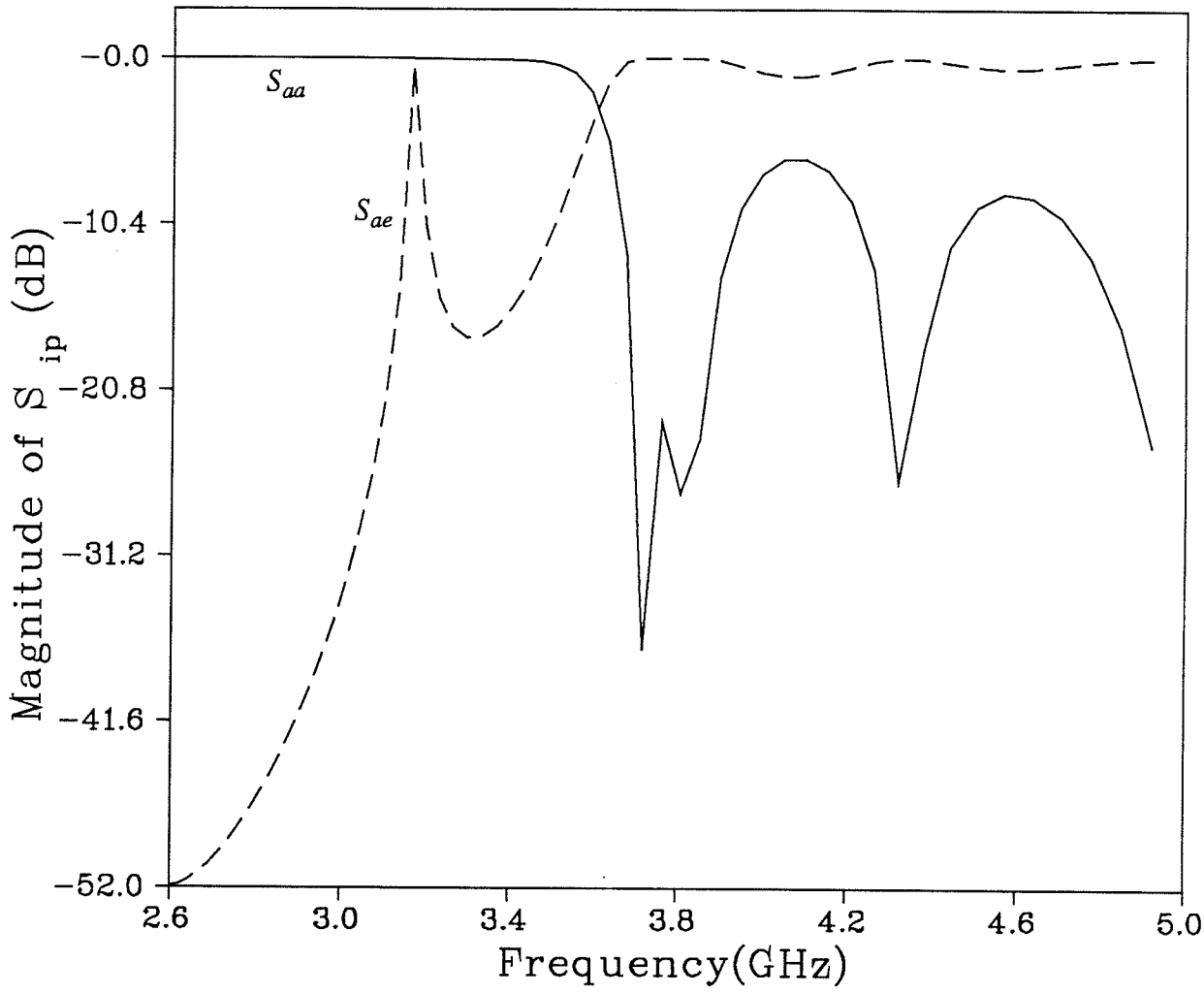

Fig. 4-16: Magnitude of S_{ip} for multiple-step with $L = L_t = 7.98$ cm.

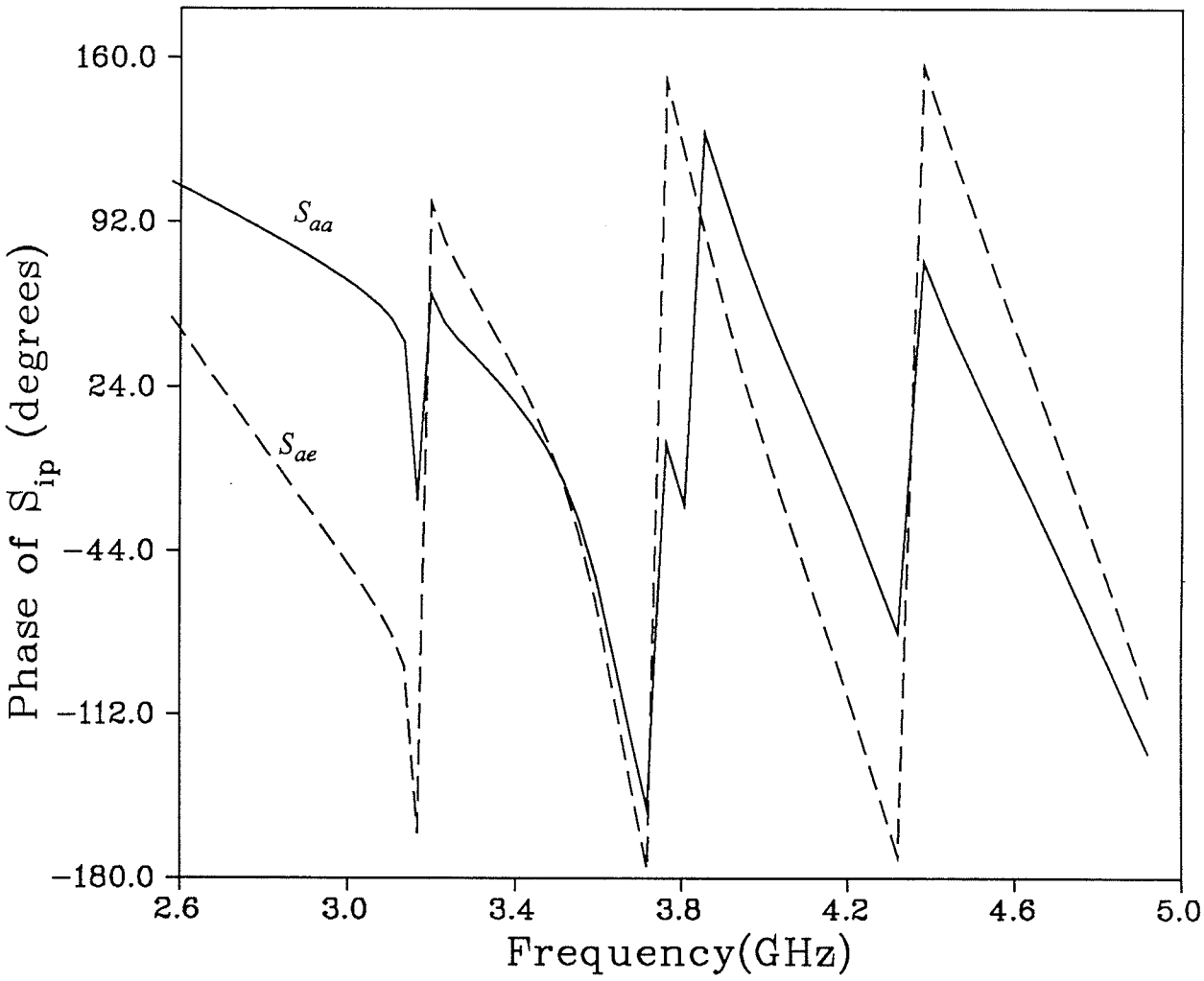

Fig. 4-17: Phase of S_{ip} for multiple-step with $L = L_t = 7.98$ cm.

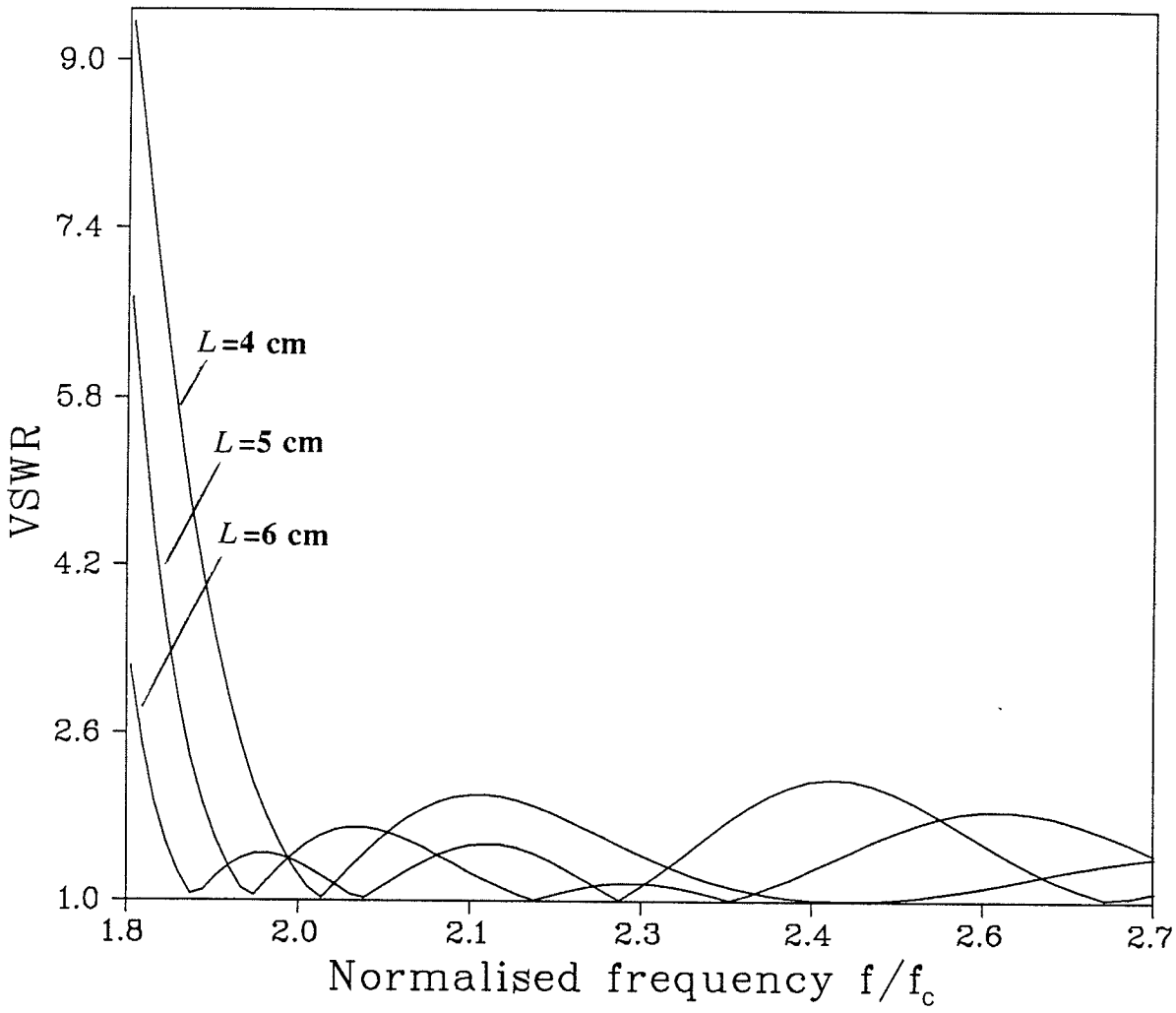

Fig. 4-18: Magnitude of *VSWR* for multiple-step with L as aparameter and L_t = 7.98 cm.

CHAPTER 5

DISCUSSION AND CONCLUSIONS

A moment method solution for the multiple-step discontinuity in rectangular waveguides is given in this thesis. The solution is expressed in terms of aperture admittance matrices, one for each region. The presentation is confined to a single-step in Chapter 2, then the analysis is extended to double-step in Chapter 3, where two coupled set of equations are obtained and expressed in matrix form. Finally the method is applied to the multiple-step discontinuity in Chapter 4 using a cascading procedure, with the only restriction being that L_t should be sufficiently large compared to the wavelength.

De Smedt and Denturck [13] obtained the scattering matrix for a symmetric double-step discontinuity in terms of the single-step discontinuity, their solution is lengthy (in terms of the amount of computation) because it requires computation of the scattering matrix coefficients for each junction while the separation length has to be sufficiently large compared to the wavelength. This is in contrast to our solution which handles two consecutive junctions at a time, and by doing this the amount of computation is reduced to one half. Furthermore, the junction to junction separation is not restricted in our case in principle, although shorter separations require longer computation time to achieve reasonable convergence.

The simplicity of the moment method can be noted in the way the continuity conditions across the junctions are satisfied. By using the Equivalence Principle, the tangential electric field is automatically satisfied by replacing the apertures by electric walls each carrying magnetic current sheets on both sides of the apertures, leaving

only the tangential magnetic field to deal with.

In Chapter 2 and 4, the comparison with experimental data obtained by De Smedt and Denturck [13] shows significant agreement since this problem has no exact solution to compare with.

In Chapter 4, the symmetric double-step discontinuity has been formulated by applying the Equivalence Principle and the Bisection Theorem [25]; the field analysis has been simplified by considering the two special cases of even and odd excitations modes and then superimposing the results to obtain the solution of the problem.

The magnitude of the reflection and transmission coefficient improves when three or more waveguide discontinuities are connected in a cascade as shown in the last section of Chapter 4 by getting more ripples compared with the results obtained for the double-step discontinuity [17]. The other way we obtained better results was that by decreasing the value of the length L from 7.98 to 4 cm. There seems to be no way to determine the accuracy of the results obtained for cascaded junctions without comparison with available numerical or experimental data.

The scattering matrix coefficients are applicable for ridged and oversized double-step waveguide discontinuities as shown in Chapter 4. The purpose of analyzing these particular cases was to obtain a reliable solution for design of waveguide steps which are possible to analyse by other methods only with restriction on dimensions and mode spectrum. This is particularly true since the moment method solution proved to be quite flexible for handling such structures and quite accurate when compared with available data.

The higher order modes of excitation are taken into account in the analysis, and the ripples in the frequency response of the input reflection coefficient illustrate the relevance of our solution for the design of waveguide junctions.

Various values of both lengths L and L_t are considered, while the formulation and convergence do not seem to suffer by varying both lengths. However, the frequency range taken is confined between 2.6 and 19 GHz.

5.1 Suggestions for future research

Although we have investigated the moment method solution up to four discontinuities, it is obviously of interest to extend the effort to N step discontinuities.

Another potential study involves employing the moment method in two different co-ordinates systems such as the problem of circular-to-rectangular waveguide junctions, waveguide-horn junction, *etc*.

Finally, the method can also be adapted to the coupling between two horns, coupling between two waveguides particularly since the method has already been applied to study the coupling between two slits.

APPENDIX A

ANALYSIS OF ASYMMETRICAL DIAPHRAGMS IN RECTANGULAR WAVEGUIDES

A particularly important problem in electromagnetic theory is the analysis of diaphragms or irises in rectangular waveguides. So far, a few special discontinuities have exact solutions; otherwise a numerical solution is suggested.

Wu *et al* [11] have used the moment method procedure to present a solution to scattering by irises in rectangular waveguides. In their solution, the evanescent wave is presented by the extra induced current density on the conducting surfaces which is localized at the discontinuity, then the moment method with the point-matching technique is applied to solve for the scattering matrix coefficients and the induced current density. It should be noted that Ray theory has also been applied to investigate this problem by Yee and Felsen [20,21].

We present here a moment method procedure which is straightforward and parallel to the analysis in Chapter 2, the only difference in this case being that the cross-sections of the waveguides are the same and also the aperture size S is arbitrary.

Consider an infinitely long rectangular waveguide having a discontinuity at z=0 as shown in Fig. A-1. The transverse components of the electromagnetic field in modal form are given as follows [31].

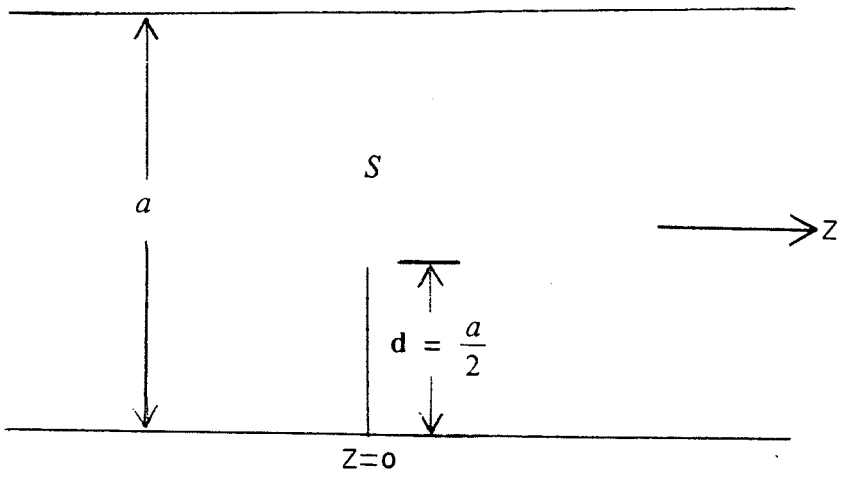

Fig. A-1: Geometry of an asymmetrical diaphragm.

$$E_t = \begin{cases} \sum_i a_i e^{-j\gamma_{ai} z} e_{ai} + \sum_i d_i e^{j\gamma_{ai} z} e_{ai} & (z < 0) \\ \sum_i b_i e^{-j\gamma_{ai} z} e_{ai} & (z > 0) \end{cases} \tag{A-1}$$

$$H_t = \begin{cases} \sum_i a_i Y_{ai} e^{-j\gamma_{ai} z} u_z \times e_{ai} - \sum_i d_i Y_{ai} e^{j\gamma_{ai} z} u_z \times e_{ai} & (z < 0) \\ \sum_i b_i Y_{ai} e^{-j\gamma_{ai} z} u_z \times e_{ai} & (z > 0) \end{cases} \tag{A-2}$$

a_i, b_i, and d_i are complex coefficients of the incident, transmitted, and reflected modes, respectively.

Following the procedure outlined in Chapter 2, the scattering matrix for this structure can be written as

$$S_{11} = H_a \bar{Y}_a^{-1} W_a^T Y_a - U \tag{A-1}$$

and for the submatrix S_{21}, we have

$$S_{21} = H_a \bar{Y}_a^{-1} W_a^T Y_a \tag{A-2}$$

where the subscript 1 refers to the left waveguide and 2 refers to the right waveguide. Since the structure is symmetric about z=0, the submatrices S_{12} and S_{22} are identical to S_{21} and S_{11}, respectively, *i.e.*

$$S_{12} = S_{21} \tag{A-3}$$

and

$$S_{22} = S_{11} \tag{A-4}$$

In Fig. A-2 we have plotted the magnitude of the reflection coefficient of a perfectly thin diaphragm located at the lower wall (z=0) with a length equal to $a/2$. The aperture is divided into a number of subsections 3,5,...,11. However 11 subsections and 7 modes (*i.e.* N=7) yield to an excellent accuracy.

The results are verified by comparing with the exact solution obtained by Collin [5]. The agreement is excellent between the two solutions, particularly in the rang $0.5 < a/\lambda < 0.85$. On the other hand, the agreement between the exact and ray theory solution is poor especially near the cutoff frequencies to which the solution can not be applied [45].

Fig. A-3 show the magnitude of the transmission coefficient compared with the exact and ray theory solution, the agreement is excellent with the exact solution for values $0.7 < a/\lambda$, while Fig. A-4 show the phase of the reflection coefficient plotted in degrees.

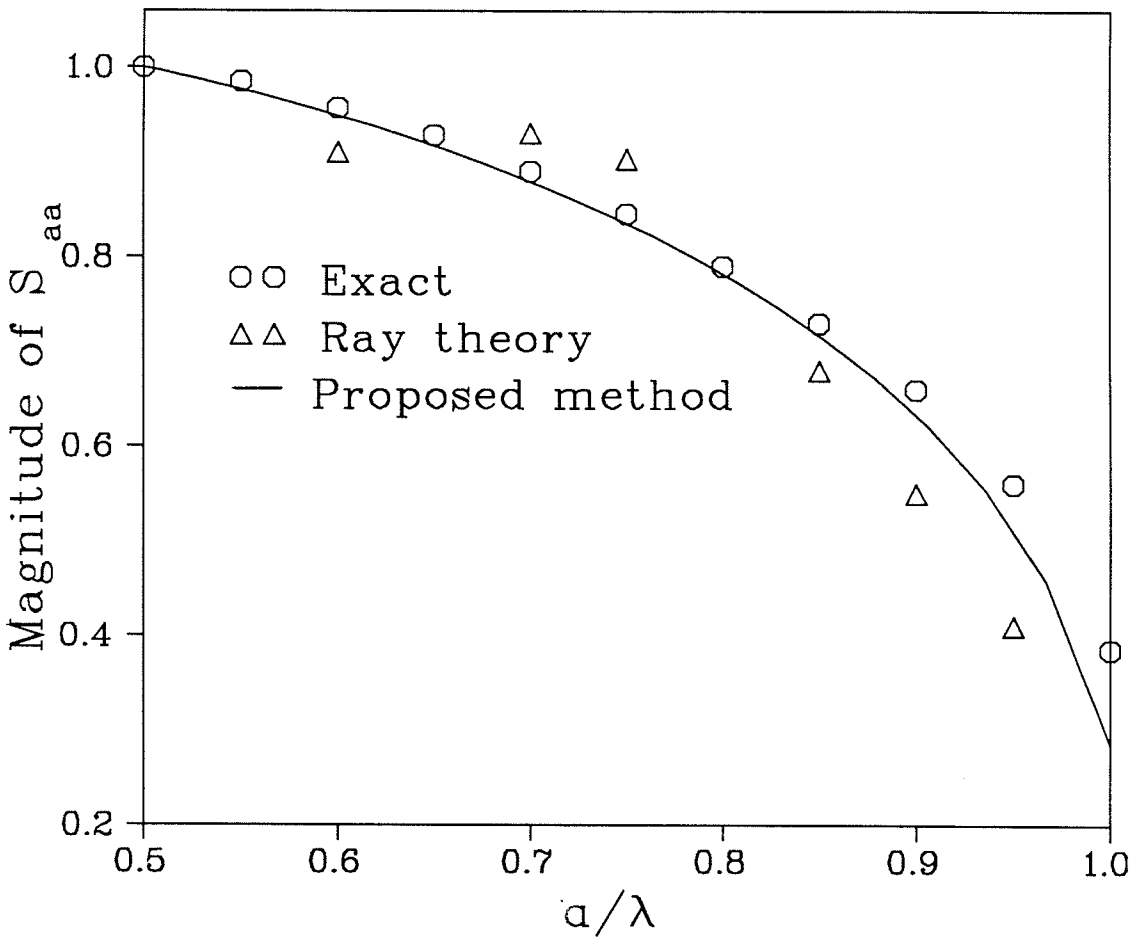

Fig. A-2: Magnitude of S_{aa} for an asymmetrical diaphragm with d = $\frac{a}{2}$.

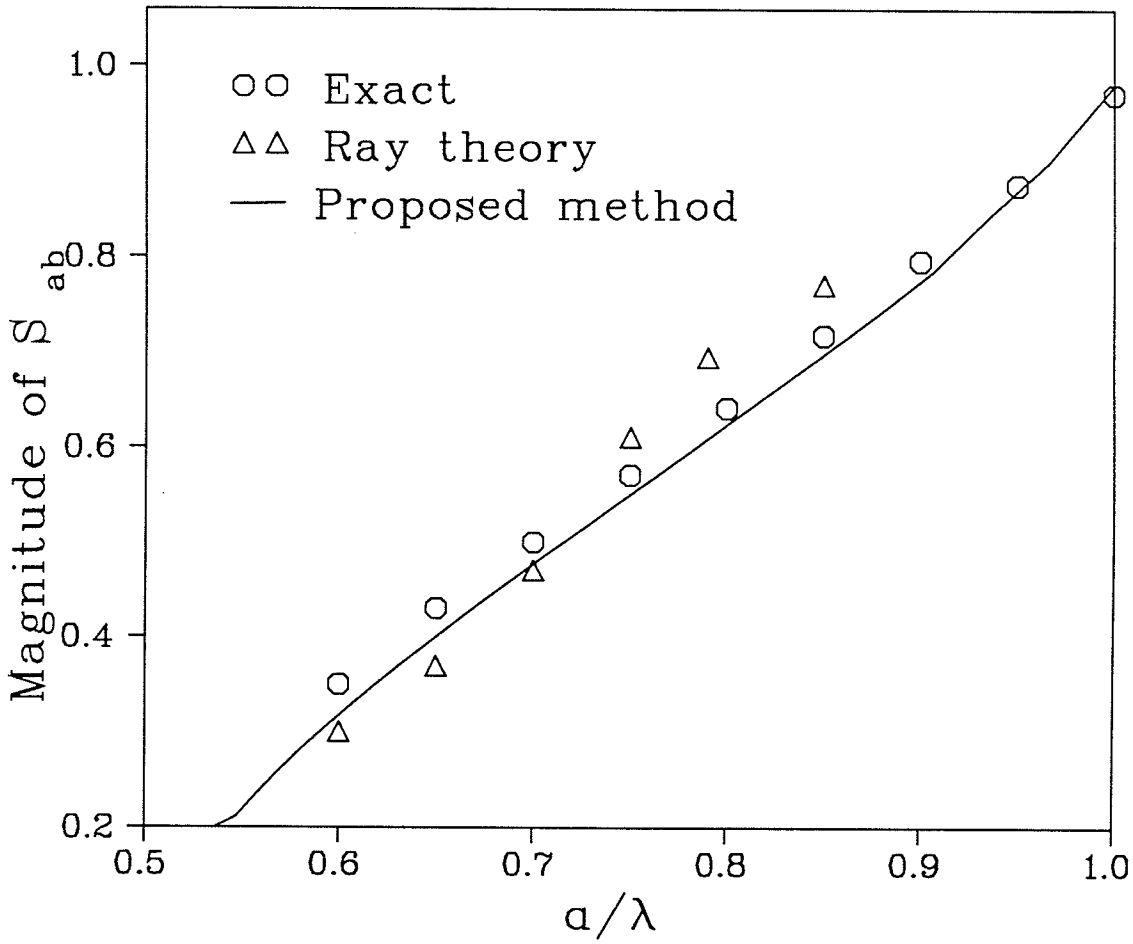

Fig. A-3: Magnitude of S_{ab} for an asymmetrical diaphragm with d = $\frac{a}{2}$.

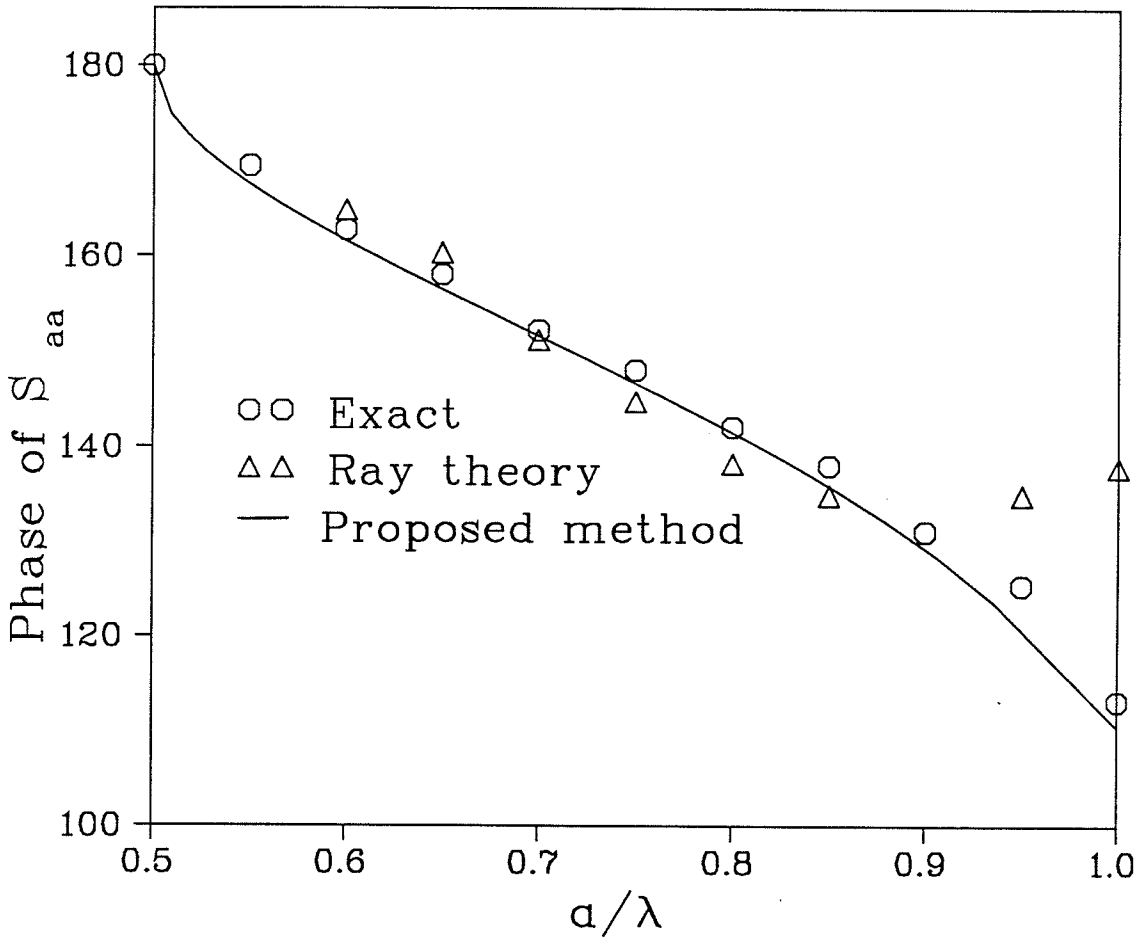

Fig. A-4: Phase of S_{aa} for an asymmetrical diaphragm with d = $\frac{a}{2}$.

APPENDIX B

DERIVATION OF THE SCATTERING MATRIX FOR CASCADED JUNCTIONS

In this appendix we present a derivation to the equations in section 4.6 as follows.

$$b_1^{(A)} = S_{aa}^{(d)}\, a_1^{(A)} + S_{ac}^{(d)}\, b_1^{(C)} \tag{B-1}$$

$$a_1^{(C)} = S_{ca}^{(d)}\, a_1^{(A)} + S_{cc}^{(d)}\, b_1^{(C)} \tag{B-2}$$

$$b_1^{(C)} e^{\gamma_1 L_t} = S_{cc}^{(d)}\, e^{-\gamma_1 L_t}\, a_1^{(C)} + S_{ce}^{(d)}\, a_1^{(E)} \tag{B-3}$$

$$b_1^{(E)} = S_{ec}^{(d)}\, e^{-\gamma_1 L_t}\, a_1^{(C)} + S_{ee}^{(d)}\, a_1^{(E)} \tag{B-4}$$

Substituting (B-3) into (B-2) and then solving for $a_1^{(C)}$, we obtain

$$a_1^{(C)} = \frac{S_{ca}^{(d)}}{1 - S_{cc}^{(d)2}\; e^{-2\gamma_1 L_t}}\, a_1^{(A)} + \frac{S_{cc}^{(d)}\, S_{ce}^{(d)}\, e^{-\gamma_1 L_t}}{1 - S_{cc}^{(d)2}\; e^{-2\gamma_1 L_t}}\; a_1^{(E)} \tag{B-5}$$

Again, substituting (B-5) into (B-4) and simplifying, we obtain

$$b_1^{(E)} = \underbrace{\frac{S_{ec}^{(d)}\, S_{ca}^{(d)}\, e^{-\gamma_1 L_t}}{1 - S_{cc}^{(d)2}\; e^{-2\gamma_1 L_t}}}_{S_{ec}}\, a_1^{(A)} + \left(\underbrace{S_{ee}^{(d)} + \frac{S_{ec}^{(d)}\, S_{cc}^{(d)}\, S_{ce}^{(d)}\, e^{-2\gamma L_t}}{1 - S_{cc}^{(d)2}\; e^{-2\gamma_1 L_t}}}_{S_{ee}} \right) a_1^{(E)} \tag{B-6}$$

REFERENCES

1. S. B. Cohn,"Optimum design of stepped transmission-line transformers", I.R.E. Trans. Microwave Theory Tech., vol. MTT-3, pp. 16-21, Apr. 1955.

2. D. Varon,"Radial line band rejection filters in coaxial waveguides", IEEE Trans. Microwave Theory Tech., vol. MTT-15, No.12, pp. 680-687, Dec. 1967.

3. J. V. Bladel,"Dielectric resonator in waveguide below cutoff", IEEE Trans. Microwave Theory Tech., vol.MTT-29, No.4, pp. 314-322, Apr. 1981.

4. N. Marcuvitz, Waveguide Handbook, NewYork: McGraw-Hill, 1951.

5. R. E. Collin, Fields Theory of Guided Waves, NewYork: McGraw-Hill, 1960.

6. H. Poritsky and M. H. Blewett,"A method of solution of field problems by means of over-lapping regions", Quarterly Appl. Math., vol.3, No.4, pp. 336-347, 1946.

7. K. G. Goyal, Analysis of the field structure in corners and tees in rectangular waveguides, M. Sc. Thesis, Department of Electrical Engineering, University of Toronto, 1966.

8. M. F. Iskander and M. Hamid,"Scattering coefficients at a waveguide-horn junction", Proc. IEE, vol.123, pp. 123-127, 1976.

9. K. C. Kao,"Approximate solution of the H-plane right-angled corner in over-moded rectangular waveguide operating in the H_{10} mode", Proc. IEE, vol.III, No.4, pp. 624-628, April 1964.

10. S. Sinha,"Analysis of multiple-strip discontinuity in a rectangular waveguide", IEEE Trans. Microwave Theory Tech., vol. MTT-34, No.6, pp. 696-700, June

1986.

11. S. C. Wu and Y. L. Chow,"An application of moment method to waveguide scattering problem", IEEE Trans. Microwave Theory Tech., vol. MTT-20, No.11, pp. 744-749 , Nov. 1972

12. T. Vu Khac,"Solution for some waveguide discontinuities by the method of moments", IEEE Trans. Microwave Theory Tech., vol. MTT-20, pp. 416-418, 1972.

13. R. De Smedt and B. Denturck,"Scattering matrix of junction between rectangular waveguides", IEE Proc., vol.130.pt.H, No.2, pp. 183-190, March 1983.

14. T. E. Rozzi and W. F. G. Mecklenbräuker,"Wide-band network modeling of interacting inductive irises and steps", IEEE Trans. Microwave Theory Tech., vol. MTT-23, No.2, pp. 235-245, Feb. 1975.

15. T. E. Rozzi,"The variational treatment of thick interacting inductive irises", IEEE Trans. Microwave Theory Tech., vol. MTT-21, pp. 82-88, Feb. 1973.

16. A. Wexler,"Solution of waveguide discontinuities by modal analysis", IEEE Trans. Microwave Theory Tech., vol. MTT-15, pp. 508-517, Sep. 1967.

17. H. Patzelt and F. Arndt,"Double-plane steps in rectangular waveguides and their application for transformers, irises, and filters", IEEE Trans. Microwave Theory Tech., vol. MTT-30, No.5, pp. 771-776, May 1982.

18. R. Safavi-Naina and R. H. MacPhie," On solving waveguide junction scattering problems by conservation of complex power technique", IEEE Trans. Microwave Theory Tech., vol. MTT-29, No.4, pp. 337-343, Apr. 1981.

19. R. Safavi-Naina,"On solving waveguide scattering problems by the conservation of complex power", Ph.D. dissertation, University of Waterloo, Ontario, Canada , Mar.1979.

20. H. Y. Yee and L. B. Felsen,"Ray optical analysis of electromagnetic scattering in waveguides", IEEE Trans. Microwave Theory Tech., vol. MTT-17, pp. 671-683, Sept. 1969.

21. H. Y. Yee and L. B. Felsen,"Ray optics- A novel approach to scattering by discontinuities in rectangular waveguide", IEEE Trans. Microwave Theory Tech., vol.MTT-17, pp. 73-85, Feb.1969.

22. M. F. Iskander and M. A.K. Hamid,"Iterative solutions of waveguide discontinuity problems", IEEE Trans. Microwave Theory Tech., vol. MTT-25, pp. 763-767, Sept. 1977.

23. H. Auda and R. F. Harrington,"A moment method solution for waveguide junctions problems", IEEE Trans. Microwave Theory Tech. vol. MTT-35, No.7, pp. 515-520, July 1983.

24. R. F. Harrington and J. R. Mautz," A generalized network formulation for aperture problems", IEEE Trans. Antennas Propagat. vol. Ap-24, pp. 870-873, Nov. 1976.

25. R. Mittra, Computer techniques in electromagnetics, NewYork: Oxford, 1973.

26. A. S. Omar and K. Schunemann," Transmission matrix representation of finline discontinuities", IEEE Trans. Microwave Theory Tech., vol. MTT-33, No.9, pp. 765-770, Sept. 1985.

27. G. Filipsson,"A new general computer algorithm for S-matrix calculation of interconnected multiports", Proc. 11 *th* European Microwave Conference (Amsterdam), pp. 700-704, 1981.

28. G. R. Simpson,"A generalized m-port cascade connection", Proc. IEEE MTT-S Symp.,(Los Angeles), pp. 507-509, 1981.

29. R. E. Collin, Foundation for Microwave Engineering, NewYork: McGrow-Hill, 1961.

30. R. F. Harrington, Time-Harmonic Electromagnetic Fields, NewYork: McGraw-Hill, 1961.

31. R. F. Harrington, Field Computation by Moment Methods, NewYork: Macmillan, 1968.

32. Y. Leviatan,"Low-frequency characteristics modes for aperture coupling problems ", IEEE Trans. Microwave Theory Tech., vol. MTT-34, No.11, pp. 1208-1222 , Nov. 1986.

33. Y. Leviatan,"Electromagnetic coupling between two half-space regions by two slot-perforated parallel conducting screens", IEEE Trans. Microwave Theory Tech., vol. MTT-36. No.1, pp. 44-52, Jan. 1988.

34. L. Kantorovich and G. Akilov, Functional analysis in normed space, Pergamon Press, Oxford, pp. 586-587, 1964.

35. C. Balanis, Antenna Theory Analysis and Design, NewYork: Harper and Row, 1982.

36. R. F. Harrington and J. R. Mautz,"Computation of characteristic modes for conducting bodies", IEEE Trans. Antennas Propag., vol. AP-19, pp. 629-639, Sept.

1971.

37. R. F. Harrington and J. R. Mautz,"Characteristic modes for dielectric and magnetic bodies", IEEE Trans. Antennas Propag., vol.AP-20, pp. 194-198, Mar. 1972.

38. R. F. Harrington and J. R. Mautz,"Theory of characteristic modes for conducting bodies", IEEE Trans. Antennas Propag., vol.AP-19, pp. 622-628, Sept. 1971.

39. C. G. Montgomery, R. H. Dicke and E. M. Purcell, Principle of Microwave Circuits, NewYork: McGraw-Hill, 1948.

40. T. D. Shockley, C. R. Haden and C. E. Lewis,"Application of the point-matching method in determining the reflection and transmission coefficients in linearly tapered waveguides", IEEE Trans. Microwave Theory Tech., vol.MTT-16, pp. 562-564, Aug. 1968.

41. T. Sugiura and H. Suga,"The susceptance of annular metallic strip in circular waveguide with incident TE_{01} mode", IEEE Trans. Microwave Theory Tech., vol.MTT-27, No.2, pp. 160-167, Feb. 1979.

42. J. D. Wade and R. H. MacPhie,"Scattering at circular-to-rectangular waveguide junctions", IEEE Trans. Microwave Theory Tech., vol.MTT-34, No.11, pp. 1085-1091 Nov. 1986.

43. D. T. Auckland and R. F. Harrington,"Electromagnetic transmission through a filled slit in a conducting plane of finite thickness, *TE* case", IEEE Trans. Microwave Theory Tech., vol.MTT-26, No.7, pp. 499-504, July 1978.

44. A. K. Hamid, I.R. Ciric and M. Hamid,"Moment method solution of double step discontinuity in waveguides", accepted for publication, Int. J. of Electronics.

45. S. C. Kashyap, Diffraction by a slit in a thick conducting screen, Ph.D. Thesis, Department of Electrical Engineering, University of Manitoba, 1971.

46. A. K. Hamid, I.R. Ciric and M. Hamid,"Analysis of multiple-step discontinuities in rectangular waveguides", Proc. Antenna and Applied Electromagnetic Symposium, University of Manitoba, Winnipeg, Canada, August 1988.